Master's thesis

NTNU
Norwegian University of Science and Technology
Faculty of Natural Sciences
Department of Physics

Mathias Bo Mjøen Svendsen

# Curvature in Superconductor-Ferromagnet Structures

Master's thesis in Applied Physics and Mathematics
Supervisor: Dr. Sol Jacobsen
June 2021

NTNU
Norwegian University of
Science and Technology

Mathias Bo Mjøen Svendsen

# Curvature in Superconductor-Ferromagnet Structures

Master's thesis in Applied Physics and Mathematics
Supervisor: Dr. Sol Jacobsen
June 2021

Norwegian University of Science and Technology
Faculty of Natural Sciences
Department of Physics

NTNU
Norwegian University of
Science and Technology

**Abstract**

The introduction of superconducting spintronic devices is seen as one possible solution to the major energy loss due to Joule heating in current computers. Superconducting spintronic devices are both energy- and space efficient, providing the prospect of dissipationless currents and a small size compared to its semiconducting counterparts. A particularly interesting system with several potential applications in superconducting spintronics is the superconductor-ferromagnet proximity system. The key feature of such systems is the proximity effect, where superconducting correlations can tunnel into the ferromagnet. The main challenge with the superconductor-ferromagnet proximity system is the short decay lengths of the superconducting singlet correlations. One approach to solve this problem is to introduce spin-orbit coupling in the ferromagnet, an effect where the electron spin couples to its momentum, which may generate long-range triplets. However, the strength and direction of the intrinsic spin-orbit coupling is fixed in a specific sample. For superconductor-ferromagnet proximity systems to be useful in spintronic applications, an on-demand tunable spin-orbit coupling is desirable.

In this thesis, we investigate the possibility of utilizing curvature in the ferromagnet as a source of a tunable spin-orbit coupling. The addition of curvature results in a spin-orbit coupling in the normal direction proportional to the curvature itself. We have derived the Usadel equation in curvilinear coordinates, valid for torsion-free curved nanowires and thin-films. Furthermore, we investigate the limiting case of a 1D nanowire arc curved in the shape of a circle-portion both analytically in the weak proximity limit, and numerically analyzing physical observables like the magnetization and charge and spin current density. The analysis of the magnetization confirmed the presence of long-range triplets when introducing curvature in the ferromagnetic nanowire. The analysis of the charge current resulted in two main discoveries; a curvature induced long-ranged Josephson effect and a curvature-induced $0-\pi$ transition. The long-ranged Josephson effect was confirmed numerically by separating the singlet and triplet contributions to the charge current for a junction of length $L = 6\xi$. The curvature-induced $0-\pi$ transition for the charge current was found to occur at a specific length-dependent curvature. Previously, $0-\pi$ transitions have been generated by adjusting the length of a the ferromagnetic wire, a non-dynamical procedure requiring multiple samples, not suited for applications in superconducting spintronics. Both the curvature induced long-ranged Josephson effect and the curvature-induced $0-\pi$ transition providing a fully dynamical control of the transition, offers great possibilities for superconducting spintronics.

# Preface

This thesis concludes a five year master's program in applied physics and mathematics at the Norwegian University of Science and Technology, under the supervision of Dr. Sol Jacobsen at the center of QuSpin. The thesis amounts to 30 ECTS points and builds upon a project thesis written in the 9th of the 10 total semesters. The thesis is mainly theoretical with the focus on deriving a general diffusion equation for curved superconductor-ferromagnet proximity systems. However, a numerical analysis is performed in MATLAB utilizing a boundary value solver `bvp6c` to find solutions to the diffusion equation. All plots of relevant physical observables provided in the thesis are produced in MATLAB using the internal `plot` and `quiver`-functions. Most numerical calculation was performed on the supercomputer Saga at NTNU. All illustrations are made using vector graphics in Inkscape. The theoretical work in the thesis relies heavily on many-body quantum mechanics in the framework of Green's functions and on tensor calculus, where the reader is assumed to be familiar with the former. An introduction on tensor calculus is given in Section 1.3, but a complete treatise can be found in the book by Neuenschwander [33]. The work presented in the thesis resulted in a paper submitted for publication and is enclosed in the Appendix.

First of all, I would like to thank my supervisor Sol Jacobsen for your enthusiastic guidance and for always being available when I got stuck. A have thoroughly enjoyed our weekly meetings, and I have learned a lot from you. Your work ethic and passion have truly inspired me, and I am now more motivated than ever to continue in the exciting field of condensed matter physics. Hopefully, we will have the chance for collaborations in the future.

I would also like to thank Tancredi Salamone, Dr. Henning Hugdal and Dr. Morten Amundsen for our weekly curvature meetings. Even though we didn't have many chances to meet in person our Zoom meetings provided a great source of input and fruitful discussions.

Lastly, I would like to thank my family and friends for supporting me with special thanks to my brother Sindre for providing some relief from academic work through outdoor adventures and weekly climbing sessions.

Mathias Bo Mjøen Svendsen
Trondheim, Norway
June 2021

## Notation and units

To keep track of the dimensions of matrices we employ a notation where $\underline{M}$ is a 2x2 matrix, $\hat{M}$ is a 4x4 matrix and $\check{M}$ is a 8x8 matrix. A matrix sum/product with non-matching dimensions should be interpreted as taking the Kronecker product between the smallest matrix and the appropriate identity matrix before performing the matrix summation/multiplication. For example, the product $\hat{M}\check{N} + \underline{P}$ should be interpreted as $(\underline{I} \otimes \hat{M})\check{N} + (\hat{I} \otimes \underline{P})$, where $\underline{I}$ and $\hat{I}$ are the 2x2 and 4x4 identity matrix respectively.

Vectors will be denoted by a bold font $\boldsymbol{a}$ and may be expressed in terms of its components in either a parenthesis notation $\boldsymbol{a} = (a_x, a_y, a_z)$ or a notation using unit vectors $\boldsymbol{a} = a_x\hat{\boldsymbol{e}}_x + a_y\hat{\boldsymbol{e}}_y + a_z\hat{\boldsymbol{e}}_z$ in a Cartesian coordinate system. The unit vectors $\hat{\boldsymbol{e}}_i$ should not be confused with the notation for 4x4 matrices. The same vector may be expressed in a curvilinear coordinate system as $\boldsymbol{a} = (a_T, a_N, a_B)$ or $\boldsymbol{a} = a_T\hat{\boldsymbol{\mathcal{T}}}(s) + a_N\hat{\boldsymbol{\mathcal{N}}}(s) + a_B\hat{\boldsymbol{\mathcal{B}}}(s)$. We will separate between covariant, contravariant and physical vector components denoted by $a_i$, $a^i$ and $a_{(i)}$ respectively, the exception being when the vector is defined in a specific basis like in the parenthesis vector notation or in terms of the unit vectors. In these cases, physical vector components are implied.

Partial derivatives are denoted by a short-hand notation $\partial_x = \frac{\partial}{\partial x}$. The gradient is a vector containing the partial derivatives in the corresponding directions, expressed in Cartesian coordinates as $\nabla = (\partial_x, \partial_y, \partial_z)$.

The identity Pauli matrix and the Cartesian Pauli matrices in spin space are defined as

$$\underline{\sigma}_0 = \begin{pmatrix} 1 & 0 \\ 0 & 1 \end{pmatrix}, \quad \underline{\sigma}_x = \begin{pmatrix} 0 & 1 \\ 1 & 0 \end{pmatrix}, \quad \underline{\sigma}_y = \begin{pmatrix} 0 & -i \\ i & 0 \end{pmatrix}, \quad \underline{\sigma}_z = \begin{pmatrix} 1 & 0 \\ 0 & -1 \end{pmatrix}.$$

The Cartesian Pauli matrices may be combined into a Pauli spin-vector in spin space $\underline{\boldsymbol{\sigma}} = (\underline{\sigma}_x, \underline{\sigma}_y, \underline{\sigma}_z)$. The Pauli matrices in Nambu space are defined in the exact same way and will be denoted by $\underline{\tau}_i$

$$\underline{\tau}_0 = \begin{pmatrix} 1 & 0 \\ 0 & 1 \end{pmatrix}, \quad \underline{\tau}_x = \begin{pmatrix} 0 & 1 \\ 1 & 0 \end{pmatrix}, \quad \underline{\tau}_y = \begin{pmatrix} 0 & -i \\ i & 0 \end{pmatrix}, \quad \underline{\tau}_z = \begin{pmatrix} 1 & 0 \\ 0 & -1 \end{pmatrix}.$$

$\hat{\tau}_z = \mathrm{diag}(1, 1, -1, -1)$ is a 4x4 matrix extension of $\underline{\tau}_z$.

Complex conjugation of scalars and matrices are denoted by an asterisk *, while hermitian conjugation of matrices is denoted by a dagger †. Square brackets $[\cdot, \cdot]$ denotes a commutator while curly brackets $\{\cdot, \cdot\}$ denotes an anticommutator. The commutator and anticommutator of two matrices $\hat{A}$ and $\hat{B}$ are defined as follows

$$[\hat{A}, \hat{B}] = \hat{A}\hat{B} - \hat{B}\hat{A}, \qquad \{\hat{A}, \hat{B}\} = \hat{A}\hat{B} + \hat{B}\hat{A}.$$

In physics we often want to minimize the number of units and express them in terms of physical constants rather than using SI units which is heavily based on measurements. By choosing physical constants as the fundamental scale of

the corresponding physical quantity, we can set these constants to unity which has the advantage of making expressions simpler, while still keeping the physics in the equations [79]. Many such natural unit systems exists. In this thesis we will use a natural unit system where

$$\hbar = c = \epsilon_0 = \mu_0 = k_B = 1,$$

where $\hbar$ is the reduced Planck's constant, $c$ is the speed of light, $\epsilon_0$ is the vacuum permittivity, $\mu_0$ is the permeability and $k_B$ is the Boltzmann constant.

# Contents

# 1 Introduction

## 1.1 Motivation

About 5% of all energy consumption in the U.S. goes to running computers [1]. The majority of this energy will inevitably be converted to heat necessitating expensive and wasteful cooling infrastructure. In a world where information storage and high-performance computing has become essential, the computational energy is only bound to increase. A major driver to the increasing energy cost of computers is mining of cryptocurrency. It has recently been estimated that mining for bitcoins alone represents more than 100 TWh/y [2], close to the total electricity consumption of Norway and amounting to nearly 0.6% of the global electricity use. Even considering a continued shift to more "green" electricity production, the energy cost of running "hot" computers is clearly not sustainable, neither from an ecological nor a business perspective. A paradigm shift in how computations can be performed in an energy efficient manner is clearly needed.

A possible solution to this problem would be to develop powerful "cool" computers by the introduction of superconducting spintronics, where currents may flow resistance free and the spin of the electron is used as the information carrier rather than, or in combination with, the charge. Due to the net spin-polarization of quasiparticles in the superconductor the short decay lengths due to spin-flip scattering, a problem in non-superconducting spintronics, may be avoided [3], [4]. Spintronic devices have the advantage of being smaller in size compared to its charge based semiconducting counterparts, where the transport properties are dictated by the depletion layer which thickness may vary from a couple of nanometers to a few micrometers [5].

One system that offers tantalizing possibilities for applications in superconducting spintronics is the superconductor-ferromagnet (SF) proximity system. Singlet superconductivity and ferromagnetism is highly unlikely to coexist in bulk materials, but when placing a conventional superconductor in close proximity with a ferromagnet, some of the superconducting electron pairs may tunnel from the superconductor into the ferromagnet, a phenomenon called the *proximity effect* [6]. Due to the pair breaking effect present in the ferromagnet, the amplitude of the singlet superconducting electron pairs, denoted as $|\uparrow\downarrow\rangle - |\uparrow\downarrow\rangle$, will decay exponentially as a function of the length penetrated in the ferromagnet. In order for superconductor-ferromagnet proximity systems to be useful in spintronic applications, a much longer penetration depth is needed. This problem can be solved by generating the equal spin triplet state $|\uparrow\uparrow\rangle$ or $|\downarrow\downarrow\rangle$, the *long-range triplets*, which is immune to the pair breaking effect and hence decay linearly in the ferromagnet as shown in Figure 1.

The transition from the singlet state to the long-range triplet state may be understood by considering superconducting singlet correlations incident to the interface between the superconductor and the ferromagnet. Due to the spin polarization at the interface, a mixing between the incident singlet state and the opposite spin triplet state $|\uparrow\downarrow\rangle + |\uparrow\downarrow\rangle$, the *short-range triplets*, occurs. The

short-range triplet decays in an oscillatory manner as shown in Figure 1 with penetration depth depending on the spin-polarization of the ferromagnet, but is on the same order as the penetration depth of the singlet state. However, the short-range triplet may be rotated into the long-range triplet close to the interface if the ferromagnet carry an inhomogeneous exchange field. This was demonstrated theoretically by Bergeret, Volkov and Efetov in 2001 [7] and later experimentally by Keizer et al. [8] and Sosnin et al. [9] in 2006. The prerequisite for an inhomogeneous magnetic field can be problematic for practical applications since such features are rare to find intrinsically in materials and artificially generated ones are hard to control.

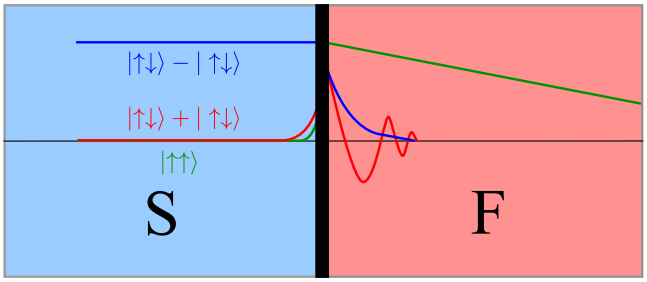


Figure 1: The amplitude of the different spin states in the superconductor (S) tunneling into the ferromagnet (F). The amplitude of the singlet state $|\uparrow\downarrow\rangle - |\uparrow\downarrow\rangle$ is indicated by the blue line, the opposite spin triplet $|\uparrow\downarrow\rangle + |\uparrow\downarrow\rangle$ by the red line, and the equal spin triplet $|\uparrow\uparrow\rangle$ by the green line.

More recently, Bergeret and Tokatly published a paper suggesting an alternative way of generating the long range triplet components by introducing spin-orbit coupling in the ferromagnet, an effect where the spin of the electrons couples to its momentum, often as a result of the lack of inversion symmetry in the ferromagnet [10]. In the paper, Bergeret and Tokatly demonstrated that introducing spin-orbit coupling may generate the long-range triplets from the short-range triplets. The long-range triplets by necessity has to be perpendicular to the ferromagnetic exchange field, while the short range triplets have to be parallel to the field. The generation of the long-range triplets is determined by a combination of the ferromagnetic exchange field and the direction and strength of the spin-orbit coupling [11], [12], [13].

The intrinsic spin-orbit strength is a material-dependent constant. For spin-orbit driven superconducting spintronics to be viable, an on-demand tunable spin-orbit coupling is needed. Voltage-gating the sample is one way of introducing such a tunable spin-orbit coupling [14]. However, the spin-orbit coupling will be constant throughout the sample. Recently, it has been shown that introducing a strain in the form of bending the material, induces a strain-driven electric field breaking the inversion symmetry resulting in a spin-orbit coupling

which relates directly to the curvature [15]. The relation between the spin-orbit strength and the curvature provides a method of tuning the spin-orbit strength by manipulation of the curvature.

One eminent novel application could be a curved superconductor-ferromagnet-superconductor proximity structure (Josephson junction) where a curved ferromagnetic wire provides a mechanism of tuning the superconducting electron pairs between the singlet and long-range triplet state by manipulating the curvature of the ferromagnet. A possible realization of such a curved Josephson junction is illustrated at the left in Figure 2. In the singlet state no spin current will pass through the junction, while in the long-range triplet state current may pass due to the long penetration depth. The alternation between the singlet and long-range triplet states functions as a current switch or a spin valve. A curvature-induced spin-orbit-tunable triplet spin-valve offers the possibility to construct logical gates driven by spin currents, where a current passing through encodes the binary 1 and no current the binary 0, rather than the standard slower and less energy efficient semiconducting electronics using electrical currents.

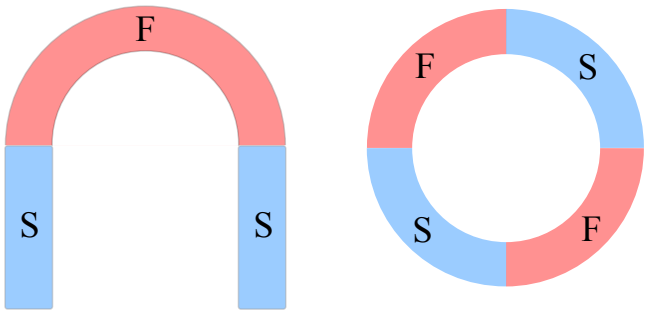


Figure 2: Potential outline of a curved Josephson (left) and a circular SQUID (right).

Another interesting application of superconductor-ferromagnet proximity systems is a SQUID (superconducting quantum interference device), which is a loop of Josephson junctions. SQUIDs are based on the fact that the maximum current flowing through the loop is periodic in the magnetic flux through the loop. Hence by monitoring the current, SQUIDs can be used for extremely precise measurements of magnetic flux. SQUIDs have a wide range of applications, from quantum computing to mapping brain activity and even measuring single electron spins. Circular nano-SQUIDs have been produced and explored experimentally [16], where the circular SQUID placed on the sharp tip of a probe provides a extremely low noise in the magnetic flux. Allthough circular SQUIDs have been tested experimentally, a full theoretical description has yet to be carried out. As established, the introduction of curvature induces long-range

triplet currents. Consequently, a circular SQUID may function as a spin-triplet SQUID [17]. A simple illustration of the outline of a semicircular SQUID is depicted at the right in Figure 2. The size of the weak link ferromagnet can be chosen much smaller compared to the superconductor.

Quantum theory of particles constrained to curved geometries has seen an increasing interest due to the experimental development of bent low-dimensional nanostructures [18], [19]. The potential for creating 2-dimensional rolled-up thin-film nanotubes has already been realized experimentally by utilizing selective etching methods on etching sensitive materials in contact with the desired thin film [20]. Lithographical methods for the creation of 1-dimensional curved nanowires have been investigated extensively where it has been shown that the partial release and the bond back of layers may be used in creating specific wrinklings in nanochannels [21]. More recently, it has been shown that fixing nanochannels in multiple points on a stretched silicon substrate and allowing the substrate to return to its original shape enables the creation of complex curved nanostructures of desired shapes [22]. Examples of such nanostructures are given in Figure 3.

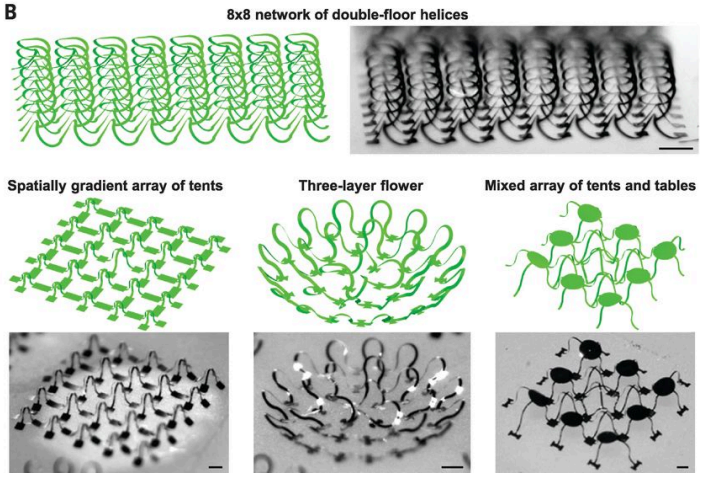


Figure 3: Examples of curved nanostructures created by fixing nanochannels in multiple points on a stretched silicon substrate and allowing the substrate to return to its original shape (Xu et. al., 2015, p.157).

The development of experimental techniques for curving low-dimensional nanostructures has opened the possibility of creating nanowires and thin films [23] with adjustable curvature for application in spin-orbit driven superconducting spintronics. Recently, Das and collaborators showed the independent control of spin and charge currents in metallic nanowires using curvature as the control parameter [24]. By placing an aluminium nanochannel over a silicon dioxide

trench, Das et. al. demonstrated that adjusting the trench depth and hence the curvature of the aluminium nanochannel, affected the charge and spin resistance. The setup provided electrical compatibility between the curved channel and other device elements which is crucial for applications in spintronic devices.

## 1.2 Fundamental concepts

*Superconductivity* is a purely quantum phenomenon observed in some materials characterized by a vanishing electrical resistance and an exclusion of external magnetic fields at sufficiently low temperatures. These characteristic properties are due to the formation of electron pairs called Cooper pairs which may form a condensate and exhibit bosonic properties. Superconductivity was first discovered in 1911 by the Dutch physicist Heike Kamerlingh Onnes [25] before the development of quantum mechanics, but it took decades before the phenomenon could be explained. The BCS theory, named after the creators Bardeen, Cooper and Schreiffer, is to date the most successful and widely used theory to describe superconductivity [26]. The theory is based on the fact that any attractive interaction between the electrons in the system, leads to the formation of Cooper pairs. The formation of Cooper pairs is not dependent of the type of attraction, only that the attraction is present. In most superconducting materials, the attraction is mediated by phonons. A simple way to understand phonon-mediated superconductivity is to consider the toy-model of two electrons moving in opposite directions in a lattice of positive ions as depicted in Figure 4. The ions on the lattice will due to the Coulomb interaction be pulled towards the electrons, causing a concentration of positive charge. Consequently, the accumulation of positive charge leads to a Coulomb interaction between the concentrated positive charge and the moving electrons causing an effective attraction between the two electrons forming a Cooper pair.

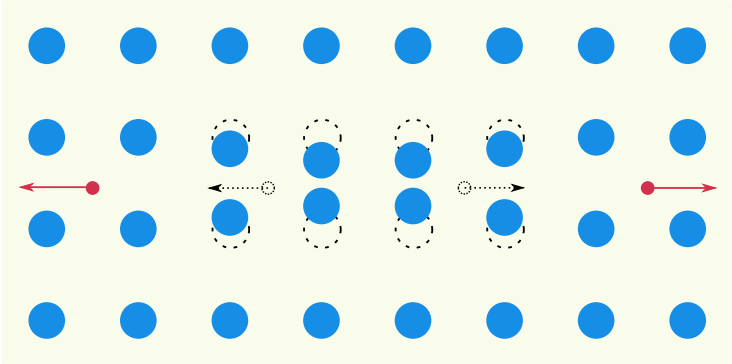

Figure 4: Two electrons (red) moving in a lattice of positive ions (blue). Through the Coulomb interaction the electrons will attract the positively charged ions and create a concentration of positive charge.

Superconductivity is a many-body quantum effect, but may be approximated as a self-consistent effective one-particle problem using a mean field theory [27]. The mean field or *order parameter* is defined as

$$\Delta(\boldsymbol{r},t) = \lambda\langle\hat{\psi}_\uparrow(\boldsymbol{r},t)\hat{\psi}_\downarrow(\boldsymbol{r},t)\rangle, \tag{1.1}$$

where $\hat{\psi}_\sigma(\boldsymbol{r},t)$ is an operator annihilating an electron with spin $\sigma$ at position $\boldsymbol{r}$ and time $t$, $\langle ...\rangle$ is a statistical average and $\lambda > 0$ is a coupling constant. In the mean field approximation, the self energy of conventional superconductivity is [28]

$$\check{\Sigma}_{SC} = \hat{\Delta}, \tag{1.2}$$

where the pair potential is defined as $\hat{\Delta} = \text{antidiag}(\Delta, -\Delta, \Delta^*, -\Delta^*)$ [29], [30]. The order parameter $\Delta$ is in general a complex number, which magnitude describes the size of the superconducting gap, the energy gain of the electrons upon forming a Cooper pair, and the complex argument describes the superconducting phase. The superconducting phase may be removed by a U(1) gauge transformation and is hence not of importance when considering only one superconductor in a system. In systems with multiple superconductors, like the Josephson junction, the phase difference is of great importance and will dictate the transport properties.

In this thesis we will focus on conventional, s-wave, singlet superconductivity. Conventional means superconductivity which can be described by BCS theory, s-wave means that the order parameter is spherically symmetric in momentum space and singlet means that the Cooper pairs are in the antisymmetric singlet state $|\uparrow\downarrow\rangle - |\uparrow\downarrow\rangle$ in the bulk of the superconductor. In order to satisfy the antisymmetry of the electronic wavefunction, s-wave, singlet superconductivity necessarily has to be symmetric in frequency.

*Ferromagnetism* is the phenomenon characterized by the spontaneous magnetization due to the alignment of electron spins in domains of the material caused by the exchange interaction [31]. This magnetic ordering breaks down at a certain material dependent temperature known as the Curie-temperature. The exchange interaction can be considered as an effective field $\boldsymbol{h}$ called the *exchange field* which describes the spin-dependent part of the electron energy [32] proportional to the magnetization of the material.

Ferromagnetic materials may form permanent magnets when exposed to an external magnetic field. These magnetic properties will still be present in the ferromagnet when turning the external field off.

The self energy from weakly spin-polarized ferromagnets is proportional to its exchange field [28]

$$\check{\Sigma}_{FM} = \boldsymbol{h}\cdot\hat{\boldsymbol{\sigma}}, \tag{1.3}$$

where $\hat{\boldsymbol{\sigma}} = \text{diag}(\boldsymbol{\sigma}, \boldsymbol{\sigma}^*)$ and $\boldsymbol{\sigma} = (\underline{\sigma}_x, \underline{\sigma}_y, \underline{\sigma}_z)$ is the Pauli spin-vector. For strongly spin-polarized ferromagnets polarization effects become important and a polarization self energy term needs to be included.

In this thesis we will consider proximity effects between conventional, s-wave superconductors and weakly spin-polarized ferromagnets in both superconductor-

ferromagnet (SF) and superconductor-ferromagnet-superconductor (SFS) proximity systems where the ferromagnet may be curved into desired shapes.

## 1.3 Tensor notation

In physics, we often search for physical laws that are independent of the chosen coordinate systems. Newton's second law of motion $\boldsymbol{F} = m\boldsymbol{a}$ can serve as an example. If we consider a particle moving in three dimensions affected by some force $\boldsymbol{F} = F_x\boldsymbol{e}_x + F_y\boldsymbol{e}_y + F_z\boldsymbol{e}_z$, we can write Newton's second law for the particle's motion as

$$F_x\boldsymbol{e}_x + F_y\boldsymbol{e}_y + F_z\boldsymbol{e}_z = m(\ddot{x}\boldsymbol{e}_x + \ddot{y}\boldsymbol{e}_y + \ddot{z}\boldsymbol{e}_z). \tag{1.4}$$

Supposing that the particle follows some orbital motion, the choice of a spherical coordinates system may be practical. In spherical coordinate Newton's second law for the particle's motion takes the form

$$\begin{aligned} F_r\boldsymbol{e}_r + F_\theta\boldsymbol{e}_\theta + F_\phi\boldsymbol{e}_\phi = {} & m(\ddot{r} - r\dot{\theta}^2 - r\dot{\phi}^2\sin^2(\theta))\boldsymbol{e}_r \\ & + m(r\ddot{\theta} + 2\dot{r}\dot{\phi} - r\dot{\phi}^2\sin(\theta)\cos(\theta))\boldsymbol{e}_\theta \\ & + m(r\ddot{\phi}\sin(\theta) + 2\dot{r}\dot{\phi}\sin(\theta) + 2r\dot{\theta}\dot{\phi}\cos(\theta))\boldsymbol{e}_\phi. \end{aligned} \tag{1.5}$$

By comparing the two equations, we see that a change of coordinate system has produced additional terms, meaning that Newton's equation $\boldsymbol{F} = m\boldsymbol{a}$ as stated above is dependent on the choice of coordinates. In order to write equations, like Newton's second law, that are invariant with respect to a change of coordinates we have to introduce the language of tensors[1]. In this thesis, we will define a curved coordinate system following our curved ferromagnet. In order to rewrite relevant equations from Cartesian to curved coordinates, tensor notation will prove to be a very useful tool.

A tensor is a mathematical object independent of a specific basis, defined by the way it transforms under a change of coordinates. Tensors can be classified by its rank. A rank 0 tensor can be described by $N^0 = 1$ number in N dimensions and can thus be represented as a scalar. Furthermore, a rank 1 tensor can be described $N^1{=}N$ numbers and can thus be represented as a vector. Continuing the reasoning, a tensor of rank 2 can be described by $N^2$ numbers equivalent to a matrix[2]. Tensors of higher rank are more complicated as they cannot be represented by any familiar mathematical object, but can be described with $N^{\text{rank}}$ numbers.

The rank of a tensor is manifested in the number of indices needed to describe the object. Consider the following two rank 1 tensors (vectors) $A_i$, $B^i$. The placement of the index determines the transformation property of the tensor. A

[1] The entirety of this section is based on the book *Tensor calculus for physics* by Dwight Neuenschwander [33].

[2] An important note is that although all rank 2 tensors may be represented as a square matrix, not all square matrices, like the Green's function matrix to be introduced later, are tensors.

rank 1 tensor with a lowered index transforms *covariantly*, while a rank 1 tensor with a raised index transforms *contravariantly* under a change of coordinates $x \to x'$

$$A'_i = \frac{\partial x^j}{\partial x'^i} A_j, \tag{1.6}$$

$$B'^i = \frac{\partial x'^i}{\partial x^j} B^j, \tag{1.7}$$

where we have introduced Einstein summation which implies a summation over each repeated index in a product. A rank 1 tensor following the transformation rule in equation (1.6) is called a *covariant* vector. Similarly, a rank 1 tensor following the transformation rule in equation (1.7) is called a *contravariant* vector. Tensors of higher rank follow a similar transformation rule. A tensor of rank $k + l$ with $k$ lowered and $l$ raised indices $T_{i_1 \dots i_k}{}^{j_1 \dots j_l}$ transforms as a product of $k$ covariant and $l$ contravariant vectors

$$T'_{i_1 \dots i_k}{}^{j_1 \dots j_l} = \frac{\partial x^{m_1}}{\partial x'^{i_1}} \cdots \frac{\partial x^{m_k}}{\partial x'^{i_k}} \frac{\partial x'^{j_1}}{\partial x^{n_1}} \cdots \frac{\partial x'^{j_l}}{\partial x^{n_l}} T_{m_1 \dots m_k}{}^{n_1 \dots n_l}. \tag{1.8}$$

A particularly useful tensor is the *metric tensor*, often called the fundamental tensor due to its importance in tensor calculus. The metric tensor may be expressed in terms of the total differential coordinate displacement. In Cartesian coordinates the differential coordinate displacement is given by

$$d\boldsymbol{R} = dx\hat{\boldsymbol{e}}_x + dy\hat{\boldsymbol{e}}_y + dz\hat{\boldsymbol{e}}_z. \tag{1.9}$$

The same differential coordinate displacement expressed in spherical coordinates is given by

$$d\boldsymbol{R} = d\rho\hat{\boldsymbol{e}}_\rho + \rho d\theta\hat{\boldsymbol{e}}_\theta + \rho \sin\theta d\phi\hat{\boldsymbol{e}}_\phi. \tag{1.10}$$

In order to generalize the differential coordinate displacement for an arbitrary coordinate system we may introduce scale factors $h_i$

$$d\boldsymbol{R} = \sum_i h_i dx^i \hat{\boldsymbol{e}}_i. \tag{1.11}$$

The scale factors have the function of endowing each coordinate displacement with the correct unit. The length of the differential coordinate displacement is found by taking the scalar product with itself

$$(dR)^2 = \sum_{i,j} h_i h_j \hat{\boldsymbol{e}}_i \cdot \hat{\boldsymbol{e}}_j dx^i dx^j = \eta_{ij} dx^i dx^j, \tag{1.12}$$

where we finally have introduced the covariant form of the metric tensor $\eta_{ij} = h_i h_j \hat{\boldsymbol{e}}_i \cdot \hat{\boldsymbol{e}}_j$. For orthogonal coordinate systems the scalar product between the unit vectors is equal to the Kronecker delta and the metric is diagonal

$$\eta_{ij} = h_i h_j \delta_{ij}. \tag{1.13}$$

Taking the examples of coordinate displacements in Cartesian and spherical coordinates given in equation (1.9) and (1.10) respectively, the covariant metric tensor may be represented as a square matrix in the following way

$$\eta_{ij}^{\text{Cartesian}} = \begin{pmatrix} 1 & 0 & 0 \\ 0 & 1 & 0 \\ 0 & 0 & 1 \end{pmatrix}, \qquad \eta_{ij}^{\text{Spherical}} = \begin{pmatrix} 1 & 0 & 0 \\ 0 & \rho^2 & 0 \\ 0 & 0 & \rho^2 \sin^2\theta \end{pmatrix}. \tag{1.14}$$

A fundamental property of the covariant (contravariant) metric tensor is that, when contracted with a contravariant (covariant) vector, it produces the corresponding covariant (contravariant) vector

$$A_i = \eta_{ij} A^j, \qquad A^i = \eta^{ij} A_j. \tag{1.15}$$

The metric tensor has the similar effect when contracted with a covariant/contravariant index of a tensor

$$T_{i_1 \dots i_{n-1}}{}^{k}{}_{i_{n+1} \dots i_m}{}^{j_1 \dots j_l} = \eta^{k i_n} T_{i_1 \dots i_m}{}^{j_1 \dots j_l}, \tag{1.16}$$

$$T_{i_1 \dots i_m}{}^{j_1 \dots j_{r-1}}{}_{s}{}^{j_{r+1} \dots j_l} = \eta_{s j_r} T_{i_1 \dots i_m}{}^{j_1 \dots j_l}. \tag{1.17}$$

From equation (1.16) and (1.17) it can be seen that the contravariant metric tensor raises the index, while the covariant metric lowers the index.

As explained, covariant/contravariant tensors follow specific transformation properties. But what about derivatives of such objects? One might naively assume that the derivative of a tensor is automatically a tensor, but as we will see, this is not the case. Consider a contravariant vector $x^i$ in a coordinate system $\mathcal{S}$. Using the transformation property given in equation (1.7), the contravariant vector $x^i$ may be expressed in a primed coordinate system $\mathcal{S}'$ as

$$x'^i = \frac{\partial x'^i}{\partial x^j} x^j. \tag{1.18}$$

The transformation rule for the derivative of a contravariant vector can be found by differentiating equation (1.18) with respect to some scalar $t$

$$\frac{dx'^i}{dt} = \frac{\partial x'^i}{\partial x^j}\frac{dx^j}{dt} + x^j \frac{d}{dt}\left(\frac{\partial x'^i}{\partial x^j}\right) = \frac{\partial x'^i}{\partial x^j}\frac{dx^j}{dt} + x^j \frac{\partial^2 x'^i}{\partial x^j \partial x^k}\frac{dx^k}{dt}. \tag{1.19}$$

From equation (1.19) one can observe a term involving second derivatives in addition to the usual contravariant transformation term. The additional term is in general non-zero. Hence ordinary derivatives of tensors are not necessarily tensors. This seems to ruin the purpose of introducing tensor calculus since the overall goal was to keep equations invariant of the choice of coordinates. The method to resolve this problem is to redefine the derivative operator in such a way that this additional term in the transformation cancels and thus preserving the tensorial nature of the transformation. This redefinition of the derivative is called the *coordinate covariant derivative*, first introduced by Ricci and Levi-Civita in 1900 [34], and will here be denoted by $\mathcal{D}$. The coordinate covariant

derivative with respect to a coordinate $x^i$ of a contravariant vector $A^j$ is defined as

$$\mathcal{D}_i A^j = \partial_i A^j + \Gamma^j_{ik} A^k, \tag{1.20}$$

where $\Gamma^j_{ik}$ is known as the Christoffel symbol or the affine connection and is related to the metric tensor

$$\Gamma^k_{ij} = \frac{1}{2}\eta^{kl}(\partial_j \eta_{li} + \partial_i \eta_{lj} - \partial_l \eta_{ij}). \tag{1.21}$$

The Christoffel symbol itself is not a tensor, but ensures that the coordinate covariant derivative of a tensor remains a tensor. The coordinate covariant derivative of a covariant vector follows a similar definition, albeit a relative minus sign

$$\mathcal{D}_i A_j = \partial_i A_j - \Gamma^k_{ij} A_k. \tag{1.22}$$

We have now introduced the language of tensors, defined how they transform and how to impose derivatives of tensors to have the right transformation properties, namely by introducing the coordinate covariant derivative. An important and often overlooked note, is how to relate these covariant and contravariant vectors with the *physical vector* defined in a certain basis. Since the scalar product of two vectors $\boldsymbol{A}$ and $\boldsymbol{B}$ is a rank 0 tensor (scalar) it should not depend on the choice of coordinate. Hence we may write

$$\boldsymbol{A} \cdot \boldsymbol{B} = \sum_i A_i B^i = \sum_{ij} \eta_{ij} A^i B^j = \sum_{ij} h_i \delta_{ij} A^i B^j = \sum_i A_{(i)} B_{(i)}, \tag{1.23}$$

where $A_{(i)}$ and $B_{(i)}$ are the physical components of the vectors $\boldsymbol{A}$ and $\boldsymbol{B}$. Equation (1.23) yields a relationship between the contravariant vector components and the physical vector components

$$A^i = \frac{A_{(i)}}{h_i}. \tag{1.24}$$

By relating the contravariant vector to the covariant a similar relationship is achieved

$$A_i = h_i A_{(i)}. \tag{1.25}$$

This may be generalized to a rank $k + l$ with $k$ lowered and $l$ raised indices

$$T_{i_1 \ldots i_k}{}^{j_1,\ldots,j_l} = \frac{h_{i_1} \cdots h_{i_k}}{h_{j_1} \cdots h_{j_l}} T_{(i_1)\ldots(i_k)(j_1)\ldots(j_l)}. \tag{1.26}$$

This concludes the introduction to tensor notation. For a more complete treatise in tensor calculus, see [33].

## 1.4 Structure

The goal of this thesis is to derive the Usadel equation in curved coordinates and solve it numerically in order to investigate the influence of curvature on physical observables. We will start with a small recap of the quasiclassical Green's function theory of superconductor-ferromagnet heterostructures and the necessary assumptions used to derive the quasiclassical Usadel equation and appropriate boundary conditions in Section 2. In Section 3 we will introduce a general curvilinear coordinate system used to describe the position in the curved ferromagnet. We will demonstrate mathematically how the curvature in the ferromagnet results in spin-orbit coupling which may be described as a background SU(2) field, before we finally derive the Usadel equation in curvilinear coordinates for torsion-free thin films, which will include the spin-orbit field. Section 3 is heavily based on tensor notation, and we will use the conventions for covariant/contravariant/physical tensor components formulated in Section 1.3. The rest of the thesis focuses on the limiting case of a 1D nanowire formed as a portion of a circle. In this case the metric tensor is Cartesian-like and the conventions for covariant/contravariant/physical components may be dropped. In Section 4 we will derive a Riccati parametrized Usadel equation for the 1D nanowire and explore the weak proximity equations with focus on the equivalence with a straight wire with a rotating exchange field. In Section 5 and 6, physical observables like the magnetization and the spin-current will be investigated using a differential equation solver in Matlab. Finally, in Section 7 we will summarize the main results as well as outline a few possible continuations of the work performed in this thesis.

# 2 Quasiclassical theory of superconductor-ferromagnet proximity systems

Most modern treatments of problems in condensed matter physics is based on two classes of methods; functional integral methods and Green's function methods. In the former, functional integrals are used to compute the sum (or integral) over configurations of states the system can be in. In this thesis we will utilize Green's functions, describing correlations between particles. More specifically, we will use the Keldysh Green's functions [35], [36] which in the dirty, quasiclassical limit, follows a 2nd order differential equation known as the Usadel equation.

## 2.1 Keldysh quasiclassical Green's function method

A Green's function $G_{\sigma\sigma'}(\boldsymbol{r},t,\boldsymbol{r}',t')$ is defined as the probability amplitude of a particle with spin $\sigma$ at a position $\boldsymbol{r}$ at a time $t$ appearing at a different position $\boldsymbol{r}'$ at a time $t'$ with spin $\sigma'$. In the formulation of second quantization, this may be expressed mathematically as a expectation value of a time-ordered product of a creation operator $\hat{\psi}$ and an annihilation operator $\hat{\psi}^\dagger$

$$G_{\sigma\sigma'}(\boldsymbol{r},t,\boldsymbol{r}',t') = -i\langle T\hat{\psi}_\sigma(\boldsymbol{r},t)\hat{\psi}^\dagger_{\sigma'}(\boldsymbol{r}',t')\rangle, \tag{2.1}$$

where $\langle ...\rangle$ denotes both a thermal and quantum average and $T$ is the time-ordering operator which orders the product of fermionic operators in chronological order with the largest time to the left [29], [30]. In the Keldysh formalism we introduce a set of Green's functions describing correlations between electrons and holes

$$G^R_{\sigma\sigma'}(\boldsymbol{r},t,\boldsymbol{r}',t') = -i\langle\{\hat{\psi}_\sigma(\boldsymbol{r},t),\hat{\psi}^\dagger_{\sigma'}(\boldsymbol{r}',t')\}\rangle\theta(t-t'), \tag{2.2}$$

$$G^A_{\sigma\sigma'}(\boldsymbol{r},t,\boldsymbol{r}',t') = +i\langle\{\hat{\psi}_\sigma(\boldsymbol{r},t),\hat{\psi}^\dagger_{\sigma'}(\boldsymbol{r}',t')\}\rangle\theta(t'-t), \tag{2.3}$$

$$G^K_{\sigma\sigma'}(\boldsymbol{r},t,\boldsymbol{r}',t') = -i\langle[\hat{\psi}_\sigma(\boldsymbol{r},t),\hat{\psi}^\dagger_{\sigma'}(\boldsymbol{r}',t')]\rangle. \tag{2.4}$$

The retarded Green's function $G^R$ and advanced Green's function $G^A$ describe the propagation of electrons in the positive time direction and holes in the negative time direction respectively. The Keldysh Green's function $G^K$ describes the non-equilibrium properties of the system.

When considering superconductor proximity structures, it is advantageous to introduce a second set of Green's functions called anomalous Green's functions describing correlations between pairs of electrons, Cooper pairs. The anomalous Green's functions are in the Keldysh formalism defined as

$$F^R_{\sigma\sigma'}(\boldsymbol{r},t,\boldsymbol{r}',t') = -i\langle\{\hat{\psi}_\sigma(\boldsymbol{r},t),\hat{\psi}_{\sigma'}(\boldsymbol{r}',t')\}\rangle\theta(t-t'), \tag{2.5}$$

$$F^A_{\sigma\sigma'}(\boldsymbol{r},t,\boldsymbol{r}',t') = +i\langle\{\hat{\psi}_\sigma(\boldsymbol{r},t),\hat{\psi}_{\sigma'}(\boldsymbol{r}',t')\}\rangle\theta(t'-t), \tag{2.6}$$

$$F^K_{\sigma\sigma'}(\boldsymbol{r},t,\boldsymbol{r}',t') = -i\langle[\hat{\psi}_\sigma(\boldsymbol{r},t),\hat{\psi}_{\sigma'}(\boldsymbol{r}',t')]\rangle. \tag{2.7}$$

The Green's functions and anomalous Green's functions may be combined into 4x4 matrix structures in Nambu space [37]

$$\hat{G}^R = \begin{pmatrix} \underline{G}^R & \underline{F}^R \\ (\underline{F}^R)^* & (\underline{G}^R)^* \end{pmatrix}, \tag{2.8}$$

$$\hat{G}^A = \begin{pmatrix} \underline{G}^A & \underline{F}^A \\ (\underline{F}^A)^* & (\underline{G}^A)^* \end{pmatrix}, \tag{2.9}$$

$$\hat{G}^K = \begin{pmatrix} \underline{G}^K & \underline{F}^K \\ -(\underline{F}^K)^* & -(\underline{G}^K)^* \end{pmatrix}, \tag{2.10}$$

where the underlined components of the matrices are 2x2 submatrices containing the four different spin combinations of $\sigma\sigma' = \uparrow\uparrow, \uparrow\downarrow, \downarrow\uparrow, \downarrow\downarrow$ of the corresponding Green's function.

Finally, the three 4x4 matrices may be combined into a single 8x8 matrix in Keldysh space

$$\check{G} = \begin{pmatrix} \hat{G}^A & \hat{G}^K \\ 0 & \hat{G}^R \end{pmatrix}. \tag{2.11}$$

The beauty of the Keldysh formalism is that almost all physical observables may be expressed in terms of the components of the Green's function matrix in Keldysh space.

In thermal equilibrium, the three non-zero components of the Green's function matrix in Keldysh space are related to each other [38]

$$\hat{G}^A = -\hat{\tau}_z(\hat{G}^R)^\dagger\hat{\tau}_z, \tag{2.12}$$

$$\hat{G}^K = (\hat{G}^R - \hat{G}^A)\tanh(\frac{\beta\epsilon}{2}), \tag{2.13}$$

meaning that only one component of the Green's function matrix in Keldysh space is needed to determine the complete 8x8 matrix.

The Green's functions vary rapidly in terms of the relative coordinate $\boldsymbol{r} - \boldsymbol{r}'$, making the current form of the Green's function strenuous to work with in practice. In order to simplify, we will introduce a set of approximations, particularly useful for superconducting systems, known as the *quasiclassical approximation* [29], [30], [39]. The quasiclassical approximation is based on two main assumptions:

1. Rapid internal oscillations in the Green's function may be averaged over.
2. All momenta may be replaced by its value on the Fermi surface $\boldsymbol{p}_F$.

The validity of the assumptions are quite easy to see when considering superconductor proximity systems. Firstly, The superconducting coherence length is much larger than the typical inverse Fermi wave vector $\boldsymbol{k}_F^{-1}$, and the Green's function will act as a wavepacket varying slowly compared to $\boldsymbol{k}_F^{-1}$ with rapid internal oscillation [3]. Since we are interested in longer length scales like the superconducting coherence length and the length of the material, an average over

the internal oscillations in terms of the relative coordinate $\boldsymbol{r} - \boldsymbol{r}'$ is acceptable. This approximation is in the literature known as the gradient approximation. In order to get rid of the internal coordinates we do a Fourier transform of the relative coordinate and time, resulting in the Fourier transformed Green's function $\check{\mathcal{G}}(\boldsymbol{R}, T, \boldsymbol{p}, \epsilon)$ in terms of the center of mass coordinate and time $\boldsymbol{R}, T$, momentum $\boldsymbol{p}$ and energy $\epsilon$.

At ambient pressure, superconductivity is a low temperature phenomena. At temperatures where the superconducting phase is reached, all low energy states in the system will be filled, while all high energy states will be empty and no thermal excitation will be present. Consequently, all physics has to take place around the Fermi level justifying the replacement of all momenta with its value at the Fermi surface.

The quasiclassical Green's function denoted by $\check{g}$ depends only on the direction of the momentum and not its magnitude

$$\check{\mathcal{G}}(\boldsymbol{R}, T, \boldsymbol{p}, \epsilon) = -i\pi\delta(\xi_p)\check{g}(\boldsymbol{R}, T, \hat{\boldsymbol{p}}_F, \epsilon), \tag{2.14}$$

where $\xi_p = \frac{\boldsymbol{p}^2}{2m} - \mu$ is the kinetic energy relative to the Fermi level $\mu$ and $i\pi$ is a normalization factor. The delta function in equation (2.14) confines the Green's function to the Fermi surface. Equation (2.14) may be rewritten as an integral over the Fourier transformed Green's function

$$\check{g}(\boldsymbol{R}, T, \hat{\boldsymbol{p}}_F, \epsilon) = \frac{i}{\pi}\int_{-\xi_c}^{\xi_c} d\xi_p \check{\mathcal{G}}(\boldsymbol{R}, T, \boldsymbol{p}, \epsilon), \tag{2.15}$$

where we have introduced some cut-off energy $\xi_c$ in order to avoid the complicated behaviour of the Green's function at high energies. Similarly to equation 2.11, the quasiclassical Green's function may be expressed in matrix form as

$$\check{g} = \begin{pmatrix} \hat{g}^A & \hat{g}^K \\ 0 & \hat{g}^R \end{pmatrix}, \tag{2.16}$$

where $\hat{g}^R$, $\hat{g}^A$ and $\hat{g}^K$ are the retarded, advanced and Keldysh quasiclassical Green's functions respectively in Nambu space

$$\hat{g}^R = \begin{pmatrix} \underline{g}^R & \underline{f}^R \\ -\underline{\tilde{f}}^R & -\underline{\tilde{g}}^R \end{pmatrix}, \tag{2.17}$$

$$\hat{g}^A = \begin{pmatrix} \underline{g}^A & \underline{f}^A \\ -\underline{\tilde{f}}^A & -\underline{\tilde{g}}^A \end{pmatrix}, \tag{2.18}$$

$$\hat{g}^K = \begin{pmatrix} \underline{g}^K & \underline{f}^K \\ \underline{\tilde{f}}^K & \underline{\tilde{g}}^K \end{pmatrix}. \tag{2.19}$$

Due to the imaginary unit in equation (2.15) we have introduced a tilde conjugation, having the function of normal conjugation combined with a sign shift in the energy, $\tilde{g}(\epsilon) = g(-\epsilon)^*$.

The quasiclassical Green's functions are normalized

$$\check{g}^2 = \check{\tau}_0, \tag{2.20}$$

which may be written in terms of the retarded, advanced and Keldysh components in Nambu space

$$\hat{g}^R\hat{g}^R = \hat{\tau}_0, \qquad \hat{g}^A\hat{g}^A = \hat{\tau}_0, \qquad \hat{g}^R\hat{g}^K + \hat{g}^K\hat{g}^A = 0. \tag{2.21}$$

## 2.2 Diffusion equation

For systems of materials with a high density of non-magnetic impurities, particles will scatter to a degree where the particle momentum is ultimately left randomized. This is in the literature known as the dirty or diffusive limit. For superconductor proximity systems, the diffusive limit may be expressed mathematically as $\xi >> l$, where $\xi$ is the superconducting coherence length and $l$ is the mean free path length. The randomization of the momentum direction suggests an expansion of the quasiclassical Green's function to one isotropic part $\check{g}_s$ and one small anisotropic part $\check{g}_p$ in momentum space

$$\check{g} = \check{g}_s + \hat{\boldsymbol{p}}_F \cdot \check{g}_p. \tag{2.22}$$

$\check{g}_p$ is considered to be so small that we may neglect terms of order $\mathcal{O}(\check{g}_p^2)$.

Diffusive quasiclassical proximity systems are described by a second order differential equation in the isotropic quasiclassical Green's function, called the Usadel equation [10], [29], [30], [36], [40]

$$iD_F\nabla(\check{g}_s\nabla\check{g}_s) = [\epsilon\hat{\tau}_z - \check{\Sigma}, \check{g}_s], \tag{2.23}$$

where $D_F$ is a material-dependent constant known as the diffusion constant and $\check{\Sigma}$ is the quasiclassical self energy, the part of the particle's energy due to interactions with its surroundings. Which types of self energies that are included in the Usadel equation depends on the physical system under consideration. For a proximity systems of only s-wave conventional superconductor and weakly polarized ferromagnet components, it is sufficient to include the self energy terms given in equations (1.2) and (1.3)[3]. Hence, the Usadel equation for superconductor-ferromagnet proximity systems takes the form

$$iD_F\nabla(\check{g}_s\nabla\check{g}_s) = [\epsilon\hat{\tau}_z - \hat{\Delta} - \boldsymbol{h}\cdot\hat{\boldsymbol{\sigma}}, \check{g}_s]. \tag{2.24}$$

In order to get a unique solution from the Usadel equation we need to introduce a set of boundary conditions. In the early 80s, Zaitsev worked out a general expression for the boundary condition at the interface between two metals for an arbitrary boundary transparency valid in both the clean and dirty limit [42]. In this thesis we will rather use a set of boundary conditions known

[3]Actually, in the diffusive limit a impurity self energy term should be included, but as it turns out this term will commute with the quasiclassical Green's function and will hence drop out of the Usadel equation [36], [41].

as the Kuprianov-Lukichev boundary conditions, whose validity only extends to the dirty limit and for weak transmission regime, but in return are quite simple [43]. The Kuprianov-Lukichev boundary conditions are given by

$$\hat{g}^R_{s,a}\nabla\hat{g}^R_{s,a} = \frac{1}{2L_a\zeta_a}[\hat{g}^R_{s,1}, \hat{g}^R_{s,2}], \tag{2.25}$$

where the label $a$ denotes the material $a$, $L_a$ is the length of material $a$ and $\zeta_a = \frac{R_B}{R_a}$ is the ratio between the barrier resistance, $R_B$ and the bulk resistance in material $a$, $R_a$. The boundary condition to vacuum may be considered as a infinite barrier resistance described by the limit $\frac{1}{\zeta_a} \to 0$ in equation (2.25). In more recent years, development of more accurate boundary conditions for spin-active interfaces have been performed and may be included in the theory [44].

# 3 Diffusion equation for curved superconductor-ferromagnet proximity structures

## 3.1 Curvilinear coordinates

For systems displaying a curved symmetry, changing from a Cartesian coordinate system to a curvilinear coordinate system is beneficial. Curvilinear coordinate systems are characterized by the fact that coordinate lines may be curved. Examples of such coordinate systems includes cylindrical and spherical coordinates.

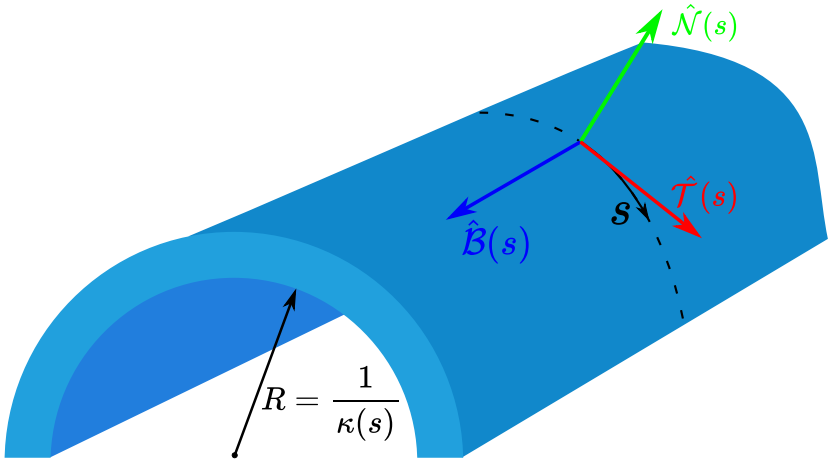


Figure 5: The curvilinear coordinate system is described by the arclength $s$ measured from some reference point and a local set of orthogonal unit vectors $\hat{\boldsymbol{\mathcal{N}}}(s)$, $\hat{\boldsymbol{\mathcal{T}}}(s)$ and $\hat{\boldsymbol{\mathcal{B}}}(s)$, normal, tangential and binormal to the curved nanostructure respectively. $R = \frac{1}{\kappa(s)}$, where $\kappa(s)$ is the curvature, is the curvature radius at the arclength point $s$.

For our purposes it is convenient to introduce a general orthogonal curvilinear coordinate system defined on the curved nanostructure as shown in Figure 5, where any point on the curved surface has a set of orthogonal basis vectors $\hat{\boldsymbol{\mathcal{N}}}(s)$, $\hat{\boldsymbol{\mathcal{T}}}(s)$ and $\hat{\boldsymbol{\mathcal{B}}}(s)$ in the normal, tangential and binormal directions respectively and a local curvature $\kappa(s)$. The benefit of this approach rather than e.g. cylindrical coordinates is the generality of the curved system it offers, allowing for investigation of arbitrarily curved three-dimensional structures. Consider a 3D-nanostructure curved only in a 2D-plane i.e. no torsion[4] is considered[5] like in the curved structure in Figure 5. Assuming that the nanostructure in the plane of curvature follows a differentiable curve, we can parametrize the

[4] Torsion signifies that the binormal unit vector depends on the arclength $s$.
[5] A similar derivation including torsion has been performed by Ortix [45]

stress-free surface in terms of the arclength and the binormal coordinate $b$, $\boldsymbol{r}(s,b) = \boldsymbol{\xi}(s) + b\hat{\boldsymbol{\mathcal{B}}}(s)$. Here we have defined the arclength parametrization of the differentiable curve in the plane of curvature, $\boldsymbol{\xi}(s)$. The three-dimensional space in the vicinity of the stress free surface $\boldsymbol{R}$, can be parametrized similarly using the normal unit vector and corresponding coordinate

$$\boldsymbol{R}(s,n,b) = \boldsymbol{r}(s,b) + n\hat{\boldsymbol{\mathcal{N}}}(s), \tag{3.1}$$

where $n$ is the curvilinear coordinate in the normal direction.

The normal, tangential and binormal unit vectors are connected through the torsion free Frenet-Serret formulas [46], [47], [48]

$$\frac{d}{ds}\hat{\boldsymbol{\mathcal{N}}}(s) = -\kappa(s)\hat{\boldsymbol{\mathcal{T}}}(s), \tag{3.2}$$

$$\frac{d}{ds}\hat{\boldsymbol{\mathcal{T}}}(s) = \kappa(s)\hat{\boldsymbol{\mathcal{N}}}(s), \tag{3.3}$$

$$\frac{d}{ds}\hat{\boldsymbol{\mathcal{B}}}(s) = 0, \tag{3.4}$$

where $\kappa(s)$ is the local curvature at the point $s$. Using equation (3.4) we can define the derivatives of the parametrized space in equation (3.1)

$$\partial_s \boldsymbol{R}(s,n,b) = (1-\kappa(s)n)\hat{\boldsymbol{\mathcal{T}}}(s), \tag{3.5}$$

$$\partial_n \boldsymbol{R}(s,n,b) = \hat{\boldsymbol{\mathcal{N}}}(s), \tag{3.6}$$

$$\partial_b \boldsymbol{R}(s,n,b) = \hat{\boldsymbol{\mathcal{B}}}(s), \tag{3.7}$$

where we have used the relation between the arclength parametrization in the plane of curvature and the tangential unit vector, $\partial_s\boldsymbol{\xi}(s) = \hat{\boldsymbol{\mathcal{T}}}(s)$. The total differential change of $\boldsymbol{R}$ can be written as

$$d\boldsymbol{R}(s,n,b) = (1-\kappa(s)n)ds\hat{\boldsymbol{\mathcal{T}}}(s) + dn\hat{\boldsymbol{\mathcal{N}}}(s) + db\hat{\boldsymbol{\mathcal{B}}}(s) = \sum_i h_{(i)}dq^i\hat{\boldsymbol{e}}_{(i)}(s), \tag{3.8}$$

$q^i$ are the curvilinear cordinates, $\hat{\boldsymbol{e}}_{(i)}(s)$ are the curvilinear unit vectors and we have introduced the scale factors in curvilinear coordinates

$$h_{(T)} = 1-\kappa(s)n, \qquad h_{(N)} = 1, \qquad h_{(B)} = 1. \tag{3.9}$$

As discussed in Section 1.3, the square of the total differential coordinate displacement may be expressed in terms of the metric tensor. Taking the square of the total differential change in $\boldsymbol{R}$ given in equation (3.8) gives

$$(dR(s,n,b))^2 = \sum_{i,j} h_{(i)}h_{(j)}\hat{\boldsymbol{e}}_{(i)}\cdot\hat{\boldsymbol{e}}_{(j)}dq^i dq^j = \eta_{ij}dq^i dq^j, \tag{3.10}$$

where we have adopted the Einstein convention in the last equality and introduced the metric tensor which may be written in terms of the scale factors as $\eta_{ij} = h_{(i)}h_{(j)}\delta_{ij}$ for orthogonal coordinate systems. Using the expression for

the scale factors given in equation (3.9), the metric tensor for our curvilinear coordinate system takes the simple diagonal matrix form

$$\eta_{ij} = \begin{pmatrix} H(s,n)^2 & 0 & 0 \\ 0 & 1 & 0 \\ 0 & 0 & 1 \end{pmatrix}, \tag{3.11}$$

where we have defined the curvature dependent scale factor

$$H(s,n) = 1 - \kappa(s)n, \tag{3.12}$$

which depends on both the arclength coordinate $s$ and the normal coordinate $n$. Later, we will show that the curvature dependent scale factor appears in e.g. the gradient operator. Hence, additional curvature-dependent terms will appear in equations including derivatives like the Usadel equation.

In order to take covariant derivatives, we need to find the Christoffel symbols. The Christoffel symbols are related to the metric tensor through the equation

$$\Gamma^k_{ij} = \frac{1}{2}\eta^{kk}(\partial_j \eta_{ki} + \partial_i \eta_{kj} - \partial_k \eta_{ij}), \tag{3.13}$$

where we have set $l = k$ compared to equation (1.21) since the curvilinear metric is diagonal. Since there is only one non-constant component of the curvilinear metric tensor, the Christoffel symbols are few and rather simple to compute. The only four non-zero components of the Christoffel symbols for a curvilinear coordinate system are

$$\begin{aligned} \Gamma^s_{ss} &= \frac{1}{H(s,n)}\partial_s H(s,n), \\ \Gamma^n_{ss} &= -H(s,n)\partial_n H(s,n), \\ \Gamma^s_{ns} &= \Gamma^s_{sn} = \frac{1}{H(s,n)}\partial_n H(s,n). \end{aligned} \tag{3.14}$$

## 3.2 Spin-orbit coupling as a result of curvature

When an electron travels with a velocity $\boldsymbol{v}$ in an electric field $\boldsymbol{E}$, the electron in its rest frame will experience a magnetic field $\boldsymbol{B} = -\boldsymbol{v} \times \boldsymbol{E}$. The electrons magnetic moment $\mu_e$ couples to the magnetic field through the Zeeman interaction with the Hamiltonian

$$H_{SO} = -\mu_e \cdot \boldsymbol{B} = \frac{eg}{2m} \boldsymbol{S} \cdot (\boldsymbol{v} \times \boldsymbol{E}), \tag{3.15}$$

where $\boldsymbol{S}$ is the spin-vector and $g$ is the g-factor, approximately equal to 2 for an electron. The Hamiltonian can be rewritten in terms of the electron momentum $\boldsymbol{p}$ and the Pauli spin matrix vector $\boldsymbol{\sigma} = 2\boldsymbol{S}$

$$H_{SO} = \frac{eg}{4m^2} \boldsymbol{\sigma} \cdot (\boldsymbol{p} \times \boldsymbol{E}). \tag{3.16}$$

The Hamiltonian in equation (3.16) manifests a coupling between the electron momentum and the spin mediated by the electric field. This coupling is known as spin-orbit coupling. Assuming the electric field is in the z-direction the Hamiltonian takes the following form

$$H_{RSO} = \frac{\alpha}{m} (\underline{\sigma}_x p_y - \underline{\sigma}_y p_x), \tag{3.17}$$

where $\alpha = \frac{egE}{4m}$. This is known as Rashba spin-orbit coupling and arises due to the lack of surface inversion symmetry due to the electric field [49]. $\alpha$ is the Rashba coefficient and describes the strength of the spin-orbit interaction. Structures with bulk inversion symmetry exhibit a different type of spin-orbit coupling known as Dresselhaus spin-orbit coupling [50].

Now, consider a piece of a cross section of a curved nanostructure as shown in Figure 6. The deformation due to the curvature of the structure results in a variable strain, which is tensile for $n > 0$ and compressive for $n < 0$. The strain along the bent direction is defined as

$$\epsilon_{ss} = \frac{L(n) - L_0}{L_0}, \tag{3.18}$$

where $L(n)$ is the length of the bent material at a length $n$ from the center and $L_0 = L(0)$ is the length of the material before bending. The strain can be expressed with the curvature $\kappa(s) = \frac{1}{R}$ as

$$\epsilon_{ss} = \frac{(R+n)\theta - R\theta}{R\theta} = \kappa(s) n. \tag{3.19}$$

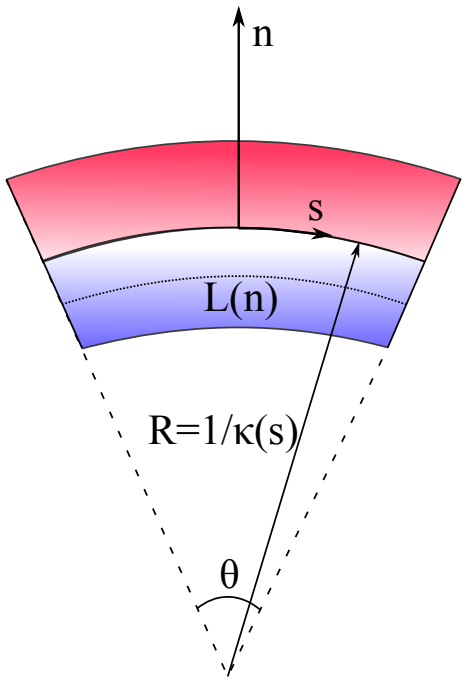


Figure 6: A piece of the cross section of a curved nanostructure where $n$ is the normal coordinate and $s$ is the arc length parameter. The red region ($n > 0$) is under tensile strain due to the curvature, while the blue region ($n < 0$) is under compressive strain. $R = 1/\kappa(s)$ is the curvature radius and $\theta$ is the curvature angle of the section. $L(n)$ is the length of the section at $n$ indicated by the dotted line.

The inhomogeneous strain along the curve results in a shift in the band energies [51], [52]. In the framework of deformation potential theory, the shift in the band energies may be treated as a varying potential which for small values of the strain are linear in strain [53]

$$V(s,n) = \lambda \epsilon_{ss}(s,n) = \lambda \kappa(s) n, \tag{3.20}$$

where $\lambda$ is a characteristic energy scale which for semiconductors is of the order of 1eV. The potential is attractive in the tensile region ($n > 0$) and repulsive in the compressive region ($n < 0$). From classical electrostatics we know that a varying potential yields an electric field $\boldsymbol{E} = -\frac{1}{e}\nabla V$. Using the gradient in curvilinear coordinates given in equation (A.6) the electric field induced by the deformation potential in equation (3.20) is

$$\boldsymbol{E}(s,n) = -\frac{\lambda n}{eH(s,n)}\partial_s(\kappa(s))\hat{\boldsymbol{\mathcal{T}}}(s) - \frac{\lambda\kappa(s)}{e}\hat{\boldsymbol{\mathcal{N}}}(s). \tag{3.21}$$

Averaging over the normal coordinate yields the average electric field at the

arclength point $s$

$$\langle \boldsymbol{E} \rangle_N(s) = -\frac{\lambda \kappa(s)}{e} \hat{\boldsymbol{\mathcal{N}}}(s), \tag{3.22}$$

where $\langle ... \rangle_N$ denotes an average over the normal coordinate $n$ and we have used the curvilinear Jacobian given in equation (A.13) in the integration over $n$. Consequently, the curvature induces an electric field in the normal direction proportional to the curvature. As previously discussed, an electric field can generate Rashba type spin-orbit coupling. Hence, using equation (3.16) the spin-orbit Hamiltonian for the curved nanostructure is

$$H_{SO} = -\frac{\alpha_N}{m} \boldsymbol{\sigma} \cdot (\boldsymbol{p} \times \hat{\boldsymbol{\mathcal{N}}}(s)), \tag{3.23}$$

where $\alpha_N = \frac{g\lambda\kappa(s)}{4m}$ is the Rashba coefficient determining the strength of the curvature-induced spin-orbit coupling. The Rashba coefficient $\alpha$ being proportional to the curvature $\kappa(s)$, provides a direct control over the spin-orbit strength by bending the structure. Since the spin-orbit coupling dictates the spin transport properties of the system, a controllable spin-orbit strength offers tantalizing possibilities for superconducting spintronic devices like the curvature-induced spin-orbit-tunable triplet spin-valve discussed in Section 1.1.

Consider a general 3-dimensional curved nanostructure. As explained earlier, the curvature in a curved nanostructure gives rise to spin-orbit coupling in the direction normal to the wire. In addition, curved nanowires may have a second, intrinsic, spin-orbit term independent of the curvature [15], [54] due to asymmetric confinement in the binormal direction. In general, we may introduce a spin-orbit vector whose components represents the spin-orbit strength due to the asymmetric confinement in the different curvilinear directions $\boldsymbol{\alpha} = \alpha_T \hat{\boldsymbol{\mathcal{T}}}(s) + \alpha_N \hat{\boldsymbol{\mathcal{N}}}(s) + \alpha_B \hat{\boldsymbol{\mathcal{B}}}(s)$ [45]. The magnitude of the spin-orbit vector determines the strength of the spin-orbit interaction, while the direction of the spin-orbit vector defines the spin-orbit axis. The Hamiltonian, neglecting potentials, of the system may be written as

$$\hat{H} = \frac{\boldsymbol{p}^2}{2m} - \frac{\boldsymbol{\alpha}}{2m} \cdot \boldsymbol{\sigma} \times \boldsymbol{p}, \tag{3.24}$$

In order to rewrite equation (3.24) to a general covariant equation we replace $\boldsymbol{p} = -i\nabla$ with coordinate covariant derivatives and rewrite the cross product in covariant form

$$\hat{H} = -\frac{1}{2m} \eta^{ij} \mathcal{D}_i \mathcal{D}_j + \frac{i}{2m} \alpha_i \mathcal{E}^{ijk} \underline{\sigma}_j \partial_k. \tag{3.25}$$

The ordinary Levi-Cevita symbol $\epsilon^{ijk}$ is not a tensor, hence to keep equations in tensorial form, we have introduced the contravariant Levi-Cevita tensor $\mathcal{E}^{ijk} = \frac{1}{\sqrt{\eta}} \epsilon^{ijk}$, where $\sqrt{\eta}$ is defined as the square root of the determinant of the metric tensor $\eta_{ij}$. The form of the last term in equation (3.25), suggests the introduction of a spin-orbit field $\boldsymbol{A}$, with a vector structure in coordinate space and a matrix structure in spin space. As a means to keep equations in covariant form, we define the contravariant spin-orbit field $\underline{A}^k = \alpha_i \mathcal{E}^{ijk} \underline{\sigma}_j$ which relates

to the components of the physical spin-orbit field through equation (1.24). The Hamiltonian may be written in terms of the contravariant spin-orbit field

$$\hat{H} = -\frac{1}{2m}\eta^{ij}\mathcal{D}_i\mathcal{D}_j + \frac{i}{2m}\underline{A}^k\partial_k. \tag{3.26}$$

Relabeling the k-index and lowering the index of the spin-orbit field by contracting with the metric tensor yields

$$\hat{H} = -\frac{1}{2m}\eta^{ij}(\mathcal{D}_i\mathcal{D}_j - i\underline{A}_i\mathcal{D}_j). \tag{3.27}$$

In equation (3.27) we have replaced the regular derivative contracted with the spin-orbit field with a covariant derivative. Since the Hamiltonian acts on a scalar wavefunction the regular and covariant derivatives are equivalent. Assuming that the spin-orbit strength is weak, i.e. the physical components components $|\underline{A}_{(i)}| \ll 1$, equation (3.27) may be expressed in the form of a charged particle moving in a magnetic field

$$\hat{H} = -\frac{1}{2m}\eta^{ij}(\mathcal{D}_i - i\underline{A}_i)^2, \tag{3.28}$$

where $\underline{A}_i$ acts as a background SU(2) gauge field [55], [56]. To ensure the correct transformation properties under local SU(2) rotations, coordinate covariant derivatives should be replaced with coordinate-gauge covariant derivatives $\mathcal{D}_i\cdot \rightarrow \tilde{\mathcal{D}}_i\cdot = \mathcal{D}_i - i[\underline{A}_i, \cdot]$ in all relevant equations [57]. The coordinate-gauge covariant derivative of a covariant vector $v_j$ is defined as

$$\tilde{\mathcal{D}}_i v_j = \partial_i v_j - \Gamma^k_{ij}v_k - i[\underline{A}_i, v_j]. \tag{3.29}$$

Just as the Cristoffel symbols ensures the coordinate covariance, the commutator with the spin-orbit field ensures gauge covariance. Hence, the name coordinate-gauge covariant derivative is chosen.

Recall our definition of the contravariant spin-orbit field

$$\underline{A}^k = \alpha_i\boldsymbol{\mathcal{E}}^{ijk}\underline{\sigma}_j = \frac{1}{\sqrt{\eta}}\alpha_i\epsilon^{ijk}\underline{\sigma}_j. \tag{3.30}$$

The specific form of the contravariant spin-orbit field in curvilinear coordinates may be found by inserting the determinant of the metric tensor which may easily be calculated from equation (3.11). By explicitly performing the Einstein summation using curvilinear coordinates in (3.30) the covariant components of the spin-orbit field may be expressed as

$$\begin{aligned}
\underline{A}_T &= H(s,n)(\alpha_{(N)}\underline{\sigma}_{(B)} - \alpha_{(B)}\underline{\sigma}_{(N)}),\\
\underline{A}_N &= (\alpha_{(B)}\underline{\sigma}_{(T)} - \alpha_{(T)}\underline{\sigma}_{(B)}),\\
\underline{A}_B &= (\alpha_{(T)}\underline{\sigma}_{(N)} - \alpha_{(N)}\underline{\sigma}_{(T)}),
\end{aligned} \tag{3.31}$$

where we have defined a local set of physical curvilinear Pauli matrices $\underline{\sigma}_{(T),(N),(B)}(s) = \boldsymbol{\sigma}\cdot\{\hat{\boldsymbol{\mathcal{T}}}(s), \hat{\boldsymbol{\mathcal{N}}}(s), \hat{\boldsymbol{\mathcal{B}}}(s)\}$ following the curved nanostructure and

$\alpha_{(T),(N),(B)}$ are the physical components of the curvilinear spin-orbit vector. By using the relation between the covariant and physical components of a vector in equation (1.25), the physical spin-orbit field in the curvilinear basis is

$$\begin{aligned}\boldsymbol{A} = &(\alpha_{(N)}\underline{\sigma}_{(B)} - \alpha_{(B)}\underline{\sigma}_{(N)})\hat{\boldsymbol{\mathcal{T}}}(s) + (\alpha_{(B)}\underline{\sigma}_{(T)} - \alpha_{(T)}\underline{\sigma}_{(B)})\hat{\boldsymbol{\mathcal{N}}}(s) \\ &+ (\alpha_{(T)}\underline{\sigma}_{(N)} - \alpha_{(N)}\underline{\sigma}_{(T)})\hat{\boldsymbol{\mathcal{B}}}(s).\end{aligned} \tag{3.32}$$

A limiting case, which will be discussed in great detail later, is the one-dimensional nanowire curved as a portion of a circle. The example of a 1D circular arc is particularly simple since the curvature is a constant and the infinitesimally thin wire allows for the assumption that the degrees of freedom in both the normal and binormal direction may be neglected. If so, the curvature function $H(s,n) = 1$ and the metric tensor reduces to the Cartesian metric tensor. In the 1D case the curvature gives rise to spin-orbit coupling in the direction normal to the wire and the asymmetric confinement in the binormal direction gives rise to a second, intrinsic, spin-orbit term independent of the curvature. If we consider no spin-orbit coupling along the wire, the spin-orbit field reduces to

$$\boldsymbol{A} = (\alpha_N\underline{\sigma}_B - \alpha_B\underline{\sigma}_N)\hat{\boldsymbol{\mathcal{T}}}(s), \tag{3.33}$$

where the notation for physical components may be dropped since for a Cartesian-like metric tensor there is no distinction between the covariant, contravariant and physical vector components. Due to the metric being a diagonal matrix of constants, coordinate covariant derivatives are equivalent to regular partial derivatives. Hence for a 1D nanowire arc we should replace all derivatives with gauge covariant derivatives[6], rather than the coordinate-gauge covariant derivative

$$\partial_i \cdot \to \tilde{\partial}_i \cdot = \partial_i \cdot - i[\underline{A}_i, \cdot], \tag{3.34}$$

similarly to the case for non-curved nanostructures [10]. The major difference in the case of a curved compared to a straight nanowire is the fact that the spin-orbit field for a curved nanowire in equation (3.33) depends on the position along the wire[7]. Hence second-order derivatives, like in the Usadel-equation, will produce additional terms proportional to the derivative of the spin-orbit field.

[6] Gauge covariant derivatives of a vector may be found by setting $\Gamma^k_{ij} = 0$ in equation (3.29)

[7] More precisely, the position dependence of the spin-orbit field lies in the curvilinear Pauli matrices which follows a Frenet-Serret type equation.

## 3.3 Usadel equation in curvilinear coordinates

The Usadel equation given in equation (2.24) may be written in covariant form by replacing derivatives with coordinate covariant derivatives and writing the scalar product using tensor notation

$$iD_F\eta^{ij}\mathcal{D}_i(\check{g}\mathcal{D}_j\check{g}) = [\epsilon\hat{\tau}_z - \hat{\Delta} - \eta^{ij}h_i\hat{\sigma}_j, \check{g}]. \tag{3.35}$$

The scalar quantities, like the energy $\epsilon$ and the order parameter $\hat{\Delta}$, are invariant and hence remain the same compared to equation (2.24). In order to include spin-orbit coupling we should replace the coordinate covariant derivatives with coordinate-gauge covariant derivatives given in equation (3.29)

$$iD_F\eta^{ij}\tilde{\mathcal{D}}_i(\check{g}\tilde{\mathcal{D}}_j\check{g}) = [\epsilon\hat{\tau}_z - \hat{\Delta} - \eta^{ij}h_i\hat{\sigma}_j, \check{g}], \tag{3.36}$$

where $\tilde{\mathcal{D}}_i v_j = \partial_i v_j - \Gamma^k_{ij}v_k - i[\hat{A}_i, v_j]$ and $\hat{A}_i = (\underline{A}_i, -\underline{A}_i^*)$ is the covariant spin-orbit field in Nambu space. Using the definition of the coordinate-gauge covariant derivative, the left-hand side of the Usadel equation may be written explicitly in terms of the covariant spin-orbit field and Cristoffel symbols

$$\begin{aligned} iD_F\eta^{ij}\tilde{\mathcal{D}}_i(\check{g}\tilde{\mathcal{D}}_j\check{g}) = iD_F\eta^{ij}\{&\partial_i(\check{g}\partial_j\check{g}) - \Gamma^k_{ij}(\check{g}\partial_k\check{g}) - i[\hat{A}_i, \check{g}\partial_j\check{g}] \\ &- i\partial_i(\check{g}[\hat{A}_j, \check{g}]) + i\Gamma^k_{ij}\check{g}[\hat{A}_k, \check{g}] - [\hat{A}_i, \check{g}[\hat{A}_j, \check{g}]]\}. \end{aligned} \tag{3.37}$$

In section 3.1 we derived the metric tensor (3.11) and Cristoffel symbols (3.14) for a curvilinear coordinate system. Since the Cristoffel symbols in equation (3.37) are contracted with a diagonal metric tensor, the only non-zero Cristoffel symbols will be the ones with equal lower indices

$$\Gamma^s_{ss} = \frac{1}{H(s,n)}\partial_s H(s,n), \qquad \Gamma^n_{ss} = -H(s,n)\partial_n H(s,n). \tag{3.38}$$

Inserting the Christoffel symbols into equation (3.37) the spin-orbit independent part of the equation may be expanded in curvilinear coordinates as

$$\begin{aligned} \eta^{ij}\{\partial_i(\hat{g}\partial_j\hat{g}) - \Gamma^k_{ij}(\hat{g}\partial_k\hat{g})\} = &\frac{1}{H(s,n)}\partial_s\left(\frac{1}{H(s,n)}\check{g}\partial_s\check{g}\right) \\ &+ \frac{1}{H(s,n)}\partial_n(H(s,n)\check{g}\partial_n\check{g}) + \partial_b(\check{g}\partial_b\check{g}). \end{aligned} \tag{3.39}$$

The term in equation (3.37) involving the coordinate covariant derivative of the spin-orbit field may be expanded in curvilinear coordinates in terms of the physical components of the spin-orbit field in the curvilinear basis

$$\begin{aligned} &\eta^{ij}\{-i\partial_i(\hat{g}[\hat{A}_j, \hat{g}]) + i\Gamma^k_{ij}\hat{g}[\hat{A}_k, \hat{g}]\} \\ &= \frac{1}{H(s,n)}\partial_s(i\hat{A}_{(T)} - \hat{g}i\hat{A}_{(T)}\hat{g}) + \frac{1}{H(s,n)}\partial_n[H(s,n)(i\hat{A}_{(N)} - \hat{g}i\hat{A}_{(N)}\hat{g})] \\ &+ \partial_b(i\hat{A}_{(B)} - \hat{g}i\hat{A}_{(B)}\hat{g}), \end{aligned} \tag{3.40}$$

where we have used the normalization condition for the quasiclassical Green's function given in (2.21). The final terms involving the spin-orbit field in equation (3.37) may be combined and expanded in curvilinear coordinates

$$\begin{aligned}
&\eta^{ij}\{-i[\hat{A}_i,\hat{g}\partial_j\hat{g}]-[\hat{A}_i,\hat{g}[\hat{A}_j,\hat{g}]]\}\\
&=-[i\hat{A}_{(T)},\hat{g}(\frac{1}{H(s,n)}\partial_s-i\hat{A}_{(T)})\hat{g}+i\hat{A}_{(T)}]\\
&-[i\hat{A}_{(N)},\hat{g}(\partial_n-i\hat{A}_{(N)})\hat{g}+i\hat{A}_{(N)}]\\
&-[i\hat{A}_{(B)},\hat{g}(\partial_b-i\hat{A}_{(B)})\hat{g}+i\hat{A}_{(B)}].
\end{aligned} \tag{3.41}$$

Combining the curvilinear expansions of the different terms in the left hand side of the Usadel equation given in equations (3.39)-(3.41) the full curvilinear Usadel equation including spin-orbit coupling may be expressed as

$$\begin{aligned}
&iD_F[\tilde{\nabla}_s(\hat{g}\tilde{\nabla}_s\hat{g})+\frac{1}{H(s,n)}\tilde{\nabla}_n(H(s,n)\hat{g}\tilde{\nabla}_n\hat{g})+\tilde{\nabla}_b(\hat{g}\tilde{\nabla}_b\hat{g})]\\
&=[\epsilon\hat{\tau}_z-\hat{\Delta}-h_{(T)}\hat{\sigma}_{(T)}-h_{(N)}\hat{\sigma}_{(N)}-h_{(B)}\hat{\sigma}_{(B)},\check{g}],
\end{aligned} \tag{3.42}$$

where we have defined the gauge covariant derivative in terms of the physical components of the spin-orbit field $\tilde{\nabla}_i\cdot=\nabla_i\cdot-i[\hat{A}_{(i)},\cdot]$ where $\nabla_i$ is the component of the curvilinear gradient $\nabla=(\frac{1}{H(s,n)}\partial_s,\partial_n,\partial_b)$ in the $i$-direction, $\hat{A}_{(i)}=(\underline{A}_i,-\underline{A}_i^*)$ and $\underline{A}_i$ is the $i$-th physical component of the spin-orbit field

$$\boldsymbol{A}=(\alpha_{(N)}\underline{\sigma}_{(B)}-\alpha_{(B)}\underline{\sigma}_{(N)},\alpha_{(B)}\underline{\sigma}_{(T)}-\alpha_{(T)}\underline{\sigma}_{(B)},\alpha_{(T)}\underline{\sigma}_{(N)}-\alpha_{(N)}\underline{\sigma}_{(T)}). \tag{3.43}$$

On the right hand side of equation (3.42) we have defined the physical curvilinear components of the exchange field vector, which is related to the Cartesian components $h_{(T),(N),(B)}=\boldsymbol{h}(x,y,z)\cdot\{\hat{\boldsymbol{\mathcal{T}}}(s),\hat{\boldsymbol{\mathcal{N}}}(s),\hat{\boldsymbol{\mathcal{B}}}(s)\}$. $\underline{\sigma}_{(T),(N),(B)}$ are the local physical curvilinear Pauli matrices defined in a similar manner.

In addition to the spin-orbit field, the introduction of curvature induces additional terms to the Usadel equation through the curvature dependent scale factor $H(s,n)$. Take for example the normal derivative term in equation (3.42). By inserting the curvature dependent scale factor given in equation (3.12) we may write the normal derivative term as

$$\frac{1}{H(s,n)}\tilde{\nabla}_n(H(s,n)\hat{g}\tilde{\nabla}_n\hat{g})=\left(\tilde{\nabla}_n+\frac{1}{1-\frac{n}{\kappa(s)}}\right)(\hat{g}\tilde{\nabla}_n\hat{g}). \tag{3.44}$$

From the above equation we see that the introduction of the curvature dependent scale factor functions similarly as a spin-orbit field as it introduces an additional term in the derivative. However, this additional term in the derivative only appears in the left-most derivative in contrast to a spin-orbit field. This is a manifestation of the fact that the Cristoffel symbols, and hence the curvature dependent scale factor, only appears when taking derivatives of tensors of rank $\geq 1$.

Due to the assumption of no torsion, scale factors do not appear in the binormal derivative term in equation (3.42).

A similar derivation can be performed in order to find the curvilinear expression for the Kuprianov-Lukichev boundary conditions given in equation (2.25). The covariant form of the Kuprianov-Lukichev boundary conditions may be written as

$$\hat{g}_a^R \mathcal{D}_i \hat{g}_a^R = \frac{1}{2L_a\zeta_a}[\hat{g}_1^R, \hat{g}_2^R], \tag{3.45}$$

where the label $a$ signifies the boundary condition for material $a$ and should not be confused with a covariant index. If we want to include spin-orbit coupling, we should change the coordinate covariant derivative with a coordinate-gauge covariant derivative

$$\hat{g}_a^R \tilde{\mathcal{D}}_i \hat{g}_a^R = \frac{1}{2L_a\zeta_a}[\hat{g}_1^R, \hat{g}_2^R], \tag{3.46}$$

Expanding the covariant Kuprianov Lukichev boundary condition in curvilinear coordinates we achieve

$$\hat{g}_a^R \tilde{\nabla}_i \hat{g}_a^R = \frac{1}{2L_a\zeta_a}[\hat{g}_1^R, \hat{g}_2^R], \tag{3.47}$$

where $\tilde{\nabla}_i$ is the gauge covariant derivative in terms of the physical spin-orbit field discussed earlier.

# 4 Nanowire arc

The simplest curved nanostructure is a nanowire arc curved in the form of a circle-portion as illustrated in Figure 7. For a circle-portion the curvature is constant $\kappa(s) = \kappa = \frac{1}{R}$, where $R$ is the radius of the full circle. Assuming that the nanowire arc residing in the xy-plane is infinitesimally thin, we may neglect the degrees of freedom in the normal and binormal direction. Consequently, the curvature dependent scale function $H(s, n) = 1$ and the metric tensor reduces to the form of a Cartesian metric tensor. For coordinate systems with a Cartesian-like metric, there is no destinction between covariant/contravariant and physical tensor components and we may drop the paranthesis notation on physical components.

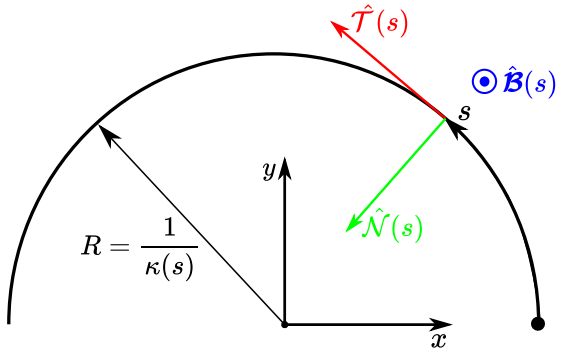


Figure 7: An illustration of a circle-portion nanowire, here chosen to be a semicircle, with a constant curvature radius $R = \frac{1}{\kappa(s)}$ residing in the xy-plane. At any arclength point s, measured from the right end of the semicircular nanowire, we have a local set of basis vectors $\hat{\boldsymbol{\mathcal{T}}}(s)$ and $\hat{\boldsymbol{\mathcal{N}}}(s)$. For a right handed curvilinear coordinate system the binormal unit vector $\hat{\boldsymbol{\mathcal{B}}}(s)$ is constant and points out of the plane.

For a 1D nanowire arc the derivatives in the binormal and normal direction disappears from the Usadel equation which takes the simple form

$$iD_F\tilde{\partial}_s(\check{g}\tilde{\partial}_s\check{g}) = [\epsilon\hat{\tau}_z - \hat{\Delta} - h_T\hat{\sigma}_T - h_N\hat{\sigma}_N - h_B\hat{\sigma}_B, \check{g}], \tag{4.1}$$

where we have defined the gauge covariant derivative $\tilde{\partial}_s \cdot = \partial_s \cdot -i[\hat{A}_T, \cdot]$ corresponding to $H(s, n) = 1$ for the coordinate gauge covariant derivative in curvilinear coordinates used in the curvilinear Usadel equation (3.42). $\hat{A}_T = \text{diag}(\underline{A}_T, -\underline{A}_T^*)$, where $\underline{A}_T = \alpha_N\underline{\sigma}_B - \alpha_B\underline{\sigma}_N$ is the tangential component of the spin-orbit field derived in Section 3.2. The curvilinear Pauli matrices are defined as

$$\underline{\sigma}_T = \boldsymbol{\sigma}\cdot\hat{\boldsymbol{\mathcal{T}}}(s), \qquad \underline{\sigma}_N = \boldsymbol{\sigma}\cdot\hat{\boldsymbol{\mathcal{N}}}(s), \qquad \underline{\sigma}_B = \boldsymbol{\sigma}\cdot\hat{\boldsymbol{\mathcal{B}}}(s), \tag{4.2}$$

where $\boldsymbol{\sigma}$ is the Cartesian Pauli spin vector. In order to find the explicit form of the Pauli matrices in curvilinear coordinates the three basis vectors are

needed. The basis vectors are related through the torsion free Frenet-Serret formulas given in equation (3.4) and can be expressed in terms of the arc length parametrization $\boldsymbol{\xi}(s)$ in the following way

$$\begin{aligned}\hat{\boldsymbol{\mathcal{T}}}(s) &= \frac{d}{ds}\boldsymbol{\xi}(s),\\ \hat{\boldsymbol{\mathcal{N}}}(s) &= \frac{1}{\kappa(s)}\frac{d^2}{ds^2}\boldsymbol{\xi}(s),\\ \hat{\boldsymbol{\mathcal{B}}}(s) &= \hat{\boldsymbol{e}}_z.\end{aligned} \tag{4.3}$$

The arc length parametrization of a circle-portion is straightforward to compute and can be expressed in the simple form $\boldsymbol{\xi}(s) = \frac{1}{\kappa}\cos(\kappa s)\hat{\boldsymbol{e}}_x + \frac{1}{\kappa}\sin(\kappa s)\hat{\boldsymbol{e}}_y$ using a Cartesian coordinate system as shown in Figure 7. Using the arclength parametrization we can express the curvilinear basis vectors in equation (4.3) for the case of a circle-portion

$$\begin{aligned}\hat{\boldsymbol{\mathcal{T}}}(s) &= -\sin(\kappa s)\hat{\boldsymbol{e}}_x + \cos(\kappa s)\hat{\boldsymbol{e}}_y,\\ \hat{\boldsymbol{\mathcal{N}}}(s) &= -\cos(\kappa s)\hat{\boldsymbol{e}}_x - \sin(\kappa s)\hat{\boldsymbol{e}}_y,\\ \hat{\boldsymbol{\mathcal{B}}}(s) &= \hat{\boldsymbol{e}}_z,\end{aligned} \tag{4.4}$$

following a right handed coordinate system.

The curvilinear Pauli matrices in equation (4.2) are now a simple task to compute

$$\underline{\sigma}_T = \begin{pmatrix} 0 & -ie^{-i\kappa s} \\ ie^{i\kappa s} & 0 \end{pmatrix},\ \underline{\sigma}_N = \begin{pmatrix} 0 & -e^{-i\kappa s} \\ -e^{i\kappa s} & 0 \end{pmatrix},\ \underline{\sigma}_B = \begin{pmatrix} 1 & 0 \\ 0 & -1 \end{pmatrix}. \tag{4.5}$$

As discussed in the end of Section 3.2, the position dependence of the curvilinear Pauli matrices in the spin-orbit field $\hat{A}_T$ induces additional terms in the second order derivatives in the Usadel equation. In the next Section these terms will be calculated explicitly, when performing a parametrization of the Usadel equation.

Tuning the curvature in the case for nanowire arcs is done by fixing one end of the wire and forming the wire into a smaller or larger portion of the full circle as shown in Figure 8. Since the curvature is inversely proportional to the radius, forming the wire into a larger portion of the full circle yields a larger curvature. Oppositely, forming it into a smaller portion yields a smaller curvature. By normalizing in terms of the length of the nanowire $L$, the curvature may be expressed as $\kappa = \frac{\pi}{L}$ for a semicircle, $\kappa = \frac{\pi/2}{L}$ for a quarter circle and so on.

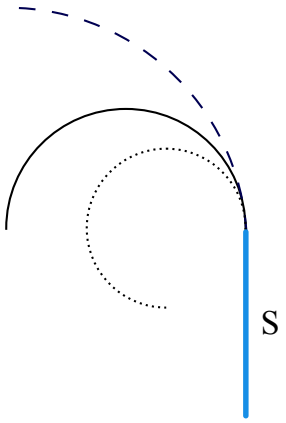


Figure 8: Fixing the end with the superconductor (S) allows for manipulating the curvature $\kappa = 1/R$, where $R$ is the circle radius, by bending the other end to form a portion of a circle. The larger the portion, the smaller the radius and hence the larger the curvature.

## 4.1 Parametrization

As discussed in Section 2.1, the retarded, advanced and Keldysh Green's functions in Nambu space are related to each other in thermal equilibrium. Hence, we can focus solely on one of the three, e.g. the retarded component. Recall the definition of the retarded quasiclassical Green's function

$$\hat{g}^R = \begin{pmatrix} \underline{g}^R & \underline{f}^R \\ -\underline{\tilde{f}}^R & -\underline{\tilde{g}}^R \end{pmatrix}. \tag{4.6}$$

The symmetry of the retarded quasiclassical Green's function suggests that a parametrization can be made in order to reduce the problem to an equation of 2x2 matrices. In quasiclassical Green's function theory, two main parametrizations are applied; $\theta$-parametrization, where the quasiclassical Green's function is expressed in terms of hyperbolic functions [30], and Riccati parametrization, where the quasiclassical Green's function is expressed in terms of a 2x2 matrix $\gamma$ [59]. $\theta$-parametrization is widely used in analytical analyses, but is potentially problematic in numerical calculations due to the divergence of hyperbolic functions. The Riccati parametrization however, is tailored for numerical work as the $\gamma$-matrix spans all values of the quasiclassical Green's function in a finite range from $0 - 1$.

The retarded quasiclassical Green's function may be expressed in terms of the Riccati matrix $\gamma$ in the following way

$$\hat{g}^R = \begin{pmatrix} N & 0 \\ 0 & -\tilde{N} \end{pmatrix} \begin{pmatrix} 1 + \gamma\tilde{\gamma} & 2\gamma \\ 2\tilde{\gamma} & 1 + \tilde{\gamma}\gamma \end{pmatrix}, \tag{4.7}$$

where $N$ is a 2x2 matrix defined as $N = (1 - \gamma\tilde{\gamma})^{-1}$. The form of the N-matrix implies some useful identities

$$N\gamma = \gamma\tilde{N}, \qquad \tilde{N}\tilde{\gamma} = \tilde{\gamma}N. \tag{4.8}$$

The derivative of $N$ may be expressed in terms of derivatives of $\gamma$

$$\partial_s N = N[(\partial_s\gamma)\tilde{\gamma} + \gamma(\partial_s\tilde{\gamma})]N. \tag{4.9}$$

In order to find the Riccati parametrized Usadel equation, the specific form of the left-hand side of the Usadel equation in (4.1) is needed

$$\begin{aligned}&\tilde{\partial}_s(\hat{g}^R\tilde{\partial}_s\hat{g}^R) = \partial_s(\hat{g}^R\tilde{\partial}_s\hat{g}^R) - i[\hat{A}_T, \hat{g}^R\tilde{\partial}_s\hat{g}^R]\\ &= \partial_s(\hat{g}^R\partial_s\hat{g}^R) - i\partial_s(\hat{g}^R\hat{A}_T\hat{g}^R - \hat{A}_T) - i[\hat{A}_T, \hat{g}^R\partial_s\hat{g}^R] - [\hat{A}_T, \hat{g}^R\hat{A}_T\hat{g}^R].\end{aligned} \tag{4.10}$$

For a nanowire arc with assymetric confinement in the binormal direction, the tangential spin-orbit field is given by $\hat{A}_T = \mathrm{diag}(\underline{A}_T, -\underline{A}_T^*)$ where $\underline{A}_T = \alpha_N\underline{\sigma}_B - \alpha_B\underline{\sigma}_N$. The curvilinear Pauli matrices follow the Frenet-Serret formulas given in equation (3.4). Consequently, the derivative of the tangential spin-orbit field is

$$\partial_s\underline{A}_T = -\kappa\alpha_B\underline{\sigma}_T. \tag{4.11}$$

The spatial variation of the spin-orbit field induces additional terms in the left-hand side of the Usadel equation proportional to the product of the curvature and the spin-orbit strength in the binormal direction.

The Riccati parametrized Usadel equation for a nanowire arc is given by

$$\begin{aligned}&D[(\partial_s^2\gamma) + 2(\partial_s\gamma)\tilde{N}\tilde{\gamma}(\partial_s\gamma)]\\ &= i(\gamma\underline{\Delta}^*\gamma - \underline{\Delta}) - i\boldsymbol{h}\cdot(\boldsymbol{\sigma}\gamma - \gamma\boldsymbol{\sigma}^*) - 2i\epsilon\gamma\\ &+ 2iD_F(\partial_s\gamma)\tilde{N}(\underline{A}_T^* + \tilde{\gamma}\underline{A}_T\gamma) + 2iD_F(\underline{A}_T + \gamma\underline{A}_T^*\tilde{\gamma})N(\partial_s\gamma)\\ &+ 2D_F(\underline{A}_T\gamma + \gamma\underline{A}_T^*)\tilde{N}(\underline{A}_T^* + \tilde{\gamma}\underline{A}_T\gamma) + D_F(\underline{A}_T^2\gamma - \gamma(\underline{A}_T^*)^2)\\ &+ iD_F\kappa\alpha_B(\underline{\sigma}_T\gamma + \gamma\underline{\sigma}_T),\end{aligned} \tag{4.12}$$

where $\boldsymbol{h}$ and $\boldsymbol{\sigma}$ are the exchange field and Pauli vector in the curvilinear basis[8].

The Riccati parametrized Kuprianov-Lukichev boundary conditions in material 1 and 2 are

$$\partial_s\gamma_1 = i(\gamma_1\underline{A}_T^* + \underline{A}_T\gamma_1) + \frac{1}{L_1\zeta_1}(1 - \gamma_1\tilde{\gamma}_2)N_2(\gamma_2 - \gamma_1), \tag{4.13}$$

$$\partial_s\gamma_2 = i(\gamma_2\underline{A}_T^* + \underline{A}_T\gamma_2) + \frac{1}{L_2\zeta_2}(1 - \gamma_2\tilde{\gamma}_1)N_1(\gamma_2 - \gamma_1). \tag{4.14}$$

In some limiting cases, the Riccati parametrized Usadel equation is simple to solve analytically. One relevant example is the bulk of a superconductor which is

[8] A full derivation of the Riccati parametrized Usadel equation for a spatially inhomogeneous spin-orbit field can be found in Appendix B

a good approximation for superconductor-ferromagnet proximity systems with a weak exchange field. In the bulk of the superconductor there exists no variations in the quasiclassical Green's function and we may neglect the derivatives in equation (4.12). Assuming no spin-orbit effects in the superconductor, the Riccati parametrized Usadel equation takes the simple form

$$\gamma_{\mathrm{BCS}}\underline{\Delta}^{*}\gamma_{\mathrm{BCS}} - \underline{\Delta} = 2\epsilon\gamma_{\mathrm{BCS}}, \tag{4.15}$$

with the solution

$$\gamma_{\mathrm{BCS}} = \frac{\sinh\theta}{\cosh\theta + 1} i\underline{\sigma}_2 e^{i\phi}, \qquad \tilde{\gamma}_{\mathrm{BCS}} = -\frac{\sinh\theta}{\cosh\theta + 1} i\underline{\sigma}_2 e^{-i\phi}, \tag{4.16}$$

where the superconducting phase $\phi$ is written explicitly, and we have defined a parameter $\theta$

$$\theta = \begin{cases} \frac{1}{2}\ln\frac{\epsilon+|\Delta|}{|\Delta|-\epsilon} - i\frac{\pi}{2} & \epsilon > |\Delta| \\ \\ \frac{1}{2}\ln\frac{\epsilon+|\Delta|}{\epsilon-|\Delta|} & \epsilon < |\Delta| \end{cases}. \tag{4.17}$$

Since we are interested in how the superconducting correlations behave inside the curved ferromagnet, we can assume a bulk solution of the gamma matrix in the superconductor and focus on the Usadel equation inside the ferromagnet.

## 4.2 Weak proximity limit

When the interface transparency between the superconductor and the ferromagnet is low, only a small number of Cooper pairs manages to tunnel from one side to the other, known as the weak proximity limit. In such a scenario the components of the $\gamma$ matrix are expected to be small, i.e. $|\gamma_{ij}| \ll 1$ and terms of the order $\mathcal{O}(\gamma^2)$ may be neglected [11]. Since $N \approx 1$ in this limit, the anomalous quasiclassical Green's function may be related directly to the gamma matrix, $\underline{f}^R \approx 2\gamma$.

The anomalous quasiclassical Green's function can be decomposed in terms of the so called d-vector $\boldsymbol{d}$, which transforms as a vector under a rotation of spin, and the scalar singlet component $f_s$ [60], [61]. The decomposition can be written in covariant form as

$$\underline{f}^R = (f_s + \eta^{ij} d_i \underline{\sigma}_j) i \underline{\sigma}_y. \tag{4.18}$$

For a nanowire arc, we can write equation (4.18) in curvilinear coordinates as

$$\underline{f}^R = (f_s + d_T \underline{\sigma}_T + d_N \underline{\sigma}_N + d_B \underline{\sigma}_B) i \underline{\sigma}_y, \tag{4.19}$$

Equation (4.19) can be expressed in matrix form

$$\underline{f}^R = 2\gamma = \begin{pmatrix} (id_T + d_N)e^{-i\kappa s} & d_B + f_s \\ d_B - f_s & (id_T - d_N)e^{i\kappa s} \end{pmatrix}, \tag{4.20}$$

using the expression for the curvilinear Pauli matrices for a nanowire arc curved as a portion of a circle given in equation (4.5). In the weak proximity limit, the Riccati parametrized Usadel equation for the nanowire arc given in equation (4.12) reduces to a linear differential equation in gamma

$$\begin{aligned} D_F \partial_s^2 \gamma = &- i\boldsymbol{h} \cdot (\boldsymbol{\sigma}\gamma - \gamma\boldsymbol{\sigma}^*) - 2i\epsilon\gamma + 2iD_F[(\partial_s\gamma)\underline{A}_T^* + \underline{A}_T(\partial_s\gamma)] \\ &+ 2D_F[\underline{A}_T\gamma\underline{A}_T^* + \gamma(\underline{A}_T^*)^2] + D_F[(\underline{A}_T)^2\gamma - \gamma(\underline{A}_T^*)^2] \\ &- iD_F[(\partial_s\underline{A}_T)\gamma + \gamma(\partial_s\underline{A}_T^*)]. \end{aligned} \tag{4.21}$$

Using the weak proximity representation of the gamma matrix given in equation (4.20), each term in the linearized Riccati parametrized Usadel equation may be expressed in matrix form. Performing matrix multiplication between the weak proximity gamma matrix and the Pauli matrices given in equation (4.5), the exchange field part of equation (4.21) is given by

$$-i\boldsymbol{h} \cdot (\boldsymbol{\sigma}\gamma - \gamma\boldsymbol{\sigma}^*) = \begin{pmatrix} (h_T f_s - ih_N f_s)e^{-i\kappa s} & -i\boldsymbol{h} \cdot \boldsymbol{d} - ih_B f_s \\ i\boldsymbol{h} \cdot \boldsymbol{d} - ih_B f_s & (h_T f_s + ih_N f_s)e^{i\kappa s} \end{pmatrix}. \tag{4.22}$$

The next issue is to tackle the spin-orbit dependent part of equation (4.21). For a 1D planar nanowire arc with asymmetric confinement in the binormal direction, the spin-orbit field is given by $\underline{A}_T = \alpha_N \underline{\sigma}_B - \alpha_B \underline{\sigma}_N$. By insertion, we find that the second last term in equation (4.21) is equal to zero for this choice of spin-orbit field. Using the Frenet-Serret formulas, the derivative of the

spin-orbit field is given by $\partial_s \underline{A}_T = -\kappa\alpha_B \underline{\sigma}_T$. Inserting this into the last term in equation (4.21), the following matrix expression is achieved

$$-D_F i[(\partial_s \underline{A}_T)\gamma + \gamma(\partial_s \underline{A}_T^*)] = D_F \kappa\alpha_B \begin{pmatrix} d_B e^{-i\kappa s} & -d_N \\ -d_N & -d_B e^{i\kappa s} \end{pmatrix}. \tag{4.23}$$

The final two spin-orbit terms may be expressed in matrix form as

$$\begin{aligned}
[(\partial_s\gamma)\underline{A}_T^* + \underline{A}_T(\partial_s\gamma)]^{(1,1)} &= e^{-i\kappa s}[\alpha_N(\partial_s - i\kappa)(id_T + d_N) + \alpha_B \partial_s d_B], \\
[(\partial_s\gamma)\underline{A}_T^* + \underline{A}_T(\partial_s\gamma)]^{(1,2)} &= \alpha_B[\partial_s(id_T) - i\kappa d_N], \\
[(\partial_s\gamma)\underline{A}_T^* + \underline{A}_T(\partial_s\gamma)]^{(2,1)} &= \alpha_B[\partial_s(id_T) - i\kappa d_N], \\
[(\partial_s\gamma)\underline{A}_T^* + \underline{A}_T(\partial_s\gamma)]^{(2,2)} &= e^{i\kappa s}[-\alpha_N(\partial_s + i\kappa)(id_T - d_N) + \alpha_B \partial_s d_B],
\end{aligned} \tag{4.24}$$

$$\begin{aligned}
[\underline{A}_T\gamma\underline{A}_T^* + \gamma(\underline{A}_T^*)^2]^{(1,1)} &= e^{-i\kappa s}[\alpha_N^2(id_T + d_N) + \alpha_N\alpha_B d_B + \alpha_B^2(id_T)], \\
[\underline{A}_T\gamma\underline{A}_T^* + \gamma(\underline{A}_T^*)^2]^{(1,2)} &= \alpha_B^2 d_B + \alpha_N\alpha_B d_N, \\
[\underline{A}_T\gamma\underline{A}_T^* + \gamma(\underline{A}_T^*)^2]^{(2,1)} &= \alpha_B^2 d_B + \alpha_N\alpha_B d_N, \\
[\underline{A}_T\gamma\underline{A}_T^* + \gamma(\underline{A}_T^*)^2]^{(2,2)} &= e^{i\kappa s}[\alpha_B^2(id_T) - \alpha_N\alpha_B d_B + \alpha_N^2(id_T - d_N)],
\end{aligned} \tag{4.25}$$

where $(i, j)$ are the components of the matrix. The last term needed is the left-hand side of equation (4.21). Taking the second derivative of the weak proximity gamma matrix given in (4.20) gives

$$\partial_s^2\gamma = \frac{1}{2}\begin{pmatrix} e^{-i\kappa s}(\partial_s - i\kappa)^2(id_T + d_N) & \partial_s^2(d_B + f_s) \\ \partial_s^2(d_B - f_s) & e^{i\kappa s}(\partial_s + i\kappa)^2(id_T - d_N) \end{pmatrix}. \tag{4.26}$$

Comparing componentwise the matrix representation of the right and left-hand side of the linearized Riccati parametrized Usadel equation in (4.21), we attain four coupled differential equations

$$\begin{aligned}
\frac{D_F}{2}(\partial_s - i\kappa)^2(id_T + d_N) = (h_T - ih_N)f_s - i\epsilon(id_T + d_N) + D_F\kappa\alpha_B d_B \\
+ 2D_F[\alpha_N^2(id_T + d_N) + \alpha_N\alpha_B d_B + \alpha_B^2(id_T)] \\
+ 2iD_F[\alpha_N(\partial_s - i\kappa)(id_T + d_N) + \alpha_B\partial_s d_B],
\end{aligned} \tag{4.27}$$

$$\begin{aligned}
\frac{D_F}{2}(\partial_s + i\kappa)^2(id_T - d_N) = (h_T + ih_N)f_s - i\epsilon(id_T - d_N) - D_F\kappa\alpha_B d_B \\
+ 2D_F[\alpha_N^2(id_T - d_N) - \alpha_N\alpha_B d_B + \alpha_B^2(id_T)] \\
+ 2iD_F[-\alpha_N(\partial_s + i\kappa)(id_T - d_N) + \alpha_B\partial_s d_B],
\end{aligned} \tag{4.28}$$

$$\begin{aligned}
\frac{D_F}{2}\partial_s^2(d_B + f_s) = -i(\boldsymbol{h}\cdot\boldsymbol{d} + h_B f_s) - i\epsilon(d_B + f_s) - D_F\kappa\alpha_B d_N \\
+ 2D_F(\alpha_B^2 d_B + \alpha_N\alpha_B d_N) - 2D_F[\alpha_B(\partial_s(d_T) - \kappa d_N)],
\end{aligned} \tag{4.29}$$

$$\begin{aligned}
\frac{D_F}{2}\partial_s^2(d_B - f_s) = i[\boldsymbol{h}\cdot\boldsymbol{d} - h_B f_s] - i\epsilon(d_B - f_s) - D_F\kappa\alpha_B d_N \\
+ 2D_F[\alpha_B^2 d_B + \alpha_N\alpha_B d_N] - 2D_F[\alpha_B(\partial_s(d_T) - \kappa d_N)].
\end{aligned} \tag{4.30}$$

The form of the equations suggests a simplification by adding and subtracting equation (4.28) from (4.27) and equation (4.30) from (4.29) respectively. Performing this simplification results in the final form of the four coupled differential equations for the curvilinear components of the d-vector and the singlet

$$\begin{aligned}\frac{iD_F}{2}\partial_s^2 d_T &= \epsilon d_T + h_T f_s + iD_F[2(\alpha_N^2+\alpha_B^2)+\kappa(\frac{\kappa}{2}+2\alpha_N)]d_T \\ &\quad + iD_F(2\alpha_N+\kappa)\partial_s d_N + 2iD_F\alpha_B\partial_s d_B,\end{aligned} \tag{4.31}$$

$$\begin{aligned}\frac{iD_F}{2}\partial_s^2 d_N &= \epsilon d_N + h_N f_s + iD_F[2\alpha_N^2+\kappa(\frac{\kappa}{2}+2\alpha_N)]d_N \\ &\quad - iD_F(2\alpha_N+\kappa)\partial_s d_T + iD_F\alpha_B(2\alpha_N+\kappa)d_B,\end{aligned} \tag{4.32}$$

$$\begin{aligned}\frac{iD_F}{2}\partial_s^2 d_B &= \epsilon d_B + h_B f_s + 2iD_F\alpha_B^2 d_B + iD_F\alpha_B(2\alpha_N+\kappa)d_N \\ &\quad - 2iD_F\alpha_B\partial_s d_T,\end{aligned} \tag{4.33}$$

$$\frac{iD_F}{2}\partial_s^2 f_s = \epsilon f_s + \boldsymbol{h}\cdot\boldsymbol{d}. \tag{4.34}$$

From the equations we see that the exchange field of the ferromagnet induces the triplets parallel to the field. In order to generate the triplets perpendicular to the field, either spin-orbit coupling or curvature is needed, but comes at the cost of a higher effective energy of the triplets. Equations (4.32) and (4.33) manifests a coupling between the normal and binormal triplets due to the spin-orbit coupling in the normal and binormal directions. Both curvature and the spin-orbit coupling in the binormal direction need to be nonzero for this coupling to be present.

In all equations (4.31)-(4.34), the curvature $\kappa$ and the spin-orbit strength due to the curvature $\alpha_N$ always appear together in an additive fashion. Since $\alpha_N$ is proportional to $\kappa$, the form of the equations suggests that the curvature acts as an enhancement of the spin-orbit coupling in the normal direction. Interestingly, from inspection of equations (4.31)-(4.34) it is simple to see that choosing the spin-orbit strength due to the curvature to be $\alpha_N = -\frac{\kappa}{2}$, all spin-orbit effects due to curvature vanish. By this choice of $\alpha_N$, we now have a theoretical way of singling out the intrinsic binormal part of the spin-orbit coupling.

### 4.2.1 Tangential exchange field with no intrinsic spin-orbit coupling

The simplest limiting case of the nanowire arc is the example of a tangential exchange field $\boldsymbol{h} = h_T\hat{\boldsymbol{\mathcal{T}}}(s)$ and no spin-orbit coupling due to the asymmetric confinement in the binormal direction $\alpha_B = 0$. We will keep $\kappa$ and set $\alpha_N = 0$ in the coupled differential equation for the d-vector and the singlet in equation (4.31)-(4.34). Since $\alpha_N$ is proportional to $\kappa$ and both $\kappa$ and $\alpha_N$ appear in an additive fashion in equations (4.31)-(4.34), the curvature works as a enhancement of the normal direction spin-orbit coupling or vice versa. Keeping $\kappa$ non-zero and $\alpha_N$ zero thus functions as a rescaling of the curvature. Setting $\alpha_N = \alpha_B = 0$ in equations (4.31)-(4.34) results in a simplified set of equations

$$\frac{iD_F}{2}\partial_s^2 d_T = h_T f_s + \epsilon_T d_T + \chi\partial_s d_N, \tag{4.35}$$

$$\frac{iD_F}{2}\partial_s^2 d_N = \epsilon_N d_N - \chi\partial_s d_T, \tag{4.36}$$

$$\frac{iD_F}{2}\partial_s^2 d_B = \epsilon_B d_B, \tag{4.37}$$

$$\frac{iD_F}{2}\partial_s^2 f_s = h_T d_T + \epsilon f_s, \tag{4.38}$$

where we have defined the effective energies for each component of the d-vector, $\epsilon_i$, and a mixing factor $\chi$

$$\epsilon_T = \epsilon + \frac{iD_F}{2}\kappa^2, \tag{4.39}$$

$$\epsilon_N = \epsilon + \frac{iD_F}{2}\kappa^2, \tag{4.40}$$

$$\epsilon_B = \epsilon, \tag{4.41}$$

$$\chi = iD_F\kappa. \tag{4.42}$$

As seen in equation (4.40) and (4.41), the curvature of the wire yields an imaginary shift in the effective energy due to inelastic scattering effects, leading to the destruction of Cooper pairs.

The physical implications of equation (4.35)-(4.38) can easily be understood by considering a superconductor in close proximity to a curved ferromagnet. The Cooper pairs in the superconductor are in the singlet state $f_s$. Approaching the interface, the exchange field leads to a mixing between the incident singlet state, and the short-range triplet state $d_T$ parallel to the exchange field manifested by equation (4.38). The curvature of the ferromagnet induces the transition from the short-range triplet to the long-range triplet $d_N$ normal to the exchange field as reflected by the mixing term in equation (4.35) and (4.36). The generation of long-range triplets depends on the mixing factor which in turn is proportional to the curvature $\kappa$. The binormal component $d_B$ is entirely decoupled from both the singlet component and the two other triplet components. Hence, the binormal component can not be generated from the singlet component and will thus not be present in the case of a nanowire arc nanowire with $\alpha_B = 0$.

The effective energy shift of both the short and long-range triplets are proportional to the curvature squared. A high curvature will thus provide a large triplet mixing factor at the cost of a higher effective energy, making the triplets less energetically favourable in comparison to the singlet.

### 4.2.2 Equivalence of a curved nanowire and a straight nanowire with a rotating exchange field

As discussed in Section 1.1, a possible way of generating long-range triplets is to introduce an inhomogeneous, rotating exchange field in the ferromagnet. In fact, there is an equivalence between a curved nanowire with a tangential exchange field and a straight wire of the same length with an exchange field which rotates in accordance with the curved wire.

For simplicity, we consider a semicircular curved nanowire and a straight nanowire along the y-axis with exchange field corresponding to the one of the curved wire as displayed in Figure 9.

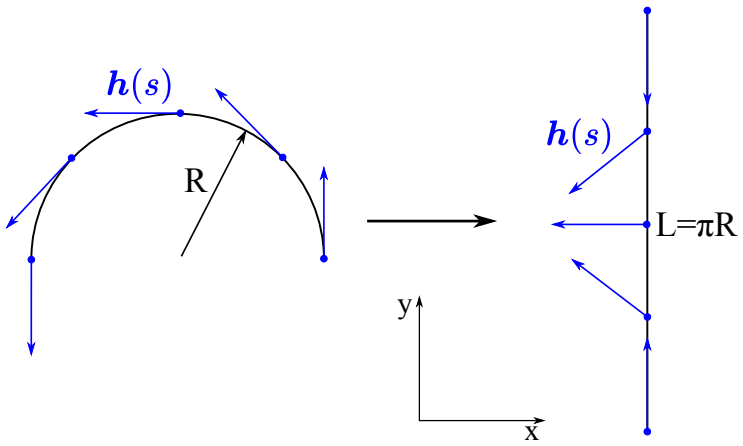


Figure 9: The semicircular nanowire with tangential exchange field $\boldsymbol{h}(s) = h\hat{\boldsymbol{\mathcal{T}}}(s)$ and the straight wire with corresponding exchange field. The nanowire length is $L = \pi R$.

The rotating exchange field in the straight wire is given in a Cartesian basis by

$$\boldsymbol{h}(s) = -h\sin(\kappa s)\hat{\boldsymbol{x}} + h\cos(\kappa s)\hat{\boldsymbol{y}}, \tag{4.43}$$

where $s = y$ is the arclength coordinate along the straight wire. In the limit of weak proximity the singlet and triplet components in the straight wire are

described by the linearized parametrization of the Usadel equation

$$\frac{iD_F}{2}\partial_s^2 f_s = \boldsymbol{h}\cdot\boldsymbol{d} + \epsilon f_s, \tag{4.44}$$

$$\frac{iD_F}{2}\partial_s^2 \boldsymbol{d} = f_s\boldsymbol{h} + \epsilon\boldsymbol{d}. \tag{4.45}$$

Using the expression for the rotating exchange field in equation (4.43) and separating equation (4.45) component wise yields

$$\frac{iD_F}{2}\partial_s^2 f_s = -h\sin(\kappa s)d_x + \cos(\kappa s)d_y + \epsilon f_s, \tag{4.46}$$

$$\frac{iD_F}{2}\partial_s^2 d_x = -h\sin(\kappa s)f_s + \epsilon d_x, \tag{4.47}$$

$$\frac{iD_F}{2}\partial_s^2 d_y = h\cos(\kappa s)f_s + \epsilon d_y, \tag{4.48}$$

$$\frac{iD_F}{2}\partial_s^2 d_z = \epsilon d_z. \tag{4.49}$$

If there is an equivalence between the semicircular curved nanowire and the straight wire with rotating exchange field, the linearized parametrization of the Usadel equation for the semicircular wire given in equation (4.35)-(4.38) should reduce to the corresponding equations for the straight wire given in equation (4.46)-(4.49) when performing a coordinate transformation from curvilinear to Cartesian coordinates.

In Cartesian coordinates the components of the d-vectors for the semicircular wire are

$$\begin{aligned} d_T &= -\sin(\kappa s)d_x + \cos(\kappa s)d_y, \\ d_N &= -\cos(\kappa s)d_x - \sin(\kappa s)d_y, \\ d_B &= d_z. \end{aligned} \tag{4.50}$$

The equations for the d-vector for the semicircular wire contains both a first and second derivative with respect to the arclength coordinate $s$. Due to the $s$-dependence of the d-vector transformed to Cartesian coordinates in equation (4.50), extra terms will appear

$$\begin{aligned} \partial_s d_T &= -\sin(\kappa s)\partial_s d_x + \cos(\kappa s)\partial_s d_y - \kappa\cos(\kappa s)d_x - \kappa\sin(\kappa s)d_y, \\ \partial_s^2 d_T &= -\sin(\kappa s)\partial_s^2 d_x + \cos(\kappa s)\partial_s^2 d_y - 2\kappa\cos(\kappa s)\partial_s d_x \\ &\quad - 2\kappa\sin(\kappa s)\partial_s d_y + \kappa^2\sin(\kappa s)d_x - \kappa^2\cos(\kappa s)d_y, \end{aligned} \tag{4.51}$$

$$\begin{aligned} \partial_s d_N &= -\cos(\kappa s)\partial_s d_x - \sin(\kappa s)\partial_s d_y + \kappa\sin(\kappa s)d_x - \kappa\cos(\kappa s)d_y, \\ \partial_s^2 d_T &= -\cos(\kappa s)\partial_s^2 d_x - \sin(\kappa s)\partial_s^2 d_y + 2\kappa\sin(\kappa s)\partial_s d_x \\ &\quad - 2\kappa\cos(\kappa s)\partial_s d_y + \kappa^2\cos(\kappa s)d_x + \kappa^2\sin(\kappa s)d_y. \end{aligned} \tag{4.52}$$

Inserting the derivatives of the d-vector expressed in Cartesian coordinates into equation (4.35)-(4.36) gives

$$\frac{iD_F}{2}\left[-\sin(\kappa s)\partial_s^2 d_x + \cos(\kappa s)\partial_s^2 d_y\right] = E(-\sin(\kappa s)d_x + \cos(\kappa s)d_y) + hf_s, \tag{4.53}$$

$$\frac{iD_F}{2}\left[-\cos(\kappa s)\partial_s^2 d_x - \sin(\kappa s)\partial_s^2 d_y\right] = E(-\cos(\kappa s)d_x - \sin(\kappa s)d_y). \quad (4.54)$$

The expressions can be simplified into two separate differential equations for $d_x$ and $d_y$ separately. Combining the two new equations with the equation for $d_B = d_z$ and $f_s$ gives

$$\frac{iD_F}{2}\partial_s^2 d_x = -h\sin(\kappa s)f_s + \epsilon d_x, \quad (4.55)$$

$$\frac{iD_F}{2}\partial_s^2 d_y = h\cos(\kappa s)f_s + \epsilon d_y, \quad (4.56)$$

$$\frac{iD_F}{2}\partial_s^2 d_z = \epsilon d_z, \quad (4.57)$$

$$\frac{iD_F}{2}\partial_s^2 f_s = h\cos(\kappa s)d_y - h\sin(\kappa s)d_x + \epsilon f_s, \quad (4.58)$$

which is exactly the same equation as for the straight nanowire with a rotating exchange field given in equation (4.46)-(4.49).

The equivalence between the two systems is not only an interesting theoretical result. It has the clear practical benefit of allowing for a direct comparison between the result for a curved nanowire to the extensively researched nanowire with rotating field. This equivalence provides a way of troubleshooting calculations and furthermore may give pointers in the direction of investigation and research.

# 5 Magnetization

In the framework of superconductor-ferromagnet proximity systems, the magnetization is a measure of the spin-accumulation of Cooper pairs in the ferromagnet. In the quasiclassical limit the magnetization is defined as [13], [62], [63]

$$\boldsymbol{M} = M_0 \int d\epsilon \mathrm{Tr}\{\hat{\boldsymbol{\sigma}}\hat{g}^K\}, \tag{5.1}$$

where $M_0$ is the constant reference magnetization given by $M_0 = g\mu_B N_0 \Delta/16$, $\mu_B$ is the Bohr magneton, $g$ is the g-factor and $N_0$ is the density of states at the Fermi level. In thermal equilibrium the Keldysh component of the quasiclassical Green's function can be directly related to the retarded component

$$\hat{g}^K = (\hat{g}^R + \hat{\tau}_z(\hat{g}^R)^\dagger\hat{\tau}_z)\tanh(\frac{\beta\epsilon}{2}). \tag{5.2}$$

In order to get a better physical understanding of the influence of singlet/triplet pairing on the magnetization, investigation of the weak proximity limit of equation (5.1) is useful. Due to the smallness of the induced magnetism a first order approximation will vanish. A second order weak proximity limit is thus needed. Keeping terms of order $\mathcal{O}(\gamma^2)$ the retarded component of the quasiclassical Green's function will reduce to

$$\hat{g}^R \approx \begin{pmatrix} 2\gamma\tilde{\gamma}+1 & 2\gamma \\ -2\tilde{\gamma} & -2\tilde{\gamma}\gamma - 1 \end{pmatrix}, \tag{5.3}$$

and the adjoint is given by

$$(\hat{g}^R)^\dagger \approx \begin{pmatrix} 2\tilde{\gamma}^\dagger\gamma^\dagger+1 & -2\tilde{\gamma}^\dagger \\ 2\gamma^\dagger & -2\gamma^\dagger\tilde{\gamma}^\dagger - 1 \end{pmatrix}. \tag{5.4}$$

Using the second order approximation of the retarded component of the quasiclassical Green's function in equation (5.2), the Keldysh component in the second order weak proximity limit can be written in terms of the components of the gamma matrix. For the case of a nanowire arc curved in the form of a portion of a circle, the spin vector may be constructed from the curvilinear Pauli matrices given in equation (4.5). The magnetization in the tangential direction can be expressed to second order in the component $\gamma_{ij}$ as

$$\begin{aligned} M_T = 2M_0 \int d\epsilon \{ & [ie^{i\kappa s}(\gamma_{11}\tilde{\gamma}_{12} + \gamma_{12}\tilde{\gamma}_{22}) + \text{c.c.}] \\ & -[ie^{i\kappa s}(\gamma_{11}\tilde{\gamma}_{21} + \gamma_{21}\tilde{\gamma}_{22}) + \text{c.c.}] \\ & +[ie^{-i\kappa s}(\gamma_{12}\tilde{\gamma}_{11} + \gamma_{22}\tilde{\gamma}_{12}) + \text{c.c.}] \\ & -[ie^{-i\kappa s}(\gamma_{21}\tilde{\gamma}_{11} + \gamma_{22}\tilde{\gamma}_{21}) + \text{c.c.}]\} \tanh(\frac{\beta\epsilon}{2}), \end{aligned} \tag{5.5}$$

where c.c. denotes the complex conjugate. Note that the complex conjugate and the tilde conjugation are not equivalent and has to be treated separately, but

due to the integration over all energies a simplification can be made. Consider the following integral

$$\int d\epsilon(\gamma_{ij}(\epsilon)\tilde{\gamma}_{kl}(\epsilon))^* \tanh(\frac{\beta\epsilon}{2}) = \int d\epsilon\gamma_{ij}^*(\epsilon)\gamma_{kl}(-\epsilon)\tanh(\frac{\beta\epsilon}{2}). \tag{5.6}$$

Since the integral runs over all energies $\epsilon$, we can without loss of generality let $\epsilon \to -\epsilon$ in the integrand. Hence, the integral can be written as

$$\begin{aligned}\int d\epsilon\gamma_{ij}^*(\epsilon)\gamma_{kl}(-\epsilon)\tanh(\frac{\beta\epsilon}{2}) &= \int d\epsilon\gamma_{ij}^*(-\epsilon)\gamma_{kl}(\epsilon)\tanh(-\frac{\beta\epsilon}{2}) \\ = -\int d\epsilon\gamma_{ij}^*(-\epsilon)\gamma_{kl}(\epsilon)\tanh(\frac{\beta\epsilon}{2}) &= -\int d\epsilon\tilde{\gamma}_{ij}(\epsilon)\gamma_{kl}(\epsilon)\tanh(\frac{\beta\epsilon}{2}).\end{aligned} \tag{5.7}$$

Using this, equation (5.5) can be simplified to

$$\begin{aligned}M_T = 4M_0 \int d\epsilon[&ie^{i\kappa s}(\gamma_{11}\tilde{\gamma}_{12} + \gamma_{12}\tilde{\gamma}_{22}) + ie^{-i\kappa s}(\gamma_{12}\tilde{\gamma}_{11} + \gamma_{22}\tilde{\gamma}_{12}) \\ &- ie^{-i\kappa s}(\gamma_{21}\tilde{\gamma}_{11} + \gamma_{22}\tilde{\gamma}_{21}) - ie^{i\kappa s}(\gamma_{11}\tilde{\gamma}_{21} + \gamma_{21}\tilde{\gamma}_{22})]\tanh(\frac{\beta\epsilon}{2}).\end{aligned} \tag{5.8}$$

This can be further simplified to

$$\begin{aligned}M_T = 4M_0 \int d\epsilon[&ie^{-i\kappa s}(\tilde{\gamma}_{11}(\gamma_{12} - \gamma_{21}) + \gamma_{22}(\tilde{\gamma}_{12} - \tilde{\gamma}_{21})) \\ &+ ie^{i\kappa s}(\gamma_{11}(\tilde{\gamma}_{12} - \tilde{\gamma}_{21}) + \tilde{\gamma}_{22}(\gamma_{12} - \gamma_{21}))\tanh(\frac{\beta\epsilon}{2}).\end{aligned} \tag{5.9}$$

Inserting the d-vector formulation of the gamma matrix in curvilinear coordinates given in equation (4.20) in equation (5.9), the final expression for the magnetization in the second order weak proximity limit is obtained

$$M_T = 4M_0 \int d\epsilon(\tilde{d}_T f_s - d_T \tilde{f}_s)\tanh(\frac{\beta\epsilon}{2}). \tag{5.10}$$

Performing a similar derivation yields the following expression for the second order weak proximity magnetization in the normal and binormal directions

$$M_N = 4M_0 \int d\epsilon(\tilde{d}_N f_s - d_N \tilde{f}_s)\tanh(\frac{\beta\epsilon}{2}). \tag{5.11}$$

$$M_B = 4M_0 \int d\epsilon(\tilde{d}_B f_s - d_B \tilde{f}_s)\tanh(\frac{\beta\epsilon}{2}). \tag{5.12}$$

The magnetization vector for a nanowire arc can hence conveniently be expressed in terms of the d-vector as

$$\boldsymbol{M} = 4M_0 \int d\epsilon(\tilde{\boldsymbol{d}} f_s - \boldsymbol{d}\tilde{f}_s)\tanh(\frac{\beta\epsilon}{2}). \tag{5.13}$$

Using a similar argumentation as in equation (5.7), equation (5.14) may be expressed in terms of the real part of the product between the d-vector and the singlet

$$\boldsymbol{M} = 8M_0 \int d\epsilon \mathrm{Re}\{\tilde{\boldsymbol{d}} f_s\} \tanh(\frac{\beta\epsilon}{2}). \tag{5.14}$$

In the second order weak proximity limit the magnetization is expressed as an energy integral of the product of the triplet d-vector and the singlet. Equation (5.14) is a general result valid for any curvilinear coordinate system by generalizing the curvilinear d-vector as $\boldsymbol{d} = d_T\hat{\boldsymbol{\mathcal{T}}}(s)+d_N\hat{\boldsymbol{\mathcal{N}}}(s)+d_B\hat{\boldsymbol{\mathcal{B}}}(s)$. The magnetization in curvilinear coordinates can be related to Cartesian coordinates using the component transformation established in equation (A.3).

In the following we will analyse the magnetization in SF nanowires, where the ferromagnetic wire is curved into portions of a circle, by numerically solving the Riccati parametrized Usadel equation given in (4.12). The interface resistance ratio is chosen to be $\zeta = 3$ and the temperature is chosen to be $T = 0.05T_C$, where $T_C$ is the critical temperature of the superconductor. Both the spin-orbit strengths and the curvature is given in units of the ferromagnet length, e.g. $\alpha = 1$ corresponds to $\alpha L = 1$. When solving the Riccati parametrized Usadel equation we assume a bulk solution in the superconductor given in equation (4.16). The expression for the magnetization in the quasiclassical limit given in (5.1) involves an integral over an infinite energy range. In order to solve the integral numerically, the introduction of a cut-off energy is needed. Here, we have found that a cut-off energy of $\epsilon_c = 15\Delta$ is a suitable choice considering accuracy, run time and weak exchange fields[9].

1D curved magnetic wires are expected to exhibit a tangential exchange field for curvatures below some material-dependent, critical curvature [64]. Hence, we have chosen a tangential exchange field $\boldsymbol{h} = \Delta(1, 0, 0)$ when calculating the magnetization.

Figure 10 shows the magnetization in the tangential (left), normal (middle) and binormal (right) directions as a function of the arclength $s$ for different curvatures. For a 1D curved nanowire with asymmetric confinement in the binormal direction, $\alpha_T = 0$. Hence the only contribution to the magnetization in the tangential direction is the exchange field and $M_T$ displays no curvature-dependence. The curvature in the nanowire induces magnetization pointing in the normal direction $M_N$ as seen in the middle column in Figure 10. In the weak proximity equation for the normal component of the magnetization in equation (5.11), the integrand is a product of the normal component of the d-vector and the singlet. Consequently, a non-zero normal component of the magnetization implies the presence of the normal component of the d-vector. Hence, from the plot of $M_N$ in Figure 10, the curvature induces the normal component of the d-vector. The normal component of the d-vector is perpendicular to the exchange field and is thus a long-range triplet.

[9]The gamma matrix varies around the value of the exchange field. Hence for a strong exchange field e.g. $20\Delta$, the cut-off energy needs to be at a higher value.

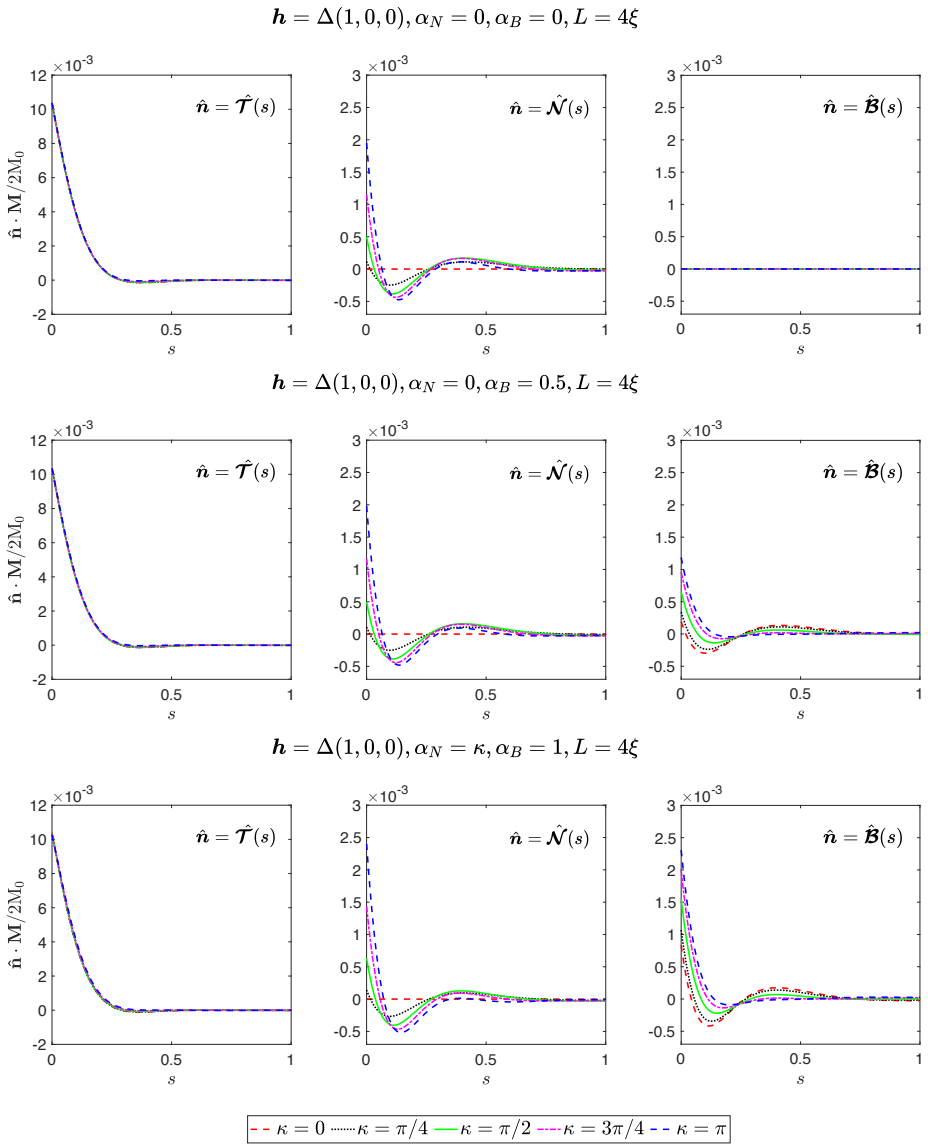


Figure 10: The normalized magnetization in the tangential (left), normal (middle) and binormal (right) directions as a function of the normalized arclength $s$ for different curvatures and spin-orbit strengths. The different curvatures are represented by different line styles and colors and the spin-orbit strength increases looking from the top panel and down according to the figure title. The exchange field is chosen to be in the tangential direction $\boldsymbol{h} = \Delta(1,0,0)$. The length of the ferromagnetic wire is $L = 4\xi$, where $\xi$ is the superconducting coherence length. All curvatures are normalized to the wire length $L$.

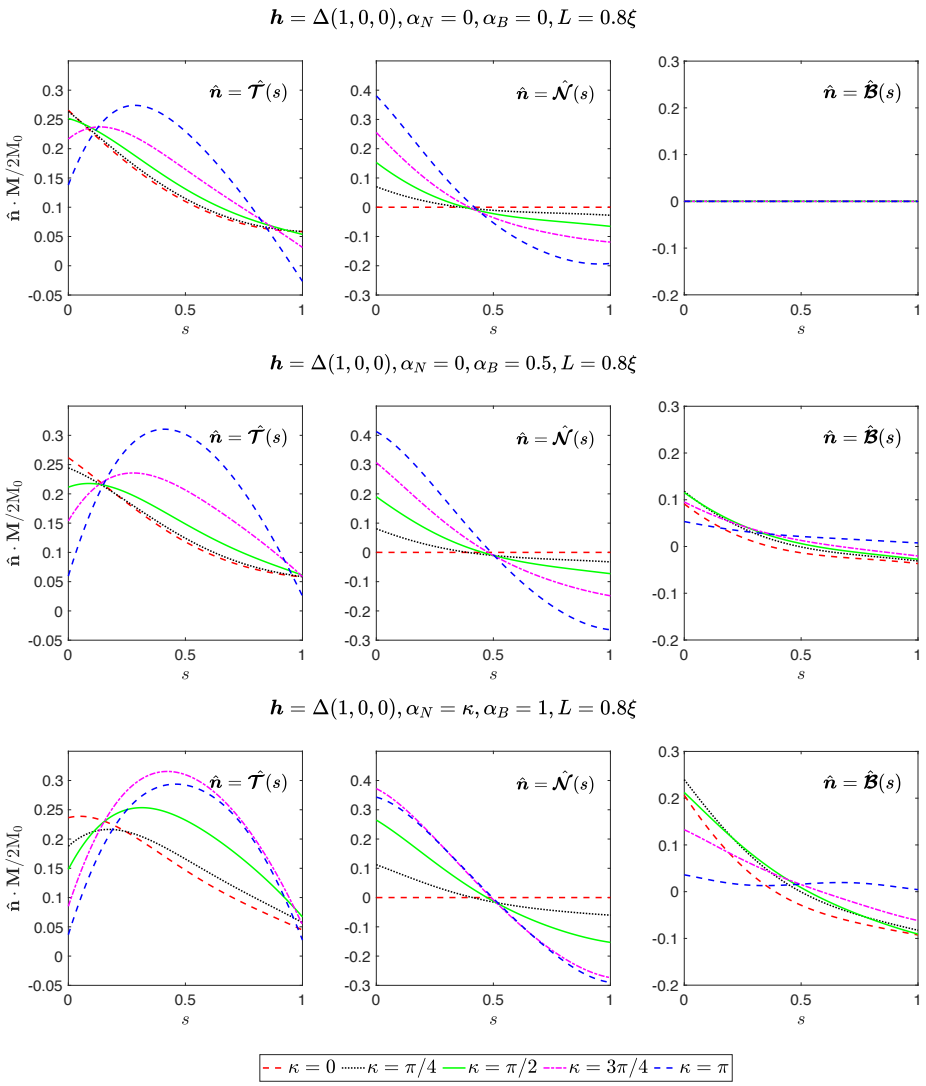


Figure 11: The normalized magnetization in the tangential (left), normal (middle) and binormal (right) directions as a function of the normalized arclength $s$ for different curvatures and spin-orbit strengths. The different curvatures are represented by different line styles and colors and the spin-orbit strength increases looking from the top panel and down according to the figure title. The exchange field is chosen to be in the tangential direction $\boldsymbol{h} = \Delta(1,0,0)$. The length of the ferromagnetic wire is $L = 0.8\xi$, where $\xi$ is the superconducting coherence length. All curvatures are normalized to the wire length $L$.

At the interface between the superconductor and the curved ferromagnetic wire ($s = 0$), $M_N$ increases upon increasing curvature. As expected, the magnetization in the normal direction vanishes for zero curvature. Rescaling the curvature by adding the curvature-dependent spin-orbit strength, $\alpha_N$ works as a strengthening of $M_N$ at the interface as seen in the middle of the last row in Figure 10.

When $\alpha_B = 0$ there is no magnetization in the binormal direction as seen in the right column in Figure 10. However, if $\alpha_B$ is nonzero, magnetization in the binormal direction is induced. The magnitude of the magnetization at the interface between the superconductor and the ferromagnet ($s = 0$), increases with increasing spin-orbit strength. The curvature will also affect the magnetization in the binormal direction, where larger curvature yields a larger magnetization at the interface. The non-zero binormal magnetization for a tangential exchange field implies the existence of the binormal component of the d-vector, which is a long-range triplet. Hence, adding curvature to a wire with intrinsic spin-orbit coupling due to asymmetric confinement in the binormal direction, induces both the $d_B$ long range triplet, due to the intrinsic spin-orbit coupling, and the $d_N$ long-range triplet, due to the curvature.

Both $M_N$ and $M_B$ are non-monotonic as a function of the arclength of the wire, but due to the short coherence length compared to the length of the wire, the magnetization in all directions tends to zero.

Figure 11 shows the magnetization for a much shorter wire length $L = 0.8\xi$. Decreasing the wire length results in a, in general, non-zero magnetization in the opposite end of the ferromagnet ($s = 1$). As for the wire length $L = 4\xi$, the magnetization in the normal direction in the wire of length $L = 0.8\xi$ is induced by adding curvature, where increasing the curvature increases the magnetization. As seen in the middle column of Figure 11, the normal component of the magnetization changes sign around the midpoint of the wire ($s = 0.5$). For non-zero $\alpha_B$ a binormal magnetization is induced. As for the case $L = 4\xi$, the magnetization increases as $\alpha_B$ is increased. The magnetization in the normal direction in the top row and the plots of the magnetization in the binormal direction in the right column in Figure 11 displays a similar behaviour. Comparing the plots, one can observe that the curvature of $\kappa = \pi$ yields a larger magnetization at the interface than a straight wire with $\alpha_B = 1$. Consequently, a curvature of $\kappa = \pi$ is expected to give spin-orbit effects greater than a straight wire with $\alpha = 1$.

Figure 12 shows evolution of the magnetization vector along the ferromagnetic semicircular nanowire of length $L = 0.8\xi$, with a tangential exchange field. The left figure shows the magnetization vector for $\alpha_N = \alpha_B = 0$, while the right figure shows the magnetization vector for $\alpha_N = 0$, $\alpha_B = 3$. The superconductor is placed at $s = 0$, the right end of the wire in Figure 12. As seen in the left figure, the magnitude of the magnetization is largest at the interface of the superconductor and the wire, and decreases along the wire. At the interface the curvature contribution to the magnetization dominates and the magnetization points in the normal direction with a slight tilt in the tangential direction due to the contribution from the tangential exchange field. In the middle of the wire

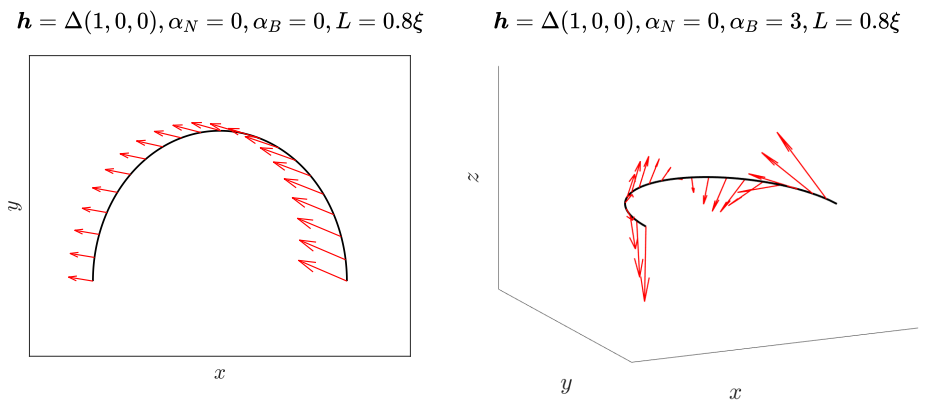


Figure 12: The magnetization vector depicted as red arrows along a semicircular wire. The superconductor is placed in the right end of the curved wire. The exchange field is chosen to be $\boldsymbol{h} = \Delta(1,0,0)$ and the curved wire is of length $L = 0.8\xi$. In the left figure the spin-orbit strengths are $\alpha_N = \alpha_B = 0$, while in the right figure $\alpha_N = 0$, $\alpha_B = 3$.

the exchange field dominates and the magnetization is almost tangential. In the left end of the wire the magnetization points in the negative normal direction and is hence dominated by the curvature contribution.

Adding a nonzero spin-orbit strength in the binormal direction induces magnetization in the binormal direction as seen at the right in Figure 12. For a relatively large spin-orbit strength $\alpha_B = 3$, the magnetization behaves in an oscillatory manner. The same oscillatory behaviour is present in straight nanowires with spin-orbit coupling [13].

# 6 Spin and charge current in curved nanostructures

## 6.1 Weak proximity current density

Placing a superconductor in both ends of a ferromagnetic wire allows for currents of both charge and spin to flow through the junction. The introduction of curvature in the ferromagnetic wire results in the generation of long-range triplet which in terms can give long-ranged currents through the junction. In order to investigate the influence of curvature on the current through the junction we will analyse the weak proximity current density equations, but first, we will take a step back and consider a straight wire with intrinsic spin-orbit coupling.

### 6.1.1 Straight nanowire with intrinsic Rashba spin-orbit coupling

In the quasiclassical approximation, the spin current density in a superconductor-ferromagnet heterostructure with intrinsic spin-orbit coupling is given by [63], [65]

$$j_{\mathrm{S},i} = j_{\mathrm{S},0} \int d\epsilon \mathrm{Tr}\{\hat{\tau}_z \hat{\sigma}_i (\hat{g}\tilde{\nabla}\hat{g})^K\}, \tag{6.1}$$

where $j_{\mathrm{S},0} = \frac{N_0 D_F}{8}$ and $\tilde{\nabla}\cdot = \nabla \cdot -i[\hat{A}, \cdot]$ is the Gauge covariant derivative with $\hat{A} = \mathrm{diag}(\boldsymbol{A}, -\boldsymbol{A}^*)$, where $\boldsymbol{A} = (\underline{A}_x, \underline{A}_y, \underline{A}_z)$ is the spin-orbit field introduced due to the intrinsic spin-orbit coupling in the ferromagnet. In the case of Rashba spin-orbit coupling the only nonzero component of the spin-orbit field is $\underline{A}_z = \alpha(\underline{\sigma}_x - \underline{\sigma}_y)$.

In thermal equilibrium, the spin current density may be written solely in terms of the retarded quasiclassical Green's function

$$j_{\mathrm{S},i} = j_{\mathrm{S},0} \int d\epsilon \mathrm{Tr}\{\hat{\tau}_z \hat{\sigma}_i [\hat{g}^R \tilde{\nabla} \hat{g}^R + \hat{\tau}_z (\hat{g}^R \tilde{\nabla} \hat{g}^R)^\dagger \hat{\tau}_z]\} \tanh \frac{\beta\epsilon}{2}. \tag{6.2}$$

In the second order weak proximity limit, the retarded quasiclassical Green's function may be written in terms of the gamma matrix as

$$\hat{g}^R \approx \begin{pmatrix} 2\gamma\tilde{\gamma} + 1 & 2\gamma \\ -2\tilde{\gamma} & -2\tilde{\gamma}\gamma - 1 \end{pmatrix}. \tag{6.3}$$

In equation (6.2), the reoccurring term is the derivative term $\hat{g}^R \tilde{\nabla} \hat{g}^R$. Considering a ferromagnetic wire situated along the z-direction with Rashba spin-orbit coupling in the corresponding direction, which is the case for nanowires with radially broken inversion symmetry in the $x + y$ direction, the derivative term takes the form

$$\hat{g}^R \tilde{\nabla} \hat{g}^R = \hat{g}^R \partial_z \hat{g}^R - i[\hat{A}_z, \hat{g}^R] = \hat{g}^R \partial_z \hat{g}^R - i\hat{g}^R \hat{A}_z \hat{g}^R + i\hat{A}_z, \tag{6.4}$$

where the normalization condition for the quasiclassical Green's function was utilized in the last step. Using the second order weak proximity representation

of the quasiclassical Green's function in equation (6.3), the term involving the derivative in equation (6.4) can be expressed to second order in matrix form as

$$\hat{g}^R\partial_z\hat{g}^R = 2\begin{pmatrix}(\partial_z\gamma)\tilde{\gamma}-\gamma(\partial_z\tilde{\gamma}) & \partial_z\gamma \\ \partial_z\tilde{\gamma} & (\partial_z\tilde{\gamma})\gamma-\tilde{\gamma}(\partial_z\gamma)\end{pmatrix}. \tag{6.5}$$

Similarly, the spin-orbit dependent part in equation (6.4) can be expressed in matrix form as

$$\begin{aligned}&-i\hat{g}^R\hat{A}_z\hat{g}^R + i\hat{A}_z \\ &=\begin{pmatrix}-2i\underline{A}_z\gamma\tilde{\gamma}-2i\gamma\tilde{\gamma}\underline{A}_z-4i\gamma\underline{A}_z^*\tilde{\gamma} & -2i\underline{A}_z\gamma-2i\gamma\underline{A}_z^* \\ 2i\tilde{\gamma}\underline{A}_z+2i\underline{A}_z^*\tilde{\gamma} & 2i\underline{A}_z^*\tilde{\gamma}\gamma+2i\tilde{\gamma}\gamma\underline{A}_z^*+4i\tilde{\gamma}\underline{A}_z\gamma\end{pmatrix}.\end{aligned} \tag{6.6}$$

The adjoint of equation (6.5) and (6.6) is

$$(\hat{g}^R\partial_z\hat{g}^R)^\dagger = 2\begin{pmatrix}\tilde{\gamma}^\dagger(\partial_z\gamma^\dagger)-(\partial_z\tilde{\gamma}^\dagger)\gamma^\dagger & \partial_z\tilde{\gamma}^\dagger \\ \partial_z\gamma^\dagger & \gamma^\dagger(\partial_z\tilde{\gamma}^\dagger)-(\partial_z\gamma^\dagger)\tilde{\gamma}^\dagger\end{pmatrix}, \tag{6.7}$$

$$\begin{aligned}
[-i\hat{g}^R\hat{A}_z\hat{g}^R+i\hat{A}_z)^\dagger]^{(1,1)} &= 2i\tilde{\gamma}^\dagger\gamma^\dagger\underline{A}_z^\dagger+2i\underline{A}_z^\dagger\tilde{\gamma}^\dagger\gamma^\dagger+4i\tilde{\gamma}^\dagger(\underline{A}_z^*)^\dagger\gamma^\dagger, \\
[-i\hat{g}^R\hat{A}_z\hat{g}^R+i\hat{A}_z)^\dagger]^{(1,2)} &= -2i\underline{A}_z^\dagger\tilde{\gamma}^\dagger-2i\tilde{\gamma}^\dagger(\underline{A}_z^*)^\dagger, \\
[-i\hat{g}^R\hat{A}_z\hat{g}^R+i\hat{A}_z)^\dagger]^{(2,1)} &= 2i\gamma^\dagger\underline{A}_z^\dagger+2i(\underline{A}_z^*)^\dagger\gamma^\dagger, \\
[-i\hat{g}^R\hat{A}_z\hat{g}^R+i\hat{A}_z)^\dagger]^{(2,2)} &= -2i\gamma^\dagger\tilde{\gamma}^\dagger(\underline{A}_z^*)^\dagger-2i(\underline{A}_z^*)^\dagger\gamma^\dagger\tilde{\gamma}^\dagger-4i\gamma^\dagger\underline{A}_z^\dagger\tilde{\gamma}^\dagger.
\end{aligned} \tag{6.8}$$

Inserting the matrices in equation (6.5), (6.6) and the adjoints in equation (6.7), (6.8) into equation (6.2), the trace of the product of 4x4 matrices may be considered as two separate trace-terms of products of 2x2 matrices

$$\begin{aligned}&\mathrm{Tr}\{\hat{\tau}_z\hat{\sigma}_i[\hat{g}^R\tilde{\nabla}\hat{g}^R+(\hat{\tau}_z\hat{g}^R\tilde{\nabla}\hat{g}^R\hat{\tau}_z)^\dagger]\} \\ &=2\mathrm{Tr}\{\underline{\sigma}_i[(\partial_z\gamma)\tilde{\gamma}-\gamma(\partial_z\tilde{\gamma})+\tilde{\gamma}^\dagger(\partial_z\gamma^\dagger)-(\partial_z\tilde{\gamma}^\dagger)\gamma^\dagger-i\underline{A}_z\gamma\tilde{\gamma} \\ &-i\gamma\tilde{\gamma}\underline{A}_z-2i\gamma\underline{A}_z^*\tilde{\gamma}+i\tilde{\gamma}^\dagger\gamma^\dagger\underline{A}_z^\dagger+i\underline{A}_z^\dagger\tilde{\gamma}^\dagger\gamma^\dagger+2i\tilde{\gamma}^\dagger(\underline{A}_z^*)^\dagger\gamma^\dagger]\}-\text{t.c.},\end{aligned} \tag{6.9}$$

where t.c. denotes the tilde conjugation of the previous trace. Since the nanowire is directed in the z-direction, the most interesting component of the current is the z-component. Carrying out the matrix multiplications in the trace with $\underline{\sigma}_i=\underline{\sigma}_z$ and performing the trace, yields the following expression in terms of the components of the gamma matrix

$$\begin{aligned}&\mathrm{Tr}\{\hat{\tau}_z\hat{\sigma}_z[\hat{g}^R\tilde{\nabla}\hat{g}^R+(\hat{\tau}_z\hat{g}^R\tilde{\nabla}\hat{g}^R\hat{\tau}_z)^\dagger]\} \\ &=4[\tilde{\gamma}_{11}\partial_z\gamma_{11}-\gamma_{11}^*\partial_z\tilde{\gamma}_{11}^*-\tilde{\gamma}_{22}\partial_z\gamma_{22}+\gamma_{22}^*\partial_z\tilde{\gamma}_{22}^*] \\ &-2\alpha[(i+1)\gamma_{11}\tilde{\gamma}_{21}+(i-1)\gamma_{12}\tilde{\gamma}_{11}]+2\alpha[(i+1)\gamma_{21}\tilde{\gamma}_{22}+(i-1)\gamma_{22}\tilde{\gamma}_{12}] \\ &+2\alpha[(i+1)\gamma_{12}^*\tilde{\gamma}_{11}^*+(i-1)\gamma_{11}^*\tilde{\gamma}_{21}^*]-2\alpha[(i+1)\gamma_{22}^*\tilde{\gamma}_{12}^*+(i-1)\gamma_{21}^*\tilde{\gamma}_{22}^*] \\ &-\text{t.c.}\end{aligned} \tag{6.10}$$

Since the trace in equation (6.10) is in the integrand of equation (6.2), the relation derived in equation (5.7) can be utilized. Consequently, we get a simplified

expression for the trace

$$\begin{aligned}&\mathrm{Tr}\{\hat{\tau}_z\hat{\sigma}_z[\hat{g}^R\tilde{\nabla}\hat{g}^R+(\hat{\tau}_z\hat{g}^R\tilde{\nabla}\hat{g}^R\hat{\tau}_z)^\dagger]\}\\&=-2\alpha(i+1)\gamma_{11}(\tilde{\gamma}_{21}+\tilde{\gamma}_{12})-2\alpha(i-1)\tilde{\gamma}_{11}(\gamma_{21}+\gamma_{12})\\&+2\alpha(i+1)\tilde{\gamma}_{22}(\gamma_{21}+\gamma_{12})+2\alpha(i-1)\gamma_{22}(\tilde{\gamma}_{21}+\tilde{\gamma}_{12})\\&+8[\tilde{\gamma}_{11}\partial_z\gamma_{11}-\tilde{\gamma}_{22}\partial_z\gamma_{22}]-\text{t.c.}\end{aligned}\tag{6.11}$$

In Cartesian coordinates the gamma matrix can be written in terms of the components of the d-vector and the singlet

$$\gamma=\frac{1}{2}\begin{pmatrix}id_y-d_x & d_z+f_s\\ d_z-f_s & id_y+d_x\end{pmatrix}.\tag{6.12}$$

Inserting the components of the gamma matrix into the trace in equation (6.11) yields, after simplifications,

$$\begin{aligned}\mathrm{Tr}\{\hat{\tau}_z\hat{\sigma}_z[\hat{g}^R\tilde{\nabla}\hat{g}^R+(\hat{\tau}_z\hat{g}^R\tilde{\nabla}\hat{g}^R\hat{\tau}_z)^\dagger]\}&=4i\alpha[d_x\tilde{d}_z-d_y\tilde{d}_z-\tilde{d}_yd_z+\tilde{d}_xd_z]\\&+4i[\tilde{d}_y\partial_zd_x-\tilde{d}_x\partial_zd_y]-\text{t.c.}\end{aligned}\tag{6.13}$$

Inserting the trace in equation (6.13), the weak proximity spin current density may be written in terms of the d-vector as

$$\begin{aligned}j_{\mathrm{S},z}=4ij_{\mathrm{S},0}\int d\epsilon[&\tilde{d}_y\partial_zd_x-\tilde{d}_x\partial_zd_y+d_y\partial_z\tilde{d}_x-d_x\partial_z\tilde{d}_z\\&+2\alpha(d_x\tilde{d}_z-d_y\tilde{d}_z-\tilde{d}_yd_z+\tilde{d}_xd_z)\tanh\frac{\beta\epsilon}{2}.\end{aligned}\tag{6.14}$$

Using equation (5.7), the expression for the spin current density can be given in terms of the imaginary components of the product of singlets and triplets

$$j_{\mathrm{S},z}=8j_{\mathrm{S},0}\int d\epsilon[\mathrm{Im}\{\tilde{d}_x\partial_zd_y-\tilde{d}_y\partial_zd_x\}+2\alpha\mathrm{Im}\{d_y\tilde{d}_z-d_x\tilde{d}_z\}]\tanh\frac{\beta\epsilon}{2}.\tag{6.15}$$

As expected the weak proximity spin current is independent of the singlet $f_s$, who carry no net spin.

### 6.1.2 Nanowire arc with curvature-induced Rashba spin-orbit coupling

In the quasiclassical approximation, the spin current density is given by equation (6.1). For the case of a 1D nanowire arc the gradient is replaced by the derivative with respect to the arclength, $\nabla \to \partial_s$. Here we will focus on the curvature-induced spin-obit coupling, and for that purpose we assume that the spin-orbit coupling due to the asymmetric confinement in the binormal direction $\alpha_B = 0$. Furthermore, we will set $\alpha_N = 0$ and investigate the $\kappa$-dependence of the current. As discussed in Section 4.2, this choice is valid due to the fact that $\alpha_N$ works as a rescaling of $\kappa$. Assuming thermal equilibrium, the spin current density along the bent direction may be written solely in terms of the retarded quasiclassical Green's function

$$j_{\mathrm{S},s} = j_{\mathrm{S},0} \int d\epsilon \mathrm{Tr}\{\hat{\tau}_z \hat{\sigma}_T [\hat{g}^R \nabla \hat{g}^R + (\tau_3 \hat{g}^R \nabla \hat{g}^R \tau_3)^\dagger]\} \tanh \frac{\beta\epsilon}{2}, \tag{6.16}$$

where $\hat{\underline{\sigma}_T} = \mathrm{diag}(\underline{\sigma}_T, \underline{\sigma}_T^*)$ is the Pauli matrix in the tangential direction in Nambu space. Since $\alpha_B = \alpha_N = 0$ the spin-orbit field is zero and introducing gauge covariant derivatives is not necessary.

Using the weak proximity expression for the retarded quasiclassical Green's function in equation (6.3), the derivative term in equation (6.16) takes the matrix form

$$\hat{g}^R \partial_s \hat{g}^R = 2 \begin{pmatrix} (\partial_s \gamma)\tilde{\gamma} - \gamma(\partial_s \tilde{\gamma}) & \partial_s \gamma \\ \partial_s \tilde{\gamma} & (\partial_s \tilde{\gamma})\gamma - \tilde{\gamma}(\partial_s \gamma) \end{pmatrix}, \tag{6.17}$$

while the adjoint term is given by

$$(\hat{g}^R \partial_s \hat{g}^R)^\dagger = 2 \begin{pmatrix} \tilde{\gamma}^\dagger(\partial_s \gamma^\dagger) - \partial_s(\tilde{\gamma}^\dagger)\gamma^\dagger & \partial_s \tilde{\gamma}^\dagger \\ \partial_s \gamma^\dagger & \gamma^\dagger(\partial_s \tilde{\gamma}^\dagger) - \partial_s(\gamma^\dagger)\tilde{\gamma}^\dagger \end{pmatrix}. \tag{6.18}$$

Using equations (6.17) and (6.18), the trace of a product of 4x4 matrices in equation (6.16) may be written as two traces of products of 2x2 matrices

$$\begin{aligned} &\mathrm{Tr}\{\hat{\tau}_z \hat{\sigma}_T [\hat{g}^R \partial_s \hat{g}^R + (\tau_3 \hat{g}^R \partial_s \hat{g}^R \tau_3)^\dagger]\} \\ =&2\mathrm{Tr}\{\sigma_T [(\partial_s \gamma)\tilde{\gamma} - \gamma(\partial_s \tilde{\gamma}) + \tilde{\gamma}^\dagger(\partial_s \gamma^\dagger) - \partial_s(\tilde{\gamma}^\dagger)\gamma^\dagger]\} - \mathrm{t.c.} \end{aligned} \tag{6.19}$$

Inserting the expression for the Pauli matrix for a nanowire arc curved in the shape of a circle portion given in equation (4.5) and carrying out the traces yields

$$\begin{aligned} &\mathrm{Tr}\{\hat{\tau}_z \hat{\sigma}_T [\hat{g}^R \partial_s \hat{g}^R + (\tau_3 \hat{g}^R \partial_s \hat{g}^R \tau_3)^\dagger]\} \\ &= 2[ie^{i\kappa s}(\tilde{\gamma}_{12}\partial_s \gamma_{11} + \tilde{\gamma}_{22}\partial_s \gamma_{12}) - ie^{-i\kappa s}(\tilde{\gamma}_{11}\partial_s \gamma_{21} + \tilde{\gamma}_{21}\partial_s \gamma_{22})] \\ &+ 2[ie^{i\kappa s}(\tilde{\gamma}_{11}^*\partial_s \gamma_{21}^* + \tilde{\gamma}_{21}^*\partial_s \gamma_{22}^*) - ie^{-i\kappa s}(\tilde{\gamma}_{12}^*\partial_s \gamma_{11}^* + \tilde{\gamma}_{22}^*\partial_s \gamma_{12}^*)] \\ &- 2[ie^{i\kappa s}(\gamma_{11}\partial_s \tilde{\gamma}_{12} + \gamma_{12}\partial_s \tilde{\gamma}_{22}) - ie^{-i\kappa s}(\gamma_{21}\partial_s \tilde{\gamma}_{11} + \gamma_{22}\partial_s \tilde{\gamma}_{21})] \\ &- 2[ie^{i\kappa s}(\gamma_{21}^*\partial_s \tilde{\gamma}_{11}^* + \gamma_{22}^*\partial_s \tilde{\gamma}_{21}^*) - ie^{-i\kappa s}(\gamma_{11}^*\partial_s \tilde{\gamma}_{12}^* + \gamma_{12}^*\partial_s \tilde{\gamma}_{22}^*)] - \mathrm{t.c.}, \end{aligned} \tag{6.20}$$

which, when inserted in the integrand in equation (6.16), yields a simplified weak proximity expression of the spin current density by utilizing the property in equation (5.7)

$$\begin{aligned} j_{\mathrm{S},s} = 4j_{\mathrm{S},0}\int d\epsilon i e^{i\kappa s}[(\tilde{\gamma}_{21}+\tilde{\gamma}_{12})\partial_s\gamma_{11} - \gamma_{11}\partial_s(\tilde{\gamma}_{21}+\tilde{\gamma}_{12}) \\ + \tilde{\gamma}_{22}\partial_s(\gamma_{21}+\gamma_{12}) - (\gamma_{21}+\gamma_{12})\partial_s\tilde{\gamma}_{22}]\tanh\frac{\beta\epsilon}{2} - \text{t.c.} \end{aligned} \tag{6.21}$$

Using the components of the gamma matrices for a nanowire arc given in equation (4.20), the terms in equation (6.21) may be expressed in terms of the curvilinear component of the d-vector

$$\begin{aligned} \partial_s\gamma_{11} &= \frac{1}{2}e^{-i\kappa s}(\partial_s - i\kappa)(id_T + d_N), \\ \partial_s\tilde{\gamma}_{22} &= \frac{1}{2}e^{-i\kappa s}(\partial_s - i\kappa)(-i\tilde{d_T} - d_N), \\ \gamma_{21}+\gamma_{12} &= d_B. \end{aligned} \tag{6.22}$$

Inserting the components of the gamma matrix and using the expressions in equation (6.22) in equation (6.21), the final form of the tangential component of the spin current in a nanowire arc is achieved

$$j_{\mathrm{S},s} = 8j_{\mathrm{S},0}\int d\epsilon[\mathrm{Im}\{\tilde{d_N}\partial_s d_B - \tilde{d_B}\partial_s d_N\} - \kappa\mathrm{Im}\{\tilde{d_B}d_T\}]\tanh\frac{\beta\epsilon}{2}. \tag{6.23}$$

To check the validity of the result we look at the limit $\kappa \to 0$ corresponding to a straight nanowire directed along the y-axis. In this limit, $d_T \to d_y$, $d_N \to -d_x$ and $d_B \to d_z$ and equation (6.23) reduces to

$$j_{\mathrm{S},y} = 8j_{\mathrm{S},0}\int d\epsilon[\mathrm{Im}\{\tilde{d_z}\partial_s d_x - \tilde{d_x}\partial_s d_z\}]\tanh\frac{\beta\epsilon}{2}. \tag{6.24}$$

To compare this with the result for the straight nanowire given in equation (6.15), we perform a cyclic permutation of the Cartesian coordinates resulting in

$$j_{\mathrm{S},z} = 8j_{\mathrm{S},0}\int d\epsilon[\mathrm{Im}\{\tilde{d_x}\partial_s d_y - \tilde{d_y}\partial_s d_x\}]\tanh\frac{\beta\epsilon}{2}, \tag{6.25}$$

which is equivalent to equation (6.15) for zero spin-orbit coupling ($\alpha = 0$).

A similar derivation can be made for the charge current. In quasiclassical Green's function theory the charge current may be expressed in thermal equilibrium in terms of the retarded quasiclassical Green's function

$$j_{\mathrm{Q}} = j_{\mathrm{Q},0}\int d\epsilon\mathrm{Tr}\{\hat{\tau}_z[\hat{g}^R\nabla\hat{g}^R + (\tau_3\hat{g}^R\nabla\hat{g}^R\tau_3)^\dagger]\}\tanh\frac{\beta\epsilon}{2}, \tag{6.26}$$

where $j_{\mathrm{Q},0} = \frac{eN_0D_F}{4}$. Using equations (6.17) and (6.18), the trace in the equation for the charge current (6.26) is

$$\begin{aligned} &\mathrm{Tr}\{\hat{\tau}_z[\hat{g}^R\partial_s\hat{g}^R + (\tau_3\hat{g}^R\partial_s\hat{g}^R\tau_3)^\dagger]\} \\ &= 2\mathrm{Tr}\{(\partial_s\gamma)\tilde{\gamma} - \gamma(\partial_s\tilde{\gamma}) + \tilde{\gamma}^\dagger(\partial_s\gamma^\dagger) - (\partial_s\tilde{\gamma}^\dagger)\gamma^\dagger\} - \text{t.c.} \end{aligned} \tag{6.27}$$

Performing the trace results in an expression containing the components of the gamma matrix

$$\begin{aligned}&\mathrm{Tr}\{\hat{\tau}_z[\hat{g}^R\partial_s\hat{g}^R + (\tau_3\hat{g}^R\partial_s\hat{g}^R\tau_3)^\dagger]\}\\&= 8[\tilde{\gamma}_{11}\partial_s\gamma_{11} + \tilde{\gamma}_{21}\partial_s\gamma_{12} + \tilde{\gamma}_{12}\partial_s\gamma_{21} + \tilde{\gamma}_{22}\partial_s\gamma_{22}].\end{aligned} \tag{6.28}$$

The derivatives of the diagonal components produces additional terms due to the curvature dependence as seen in (6.22). Inserting the components of the gamma matrix in terms of the d-vector and the singlet into equation (6.26) we may express the charge current in terms of the components of the d-vector and the singlet

$$\begin{aligned}j_\mathrm{Q} = 4j_{\mathrm{Q},0}\int d\epsilon[&\tilde{d}_T\partial_s d_T + \tilde{d}_N\partial_s d_N + \tilde{d}_B\partial_s d_B - \tilde{f}_s\partial_s f_s\\&+ \kappa(\tilde{d}_N d_T - \tilde{d}_T d_N) - \text{t.c.}]\tanh\frac{\beta\epsilon}{2},\end{aligned} \tag{6.29}$$

which we may rewrite in terms of the real part of the integrand

$$\begin{aligned}j_\mathrm{Q} = 4j_{\mathrm{Q},0}\int d\epsilon[&\mathrm{Re}\{\tilde{d}_T\partial_s d_T + \tilde{d}_N\partial_s d_N + \tilde{d}_B\partial_s d_B - \tilde{f}_s\partial_s f_s\\&- d_T\partial_s\tilde{d}_T - d_N\partial_s\tilde{d}_N - d_B\partial_s\tilde{d}_B + f_s\partial_s\tilde{f}_s\\&+ \kappa(\tilde{d}_N d_T - \tilde{d}_T d_N)\}]\tanh\frac{\beta\epsilon}{2},\end{aligned} \tag{6.30}$$

The form of the weak proximity expression of the charge current in (6.30) suggests that we can split the charge current into five contributions $j_Q = j_{Q,T} + j_{Q,N} + j_{Q,B} - j_{Q,s} + j_{Q,\kappa}$, where the triplet (T,N,B) contribution is defined as

$$j_{Q,i} = 4j_{\mathrm{Q},0}\int d\epsilon\mathrm{Re}\{\tilde{d}_i\partial_s d_i - d_i\partial_s\tilde{d}_i\}\tanh\frac{\beta\epsilon}{2}, \tag{6.31}$$

for $i \in \{T, N, B\}$ and the singlet contribution

$$j_{Q,s} = 4j_{\mathrm{Q},0}\int d\epsilon\mathrm{Re}\{\tilde{f}_s\partial_s f_s - f_s\partial_s\tilde{f}_s\}\tanh\frac{\beta\epsilon}{2}. \tag{6.32}$$

Finally the curvature contribution is defined as

$$j_{Q,\kappa} = 8\kappa j_{\mathrm{Q},0}\int d\epsilon\mathrm{Re}\{\tilde{d}_N d_T - d_N\tilde{d}_T\}\tanh\frac{\beta\epsilon}{2}. \tag{6.33}$$

The form of the curvature contribution to the charge current in equation (6.33) suggests that the curvature of the ferromagnetic wire results in a finite charge current produced by the existence of a triplet spin expectation value. This may be interpreted as a kind of inverse Edelstein effect, which converts a spin accumulation into a charge current perpendicular to the spin current, thus effectively working as a spin-charge conversion [66], [67]. The inverse Edelstein effect has been investigated for straight Josephson junctions with spin-obit coupling as the generator [68], but as shown here, the same effect may be generated using curvature. The curvature contribution $j_{Q,\kappa}$ has a similar form to the equivalent expression for a spin-orbit contribution in a straight Josephson junction.

### 6.1.3 Curvature induced long-ranged Josephson effect and dynamical $0-\pi$ transition

By solving equation (6.16) and (6.26) numerically, we can investigate the influence of curvature on the spin and charge current in Josephson junctions. We have chosen the temperature to be $T = 0.05T_C$ where $T_C$ is the critical temperature of the superconductors. In order to solve the integral in equation (6.16) and (6.26) numerically we have chosen a suitable cut-off energy $\epsilon_C = 15\Delta$.

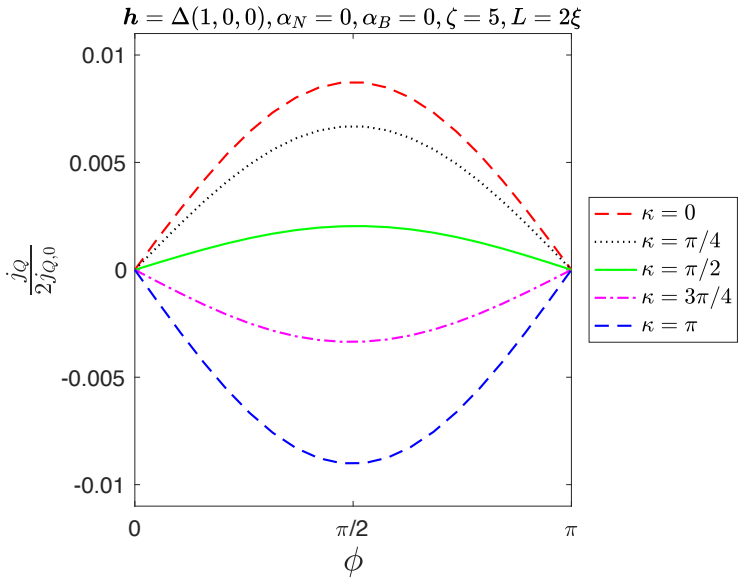


Figure 13: The charge current density normalized by the constant charge current $j_{Q,0} = \frac{eN_0D_F}{4}$ as a function of the phase difference $\phi$ of the two superconductors for different curvatures $\kappa$. The exchange field is chosen to be tangential and of strength equal to the superconducting gap $\Delta$. The spin-orbit strength in both the normal and binormal direction is set to zero and the interface resistance ratio is $\zeta = 5$. The ferromagnetic wire is of length $L = 2\xi$.

The charge current through a Josephson junction is independent of the position in the ferromagnetic wire. The value of this constant depends on the phase difference $\phi$ between the two superconductors. Figure 13 shows the charge current as a function of the phase-difference for different values of the curvature. When the phase difference is $\phi = 0$ or $\phi = \pi$ no charge current will flow through the junction. The maximum value of the charge current occurs at a phase difference of $\phi = \pi/2$. The value of the charge current at $\phi = \pi/2$ is known as the critical charge current. As seen from Figure 13, the value of the critical charge current varies with the curvature, where the maximum absolute value occurs at $\kappa = 0$ and $\kappa = \pi$. However, the charge current at $\kappa = 0$ and $\kappa = \pi$ have different signs, which may be interpreted as the current flowing in the opposite

direction. The curvature appears to switch sign at a critical curvature between $\kappa = \pi/2$ and $\kappa = 3\pi/4$. The transition between positive and negative current is known as a $0 - \pi$ transition in the literature [32].

The $0 - \pi$ transitions are not a novel phenomena, and has been extensively researched and may have application in spintronic devices and quantum computers. In most cases, the $0 - \pi$ transition is realised by changing the length of the ferromagnet in the Josephson junction [69], [70], [71]. Such a procedure is difficult to realise in practice since it would require a replacement of the ferromagnet. However, applying curvature in order to generate the $0 - \pi$ transition provides a fully dynamical control highly practical for application purposes.

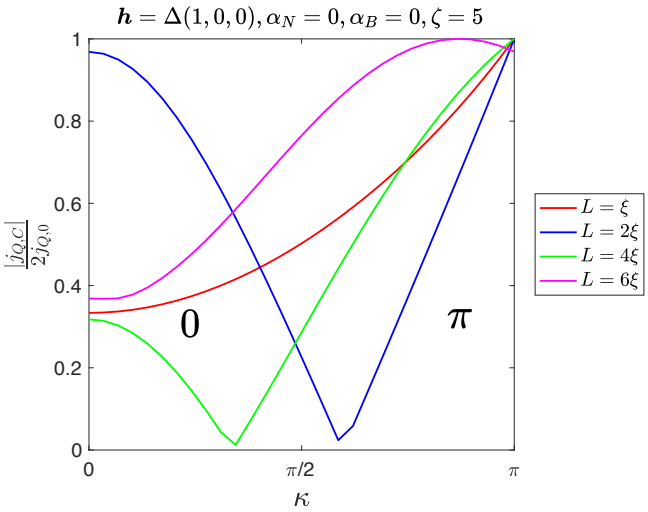


Figure 14: The absolute value of the critical charge current for different lengths of the curved ferromagnetic wire as a function of the curvature $\kappa$. The critical charge current for a given length is normalized to its maximal value. The exchange field is chosen to be tangential and of strength equal to the superconducting gap $\Delta$. The spin-orbit strength in both the normal and binormal direction is set to zero and the interface resistance ratio is $\zeta = 5$.

Figure 14 shows the absolute value of the critical charge current for different lengths of the ferromagnetic wire as a function of the curvature. The critical charge current is shown normalized to its maximum value in order to provide a comparable plot with different ferromagnetic wire lengths. Here we see that the $0 - \pi$ transition happens at roughly $\kappa_C \approx 3\pi/5$ for a Josephson junction with a ferromagnetic wire of length $L = 2\xi$. By finely tuning the curvature around this critical value of $\kappa$ we can toggle between the 0 and $\pi$ state. For a ferromagnetic wire length of $L = 4\xi$ the value of the critical curvature is shifted to a lower value $\kappa_C \approx \pi/3$. For short wire lengths $L = \xi$ and long wire lengths $L = 6\xi$ the $0 - \pi$ transition is not present with curvatures in the range $\kappa \in \{0, \pi\}$.

Adding torsion permits higher curvatures without the two superconductors in both ends to coincide in space and could possibly allow for a $0-\pi$ transition for $L = \xi$. Figure 14 suggests that the critical value of the curvature occurs at lower values for longer wire lengths and *vice versa*. The case of $L = 2\xi$ is particularly interesting since the magnitude of the critical charge current at $\kappa = 0$ and $\kappa = \pi$ is roughly equal. This is not the case for the wire of length $L = 4\xi$.

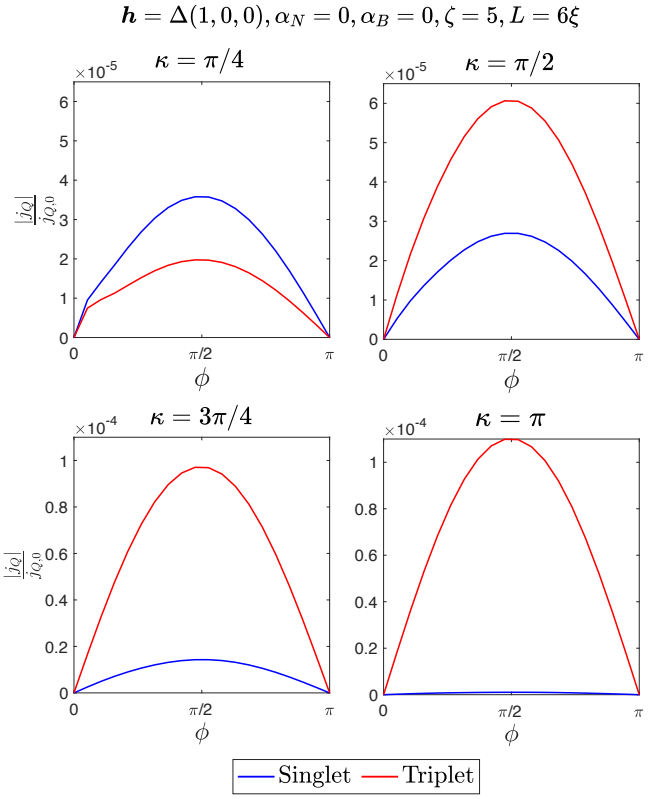


Figure 15: The absolute value of the singlet- (blue) and triplet- (red) contribution to the charge current density as a function of the phase difference $\phi$ for different curvatures $\kappa$. The exchange field is in the tangential direction with strength $\Delta$ and the length of the ferromagnet is $L = 6\xi$. The spin-orbit strength in both the normal and binormal direction is set to zero and the interface resistance ratio is $\zeta = 5$.

The $0-\pi$ transition may be explained by singling out the singlet and triplet contribution to the charge current. The transition from a singlet-dominated to a triplet-dominated system is manifested in the sign change of the charge current. The contribution to the charge current from the singlets and triplets are shown in Figure 15 where the contributions are plotted as a function of the phase difference $\phi$ for different curvatures and a ferromagnetic wire of length $L = 6\xi$.

Since the curvature is the generator of triplets, only singlet currents are present in the Josephson junction for zero curvature. Introducing curvature induces triplet correlations in the ferromagnet as seen in Figure 15. For a curvature of $\kappa = \pi/4$ the system is still dominated by the singlets. Increasing the curvature to $\kappa = \pi/2$ results in the transition to a triplet dominated charge current. For a semicircular Josephson junction ($\kappa = \pi$) the system is completely dominated by triplets and the singlet contribution to the charge current is negligible. Hence, such a semicircular Josephson junction exhibits a pure triplet current. The triplet current is present trough a long junction compared to the coherence length ($L = 6\xi$), known as the long-ranged Josephson effect [72].

## 6.2 Spin torque

In order to get a better physical understanding of spin currents in curved nanostructures it is beneficial to investigate the expectation value of the spin vector of the triplet Cooper pair. The expectation value can be expressed in terms of the d-vector [73]

$$\langle \boldsymbol{S} \rangle = i\boldsymbol{d} \times \tilde{\boldsymbol{d}}. \tag{6.34}$$

The d-vector may be decomposed in terms of the short-range triplet parallel to the exchange field and the long-range triplet normal to the exchange field, $\boldsymbol{d} = \boldsymbol{d}_{\mathrm{SR}} + \boldsymbol{d}_{\mathrm{LR}}$. As a specific example, consider an exchange field in the tangential and normal direction $\boldsymbol{h} = h_T\hat{\boldsymbol{\mathcal{T}}}(s) + h_N\hat{\boldsymbol{\mathcal{N}}}(s)$. Without loss of generality, the short- and long-range triplet components may be expressed as

$$\boldsymbol{d}_{\mathrm{SR}} = d_{\mathrm{SR}}\frac{h_T}{h}\hat{\boldsymbol{\mathcal{T}}}(s) + d_{\mathrm{SR}}\frac{h_N}{h}\hat{\boldsymbol{\mathcal{N}}}(s), \tag{6.35}$$

$$\boldsymbol{d}_{\mathrm{LR}} = g_2\frac{h_N}{h}\hat{\boldsymbol{\mathcal{T}}}(s) - g_2\frac{h_T}{h}\hat{\boldsymbol{\mathcal{N}}}(s) + g_1\hat{\boldsymbol{\mathcal{B}}}(s), \tag{6.36}$$

where $d_{SR}$, $g_1$ and $g_2$ are scalar functions and $h$ is the exchange field strength. These definitions of the short- and long-range triplets preserve the corresponding parallel and normal conditions to the exchange field. Using equation (6.36) and the formula for curvilinear cross products given in equation (A.5), the long-range and short-range contribution to the expectation value of the spin vector is

$$\langle \boldsymbol{S} \rangle_{\mathrm{LR}} = i\boldsymbol{d}_{\mathrm{LR}} \times \tilde{\boldsymbol{d}}_{\mathrm{LR}} = i(g_1\tilde{g_2} - g_2\tilde{g_1})\left[\frac{h_T}{h}\hat{\boldsymbol{\mathcal{T}}}(s) + \frac{h_N}{h}\hat{\boldsymbol{\mathcal{N}}}(s)\right], \tag{6.37}$$

$$\langle \boldsymbol{S} \rangle_{\mathrm{SR}} = 0. \tag{6.38}$$

As expected, the long-range contribution to the spin-vector expectation value is non-zero and points along the direction of the exchange field. The short-range contribution to the spin-vector expectation value is zero due to the up/down spin-structure of the short range triplets. The total expectation value of the spin vector is

$$\langle \boldsymbol{S} \rangle_{\mathrm{tot}} = i(\boldsymbol{d}_{\mathrm{SR}} + \boldsymbol{d}_{\mathrm{LR}}) \times (\tilde{\boldsymbol{d}}_{\mathrm{SR}} + \tilde{\boldsymbol{d}}_{\mathrm{LR}}) = \langle \boldsymbol{S} \rangle_{\mathrm{LR}} + \langle \boldsymbol{S} \rangle_{\mathrm{mix}} + \langle \boldsymbol{S} \rangle_{\mathrm{ex}}, \tag{6.39}$$

where we have identified a mixing and exchange term given by

$$\langle \boldsymbol{S} \rangle_{\mathrm{mix}} = S_1\left(\frac{h_T}{h}\hat{\boldsymbol{\mathcal{N}}}(s) - \frac{h_N}{h}\hat{\boldsymbol{\mathcal{T}}}(s)\right), \qquad \langle \boldsymbol{S} \rangle_{\mathrm{ex}} = S_2\hat{\boldsymbol{\mathcal{B}}}(s), \tag{6.40}$$

and $S_j = i(\tilde{d}_{\mathrm{SR}}g_j - \tilde{g}_j d_{\mathrm{SR}})$. Hence, there exists an interference term between the long-range and short-range triplets consisting of a mixing term where the spin polarization depends on the direction of the exchange field and an exchange term independent of the exchange field. The strength of the interference term depends implicitly on the curvature of the system through the scalar functions $d_{SR}$, $g_1$ and $g_2$ in the prefactor $S_j$.

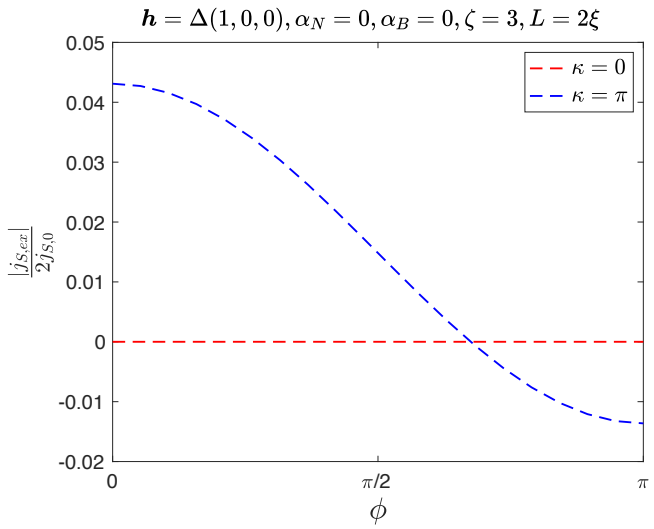


Figure 16: The normalized exchange spin current as a function of the phase difference $\phi$ for a straight wire $\kappa = 0$ and a semicircular wire $\kappa = \pi$, both of length $L = 2\xi$. The exchange field is chosen to be tangential and of strength equal to the superconducting gap $\Delta$. The spin-orbit strength in both the normal and binormal direction is set to zero and the interface resistance ratio is $\zeta = 3$.

Figure 16 shows the exchange spin current density $j_{S,\text{ex}}$ as a function of the phase difference for $\kappa = 0$ and $\kappa = \pi$ and a tangential exchange field. For a straight wire ($\kappa = 0$) with no spin-orbit coupling, no long-range triplets are generated and the superconducting correlations will be in either the singlet state, or polarized along the tangential exchange field. Consequently, there is no contribution to the exchange spin current for $\kappa = 0$ as seen in Figure 16. Introducing curvature induces an exchange spin current. The exchange spin-current is finite for both $\phi = 0$ and $\phi = \pi$ in contrast to the charge current [74]. For a phase difference of 0 and $\pi$ we thus have a pure spin-current flowing in the junction with total absence of charge currents.

The exchange spin current density $j_{S,\text{ex}}$, given in equation (6.25), may be interpreted as a field-like spin-torque acting on the magnetization, an effect present even in the absence of charge currents. Due to the misalignment of the exchange spin-expectation value given in equation (6.40) and the the tangential exchange field $\boldsymbol{h}$, the exchange spin current will act as a spin-torque in order to rotate $\boldsymbol{h}$ perpendicular to the spin, eliminating the misalignment. Such a spin-torque has been studied for straight superconductor-ferromagnet nanostructures with intrinsic spin-orbit coupling [73].

# 7 Summary, outlook and concluding remarks

Superconducting spintronics is a major emerging field in condensed matter physics, allowing for dissipationless currents and protection from spin-flip scattering. A key aspect of superconducting spintronics is the proximity effect, where properties of adjacent materials can leak into each other. A particularly interesting system is the superconductor-ferromagnet proximity system, where the magnetization in the ferromagnet tends to align electron spins allowing for spin-polarized currents. A problem with conventional superconductor-ferromagnet proximity systems is the short decay lengths of the superconducting singlet correlations. One way to resolve this is to introduce spin-orbit coupling to the ferromagnet, resulting in the generation of long-range triplets. However, for superconductor-ferromagnet proximity systems to have greater applicability in the creation of superconducting spintronic devices, a controllable, or tunable, spin-orbit coupling would be beneficial.

In this thesis we have investigated the possibility of using curvature as a tunable spin-orbit coupling in diffusive superconductor-ferromagnet proximity structures. The presence of curvature produces a strain-induced electric field breaking the inversion symmetry, resulting in a Rashba-type spin-orbit coupling with strength proportional to the curvature. Using the framework of quasiclassical Green's functions, the Usadel equation in curvilinear coordinates valid for torsion-free nanowires and thin films was derived. The weak proximity equations for the limiting case of a 1D nanowire arc curved in the shape of a circle-portion and the equivalence with a straight wire with a rotating exchange field was shown. Furthermore, the curvilinear Usadel equation was solved numerically in order to plot physical observables like the magnetization and current for 1D nanowire arcs. The magnetization and the charge current confirmed the presence of curvature-induced long-range triplets in nanowires curved as a portion of a circle.

The generality of the theory of curved proximity structures presented in Section 3 in this thesis, allows for many options of further development. Below we outline three different possible extensions of the theory of curved proximity systems.

## 7.1 Non-uniform curvature and torsion

A natural continuation in the development of the theory of diffusive curved superconductor-ferromagnet proximity structures is to consider non-constant curvature structures like an ellipse. As we derived in this thesis, the spin-orbit strength due to the curvature is proportional to the curvature itself. Hence, for ellipses the spin-orbit strength and thus also the spin-orbit field will be inhomogeneous throughout the ellipse. Elliptical quantum rings have been studied in the clean limit [75], [76] where it was found that the triplet d-vector exhibits winding along the curved profile, but has yet to be investigated for diffusive systems.

In this thesis we have only considered torsion-free structures, since the addition of torsion is expected to work as an additional curvature-like term. However, adding torsion does give a higher geometrical degree of freedom. A concrete example is the curved Josephson junction considered in Section 6. In order to avoid the two superconductors at the ends of the curved ferromagnet to coincide in space, the curvature cannot exceed $\kappa = \pi$ (a semicircle). The addition of torsion can solve this problem, allowing for a spiral wire with arbitrary curvature.

## 7.2 Curvature in other classes of materials

Due to the generality of the approach when considering curved diffusive proximity systems, the theory may be used in the study of other types of materials such as e.g. antiferromagnets. Antiferromagnets show great promise for spintronics due to their robustness towards external magnetic fields and ultrafast dynamics [77].

In this thesis we have considered curved ferromagnets in close proximity with straight superconductors. However, adding curvature to the superconductor rather than (or in combination with) the ferromagnet is possible. Adding curvature to the superconductor affects the superconducting order parameter which will depend on the curvature [78]. Consequently, the Usadel equation should be modified in order to encapsulate the curvature dependence of the order parameter. In addition, the assumption of a bulk solution in the superconductor is not expected to be a good approximation when introducing curvature in the superconductor. Hence, the Usadel equation should be solved both in the ferromagnet and the superconductor.

Curvature may be added to a combination of two superconductors and two ferromagnets in order to create an SFSF ring. As discussed in Section 1.1, such a system may be used as a SQUID (superconducting quantum interference device). Adding curvature to a superconductor induces spin-orbit coupling which affects the superconducting pairing symmetry, and allows for the generation of spin-triplets in the superconductor manifested by an amplification of the Josephson current [78]. Hence, a SFSF ring may work as a curvature-induced long-range spin-triplet SQUID.

## 7.3 2D curved thin films

One possible continuation, is to consider 2D and 3D curved structures like the thin film discussed Section 3. The Usadel equation in 1D is non-trivial to solve analytically, but can be done numerically using a partial differential equation solver like the `bvp6c` used in this thesis. However, in higher dimension (2D,3D) this is no longer an option and a more complicated numerical solution scheme is needed. To solve the 2D Usadel equation valid for curved thin films given in equation (3.42) one can utilize a numerical method known as the finite element method. The finite element method is based on discretization of the derivatives in the partial differential equation using a Taylor expansion. In 2D, such a discretization results in a grid where derivatives at a certain coordinate point

are calculated using the values at neighbouring points as pictured in Figure 17. This solution scheme sounds rather simple, but things get exponentially more difficult when considering more complicated geometries like arbitrarily curved thin films. The following introduction for the finite element method for arbitrary geometries is heavily based on the PhD thesis by Amundsen [63].

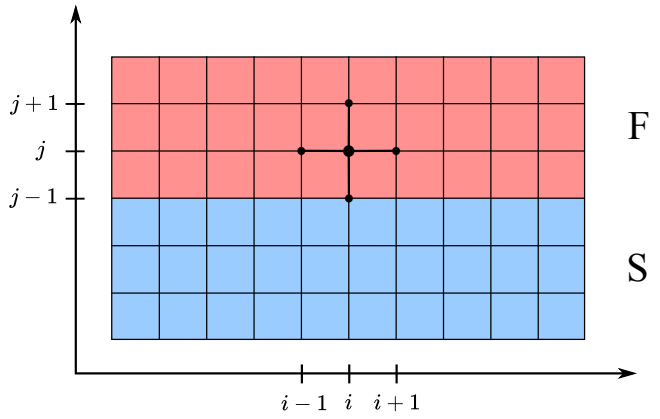


Figure 17: Discretization of a SF bilayer, showing the neighbouring points at site $(i, j)$ on the grid.

The Riccati parametrized Usadel equation may be generalized in the form

$$\nabla^2\Gamma^{(n)} = F^{(n)}(\gamma, \tilde{\gamma}, \nabla\gamma, \nabla\tilde{\gamma}), \tag{7.1}$$

where $\Gamma = (\gamma_{11}, \gamma_{12}, \gamma_{21}, \gamma_{22}, \tilde{\gamma}_{11}, \tilde{\gamma}_{12}, \tilde{\gamma}_{21}, \tilde{\gamma}_{22})$. Similarly the Riccati parametrized Kuprianov-Lukichev boundary conditions may be expressed as

$$\hat{\boldsymbol{n}} \cdot \nabla\Gamma^{(n)} = G^{(n)}(\gamma, \tilde{\gamma}). \tag{7.2}$$

Multiplying equation (7.1) with a test function $a(\boldsymbol{r})$ and performing an integration over the volume to be studied $\Omega$, results in an integral equation

$$-\int_\Omega d\boldsymbol{r}\nabla\Gamma^{(n)} \cdot \nabla a(\boldsymbol{r}) + \int_{\partial\Omega} dS\hat{\boldsymbol{n}} \cdot \nabla\Gamma^{(n)} a(\boldsymbol{r}) - \int_\Omega F^{(n)} a(\boldsymbol{r}) = 0, \tag{7.3}$$

where $\partial\Omega$ is the boundary of $\Omega$ and the divergence theorem has been used.

By discretising the space defined by $\Omega$, where each discrete point is called an element, we may expand the solution to equation (7.1) in terms of a finite set of basis functions $\phi_i$

$$\Gamma^{(n)}(\boldsymbol{r}) = \sum_i \Gamma_i^{(n)} \phi_i(\boldsymbol{r}), \tag{7.4}$$

where $\Gamma_i^{(n)}$ are some expansion coefficients to be determined. The test function $a(\boldsymbol{r})$ may be chosen to be the sum of the basis functions

$$a(\boldsymbol{r}) = \sum_i \phi_i. \tag{7.5}$$

The contribution to the integral equation (7.3) from a single element may now be written in terms of the basis functions

$$-\sum_{ij}\int_{\Omega_e} d\boldsymbol{r}\nabla\phi_i\cdot\nabla\phi_j\Gamma_i^{(n)}+\sum_{ij}\int_{\partial\Omega_e} dSG_i^{(n)}\phi_j-\sum_{ij}\int_{\Omega_e} F_i^{(n)}\phi_j=0, \quad (7.6)$$

where $\Omega_e$ is the element volume.

When considering curved geometries the elements of the discretization of the space $\Omega$ will be deformed. The deformation may be described by the basis functions

$$x=\sum_i \phi_i(\xi), \qquad y=\sum_i \phi_i(\eta), \qquad \sum_i \phi_i(\zeta), \quad (7.7)$$

where $\{\xi,\eta,\zeta\}$ are the coordinates in a corresponding straight coordinate system as pictured in Figure 18.

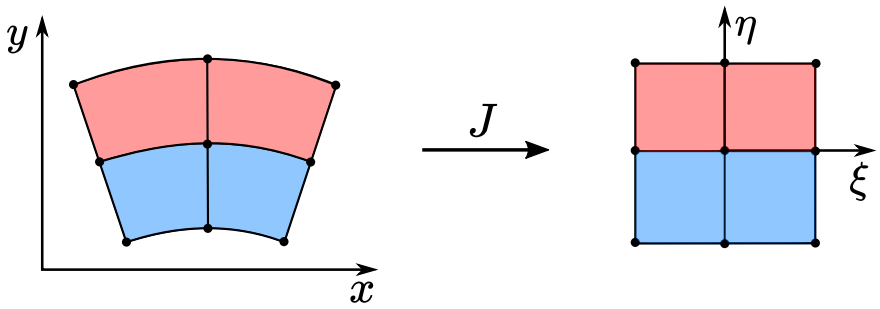


Figure 18: Transformation from a deformed element in a coordinate system $\{x,y,z\}$ to a coordinate system $\{\xi,\eta,\zeta\}$ where the element is undistorted. The transformation is described by the Jacobian matrix $J$.

The transformation from $\boldsymbol{r}=(x,y,z)$ to $\boldsymbol{\rho}=(\xi,\eta,\zeta)$ may be described by the Jacobian matrix, $J$. The coordinate differential in the integration in equation (7.6) transforms accordingly $d\boldsymbol{r}\to|J|d\boldsymbol{\rho}$. Similarly the gradients in equation (7.6) transforms as $\nabla\to J^{-1}\nabla_\rho$. Using these transformation the integrals in equation (7.6) may be evaluated using a numerical quadrature in order to determine the unknown coefficients $\Gamma_i^{(n)}$.

The benefit of using the finite element method over other methods is the generality in geometry it offers. This is especially useful in the framework of curved superconductor-ferromagnet proximity systems discussed in this thesis. Herein we have only considered Kuprianov-Lukichev boundary conditions. The addition of spin active interface boundary conditions is possible, but may require a modification of the form of the boundary condition in equation (7.2).

Finally, the numerical scheme outlined here is greatly simplified and an in depth study is needed before an eventual implementation. For a more complete introduction see [63].

## 7.4 Concluding remarks

In addition to the development of a general theory for curved diffusive superconductor-ferromagnet proximity systems, two major discoveries resulted from the work in this thesis. Firstly, the long-range Josephson effect, present in curved Josephson junctions. Secondly, a curvature-induced dynamical $0-\pi$ transition in curved Josephson junctions of certain lengths. We showed numerically that tuning the curvature around specific length-dependent curvatures works as a $0-\pi$ transition in the charge current. Both the dynamical $0-\pi$ transition and the long-range Josephson effect has potential applications in superconducting spintronic devices and quantum computers, and the curvature as the generator provides a possible physical implementation. The theory presented in this thesis in combination with the experimental development of low dimensional curved nanostructures, may enable a practical method for preparing superconducting spintronic devices, the building blocks for "cool" computers.

# References


[1] Wolpert, D. (2018). "Why Do Computers Use So Much Energy?", blog *Scientific American*. Available at: https://blogs.scientificamerican.com/observations/why-do-computers-use-so-much-energy/.

[2] Rauchs, M., Blandin, A., Dek, A. & Wu, Y. (2021). *Cambridge Bitcoin Electricity Consumption Index*, Available at:https://cbeci.org(Accessed 22 April 2021).

[3] Jacobsen, S., Ouassou, J. & Linder, J. (2017). "Superconducting Order in Magnetic Heterostructures" In: Tiwari, A. Iyer, P., Kumar, V. Swart, H. (eds) *Advanced Magnetic and Optical Materials*. Beverly: Scrivener Publishing, pp. 3-46.

[4] Linder, J. & Robinson, J. (2015). "Superconducting spintronics", *Nature Physics*, 11 (4), pp. 307-315. DOI: https://doi.org/10.1038/nphys3242.

[5] Hirohata, A., Yamada, K., Nakatani, Y., Prejbeanu, I., Diény, B., Pirro, P. & Hillebrands, B. (2020). "Review on spintronics: Principles and device applications", *Journal of Magnetism and Magnetic Materials*, 509. p. 166711. DOI: https://doi.org/10.1016/j.jmmm.2020.166711.

[6] Bulaevskii, L., Kuzii. V. & Sobyanin, A. (1977). "Superconducting system with weak coupling to the current in the ground state", *JETP Lett.*, 25 (7), pp. 290-293.

[7] Bergeret, F., Volkov, A. & Efetov, K. (2001). "Long-Range Proximity Effects in Superconductor-Ferromagnet Structures", *Phys. Rev. Lett.*, 86 (18), pp. 4096-4099. DOI: https://doi.org/10.1103/PhysRevLett.86.4096.

[8] Keizer, R., Goennenwein, S., Klapwijk, T., Miao, G., Xiao, G. & Gupta, A. (2006). "A spin triplet supercurrent through the half-metallic ferromagnet CrO2", *Nature*, 439 (2), pp. 825-827. DOI: https://doi.org/10.1038/nature04499.

[9] Sosnin, I., Cho, H., Petrashov, V.T. & Volkov, A.F. (2006). "Superconducting Phase Coherent Electron Transport in Proximity Conical Ferromagnets", *Phys. Rev. Lett.*, 96 (15), p. 157002. DOI: https://doi.org/10.1103/PhysRevLett.96.157002.

[10] Bergeret, F. & Tokatly, I. (2014). "Spin-orbit coupling as a source of long-range triplet proximity effect in superconductor-ferromagnet hybrid structures", *Phys. Rev. B*, 89 (13), p. 134517. DOI: https://doi.org/10.1103/PhysRevB.89.134517.

[11] Jacobsen, S., Ouassou, J. & Linder, J. (2015). "Critical temperature and tunneling spectroscopy of superconductor-ferromagnet hybrids with intrinsic Rashba-Dresselhaus spin-orbit coupling", *Phys. Rev. B*, 92 (2), p. 024510. DOI: https://doi.org/10.1103/PhysRevB.92.024510.

[12] Jacobsen, S. & Linder, J. (2015). "Giant triplet proximity effect in $\pi$-biased Josephson junctions with spin-orbit coupling", *Phys. Rev. B*, 92 (2), p. 024501. DOI: https://doi.org/10.1103/PhysRevB.92.024501.

[13] Jacobsen, S. & Linder, J. (2017). "Quantum kinetic equations and anomalous nonequilibrium Cooper-pair spin accumulation in Rashba wires with Zeeman splitting", *Phys. Rev. B*, 96 (13), p. 134513. DOI: https://doi.org/10.1103/PhysRevB.96.134513.

[14] Liang, D. & Gao, X.P.A. (2012). "Strong Tuning of Rashba Spin–Orbit Interaction in Single InAs Nanowires", *Nano Lett.*, 12 (6), pp. 3263–3267. DOI: https://doi.org/10.1021/nl301325h.

[15] Gentile, P., Cuoco, M. & Ortix, C. (2013). "Curvature-induced Rashba spin-orbit interaction in strain-driven nanostructures", *SPIN*, 3 (3), p. 1340002. DOI: https://doi.org/10.1142/S201032471340002X.

[16] Vasyukov, D., Anahory, Y., Embon, L., Halbertal, D., Cuppens, J., Neeman, L., Finkler, A., Segev, Y., Myasoedov, Y., Rappaport, M.L., Huber, M.E. & Zeldov, E. (2013). "A scanning superconducting quantum interference device with single electron spin sensitivity", *Nature Nanotech*, 8, pp. 639–644. DOI: https://doi.org/10.1038/nnano.2013.169.

[17] Glick, J.A., Aguilar, V., Gougam, A.B., Niedzielski, B.M., Gingrich, E.C., Loloee, R., Pratt Jr., W.P. & Birge, N.O. (2018). "Phase control in a spin-triplet SQUID", *Science Advances*, 4 (7), DOI: https://doi.org/10.1126/sciadv.aat9457.

[18] Thess, E., Lee, R., Nikolaev, P., Dai, H., Petit P., Robert, J., Xu, C., Lee, Y.H., Kim, S.G., Rinzler, A.G., Colbert, D.T., Scuseria, G.E., Tománek, D., Fischer, J.E. & Smalley R.E. (1996). "Crystalline Ropes of Metallic Carbon Nanotubes", *Science*, 273 (5274), pp. 483-487. DOI: https://doi.org/10.1126/science.273.5274.483.

[19] Prinz, V.Y., Seleznev, V.A., Gutakovsky, A.K., Chehovskiy, A.V., Preobrazhenskii, V.V., Putyato, M.A. & Gavrilova, T.A. (2000). "Free-standing and overgrown InGaAs//GaAs nanotubes, nanohelices and their arrays", *Physica E*, 6 (1), pp. 828-831. DOI: https://doi.org/10.1016/S1386-9477(99)00249-0.

[20] Schmidt, O.G., Eberl, K. (2001). "Thin solid films roll up into nanotubes", *Nature*, 410 (168), DOI: https://doi.org/10.1038/35065525.

[21] Mei, Y., Kiravittaya, S., Benyoucef, M., Thurmer, D.J., Zander, T., Deneke, C., Cavallo, F., Rastelli, A. & Schmidt, O.G. (2007). "Optical Properties of a Wrinkled Nanomembrane with Embedded Quantum Well", *Nano Lett.*, 7 (6), pp. 1676–1679. DOI: https://doi.org/10.1021/nl070653e.

[22] Xu, S., Yan, Z., Jang K., Huang, W., Fu, H., Kim, J., Wei, Z., Flavin, M., McCracken, J., Wang, R., Badea, A., Liu, Y., Xiao, D., Zhou, G., Lee, J., Chung, H.U., Cheng, H., Ren, W., Banks, A., Li, X., Paik, U., Nuzzo, R.G., Huang, Y., Zhang, Y. & Rogers, J.A. (2015). "Assembly of micro/nanomaterials into complex, three-dimensional architectures by compressive buckling", *Science*, 347 (6218), pp. 154-159. DOI: https://doi.org/10.1126/science.1260960.

[23] Volkov, O.M., Kákay, A., Kronast, F., Mönch, I., Mawass, M., Fassbender, J. & Makarov, D. (2019). "Experimental Observation of Exchange-Driven Chiral Effects in Curvilinear Magnetism", *Phys. Rev. Lett.* 123 (7), p. 077201. DOI: https://doi.org/10.1103/PhysRevLett.123.077201.

[24] Das, K.S., Makarov, D., Gentile, P., Cuoco, M., van Wees, B.J., Ortix, C. & Vera-Marun, I.J. (2019). "Independent Geometrical Control of Spin and Charge Resistances in Curved Spintronics", *Nano Lett.*, 19 (10), pp. 6839–6844. DOI: https://doi.org/10.1021/acs.nanolett.9b01994.

[25] Kamerlingh Onnes, H. (1911). "Further experiments with liquid helium. C. On the change of electric resistance of pure metals at very low temperatures etc. IV. The resistance of pure mercury at helium temperatures", *Koninklijke Nederlandse Akademie van Wetenschappen Proceedings Series B Physical Sciences*, 13 , pp. 1274-1276.

[26] Bardeen, J., Cooper, L. & Schreiffer, J. (1957). "Theory of Superconductivity", *Phys. Rev.*, 108 (5), pp. 1175-1204. DOI: https://doi.org/10.1103/PhysRev.108.1175.

[27] Tinkham, M. (1996). *Introduction to Superconductivity*, 2nd ed. McGraw-Hill, Inc., New York.

[28] Ouassou, J. (2019). "Manipulating superconductivity in magnetic nanostructures in and out of equilibrium", PhD thesis, NTNU, Trondheim.

[29] Chandrasekhar, V. (2008). "Proximity–Coupled Systems: Quasiclassical Theory of Superconductivity" In: Bennemann K., Ketterson J. (eds)b *Superconductivity.* Springer, Berlin, Heidelberg, pp. 279-313.

[30] Belzig, W., Wilhelm, F.K., Bruder, C., Schön, G. & Zaikin, A.D. (1999). "Quasiclassical Green's function approach to mesoscopic superconductivity", *Superlattices and Microstructures*, 25 pp. 1251–1288. DOI: http://doi.org/10.1006/spmi.1999.0710.

[31] Coey, J. (2010). *Magnetism and Magnetic Materials*, Cambridge University Press, New York.

[32] Buzdin, A. (2005). "Proximity effects in superconductor-ferromagnet heterostructures", *Rev. Mod. Phys.*, 77 (3), pp. 935–976. DOI: https://doi.org/10.1103/RevModPhys.77.935.

[33] Neuenschwander, D. (2014). *Tensor Calculus for Physics*, Johns Hopkins University Press, Baltimore.

[34] Ricci, M.M.G. & Levi-Civita, T. (1900). "Méthodes de calcul différentiel absolu et leurs applications", *Math. Ann.*, 54, pp. 125–201. DOI: https://doi.org/10.1007/BF01454201.

[35] Keldysh, L.V. (1965). "Diagram technique for nonequilibrium processes", *Soviet Physics JETP*, 20 (4), pp. 1018–1026.

[36] Rammer, J. (1986). "Quantum field-theoretical methods in transport theory of metals", *Reviews of Modern Physics*, 58 (2), pp. 323-359. DOI: https://doi.org/10.1103/RevModPhys.58.323.

[37] Nambu, Y. (1960). "Quasi-Particles and Gauge Invariance in the Theory of Superconductivity", *Phys. Rev.*, 117 (3), pp. 648-663. DOI: https://doi.org/10.1103/PhysRev.117.648.

[38] Linder, J., Yokoyama, T. & Sudbø, A. (2008). "The role of interface transparency and spin-dependent scattering in diffusive ferromagnet/superconductor heterostructures", *Phys. Rev. B*, 77 (17), p. 174514. DOI: https://doi.org/10.1103/PhysRevB.77.174514.

[39] Millis, A., Rainer, D. & Sauls, J.A. (1988). "Quasiclassical theory of superconductivity near magnetically active interfaces", *Phys. Rev. B*, 38 (7), pp. 4504-4515. DOI: https://doi.org/10.1103/PhysRevB.38.4504.

[40] Usadel, K.D. (1970). "Generalized Diffusion Equation for Superconducting Alloys", *Phys. Rev. Lett.*, 25 (8), pp. 507-509. DOI: https://doi.org/10.1103/PhysRevLett.25.507.

[41] Amundsen, M. & Linder, J. (2019). "Quasiclassical theory for interfaces with spin-orbit coupling", *Phys. Rev. B*, 100 (6), p. 064502. DOI: https://doi.org/10.1103/PhysRevB.100.064502.

[42] Zaĭtsev A. (1984). "Quasiclassical equations of the theory of superconductivity for contiguous metals and the properties of constricted microcontacts", *Sov. Phys. JETP*, 59 (5), pp. 1015-1024.

[43] Kuprianov, M. & Lukichev, V. (1988). "Influence of boundary transparency on the critical current of "dirty" SS'S structures", *Sov. Phys. JETP*, 67 (6), pp. 1163-1168.

[44] Eschrig, M., Cottet, A., Belzig, W. & Linder, J. (2015). "General boundary conditions for quasiclassical theory of superconductivity in the diffusive limit: application to strongly spin-polarized systems", *New J. Phys*, 17 (8), p. 083037. DOI: https://doi.org/10.1088/1367-2630/17/8/083037.

[45] Ortix, C. (2015). "Quantum mechanics of a spin-orbit coupled electron constrained to a space curve", *Phys. Rev. B*, 91 (24), p. 245412. DOI: https://doi.org/10.1103/PhysRevB.91.245412.

[46] Frenet, F. (1852). "Sur les courbes à double courbure", *Journal de Mathématiques Pures et Appliquées*, 17, pp. 437-447.

[47] Serret, J.A. (1851). "Sur quelques formules relatives à la théorie des courbes à double courbure", *Journal de Mathématiques Pures et Appliquées*, 16, pp. 193-207.

[48] Iyer, B.R. & Vishveshwara, C.V. (1993). "Frenet-Serret description of gyroscopic precession", *Phys. Rev. D*, 48 (12), pp. 5706–5720. DOI: https://doi.org/10.1103/PhysRevD.48.5706.

[49] Rashba, E. (1960). "Properties of semiconductors with an extremum loop. 1. Cyclotron and combinational resonance in a magnetic field perpendicular to the plane of the loop", *Sov. Phys. Solid State*, 2 (6), pp. 1224–1238.

[50] Dresselhaus, G. (1955). "Spin-Orbit Coupling Effects in Zinc Blende Structures", *Phys. Rev.*, 100 (2), pp. 580-586. DOI: https://doi.org/10.1103/PhysRev.100.580.

[51] Bardeen, J. & Shockley, W. (1950). "Deformation Potentials and Mobilities in Non-Polar Crystals", *Phys. Rev.*, 80 (1), pp. 72-80. DOI: https://doi.org/10.1103/PhysRev.80.72.

[52] Herring, C. & Vogt, E. (1957). "Transport and Deformation-Potential Theory for Many-Valley Semiconductors with Anisotropic Scattering", *Phys. Rev.*, 101 (3), pp. 944-961. DOI: https://doi.org/10.1103/PhysRev.101.944.

[53] Van de Walle, C. & Martin, R. (1986). "Theoretical calculations of heterojunction discontinuities in the Si/Ge system", *Phys. Rev. B*, 34 (8), pp. 5621-5634. DOI: https://doi.org/10.1103/PhysRevB.34.5621.

[54] Zhang, E., Zhang, S. & Wang, Q. (2007). "Quantum transport in a curved one-dimensional quantum wire with spin-orbit interactions", *Phys. Rev. B*, 75 (8), p. 085308. DOI: https://doi.org/10.1103/PhysRevB.75.085308.

[55] Mineev, V.P. & Volovik, G.E. (1992). "Electric dipole moment and spin supercurrent in superfluid $^3He$.", *J Low Temp Phys*, 89, pp. 823–830. DOI: https://doi.org/10.1007/BF00683888.

[56] Frönlich, J. & Studer, U.M. (1993). "Gauge invariance and current algebra in nonrelativistic many-body theory", *Rev. Mod. Phys.*, 65 (3), pp. 733-802. DOI: https://doi.org/10.1103/RevModPhys.65.733.

[57] Lewis, C.L. (2009). "Explicit gauge covariant Euler–Lagrange equation", *American Journal of Physics*, 77 (9), p. 839. DOI: https://doi.org/10.1119/1.3153503.

[58] Meijer, F., Morpurgo, A. & Klapwijk, T. (2002). "One-dimensional ring in the presence of Rashba spin-orbit interaction: Derivation of the correct Hamiltonian", *Phys. Rev. B*, 66 (3), p. 033107. DOI: https://doi.org/10.1103/PhysRevB.66.033107.

[59] Schopohl, N. & Maki, K. (1995). "Quasiparticle spectrum around a vortex line in a d-wave superconductor", *Phys. Rev. B*, 52 (1), pp. 490-493. DOI: https://doi.org/10.1103/PhysRevB.52.490.

[60] Champel, T. & Eschrig, M. (2005). "Switching superconductivity in superconductor/ferromagnet bilayers by multiple-domain structures", *Phys. Rev. B*, 71 (22), p. 220506. DOI: https://doi.org/10.1103/PhysRevB.71.220506.

[61] Mackenzie, P & Maeno, Y. (2003). "The superconductivity of $Sr_2RuO_4$ and the physics of spin-triplet pairing", *Rev. Mod. Phys.*, 75 (2), pp. 657-712. DOI: https://doi.org/10.1103/RevModPhys.75.657.

[62] Alexander, J., Orlando, T., Rainer, D. & Tedrow, P. (1985). "Theory of Fermi-liquid effects in high-field tunneling", *Phys. Rev. B*, 31 (9), pp. 5811-5825. DOI: https://doi.org/10.1103/PhysRevB.31.5811.

[63] Amundsen, M. (2020). "Proximity effects in superconducting hybrid structures with spin-dependent interactions", PhD thesis, NTNU, Trondheim.

[64] Sheka, D.D., Kravchuk, V.D. & Gaididei, Y. (2015). "Curvature effects in statics and dynamics of low dimensional magnets", *J. Phys. A: Math. Theor.*, 48 (12), p. 125202. DOI: https://doi.org/10.1088/1751-8113/48/12/125202.

[65] Alidoust, M., Linder, J., Rashedi, G. & Sudbø A. (2010). "Spin-polarized Josephson current in superconductor/ferromagnet/superconductor junctions with inhomogeneous magnetization", *Phys. Rev. B*, 81 (1), p. 014512. DOI: https://doi.org/10.1103/PhysRevB.81.014512.

[66] Shen, K., Vignale, G. & Raimondi, R. (2014). "Microscopic Theory of the Inverse Edelstein Effect", *Phys. Rev. Lett.*, 112 (9), p. 096601. DOI: https://doi.org/10.1103/PhysRevLett.112.096601.

[67] Edelstein, V.M (1990). "Spin polarization of conduction electrons induced by electric current in two-dimensional asymmetric electron systems", *Solid State Communications*, 73 (3), pp. 233-235. DOI: https://doi.org/10.1016/0038-1098(90)90963-C.

[68] Amundsen, M. & Linder, J. (2017). "Supercurrent vortex pinball via a triplet Cooper pair inverse Edelstein effect", *Phys. Rev. B*, 96 (6), p. 064508. DOI: https://doi.org/10.1103/PhysRevB.96.064508.

[69] Ryazanov, V.V., Oboznov, V.A., Rusanov, A.Yu., Veretennikov, A.V., Golubov, A.A. & Aarts, J. (2001). "Coupling of Two Superconductors through a Ferromagnet: Evidence for a $\pi$ Junction", *Phys. Rev. Lett.*, 86 (11), pp. 2427-2430. DOI: https://doi.org/10.1103/PhysRevLett.86.2427.

[70] Robinson, J.W.A., Piano, S., Burnell, G., Bell, C. & Blamire, M.G. (2006). "Critical Current Oscillations in Strong Ferromagnetic $\pi$ Junctions", *Physical Review Letters*, 97 (17), p. 177003. DOI: https://doi.org/10.1103/PhysRevLett.97.177003.

[71] Kontos, T., Aprili, M., Lesueur, J., Genêt, F., Stephanidis, B. & Boursier, R. (2002). "Josephson Junction through a Thin Ferromagnetic Layer: Negative Coupling", *Phys. Rev. Lett.*, 89 (13), p. 137007. DOI: https://doi.org/10.1103/PhysRevLett.89.137007.

[72] Golubov, A.A., Kupriyanov, M.Yu. & Il'ichev, E. (2004). "The current-phase relation in Josephson junctions", *Rev. Mod. Phys.*, 76 (2), pp. 411-469. DOI: https://doi.org/10.1103/RevModPhys.76.411.

[73] Jacobsen, S., Kulagina, I. & Linder, J. (2016). "Controlling superconducting spin flow with spin-flip immunity using a single homogeneous ferromagnet" *Sci Rep*, 6, p. 23926. DOI: https://doi.org/10.1038/srep23926.

[74] Chen, W., Horsch, P. & Manske, D. (2014). "Dissipationless spin current between two coupled ferromagnets", *Phys. Rev. B*, 89 (6), p. 064427. DOI: https://doi.org/10.1103/PhysRevB.89.064427.

[75] Ying, Z., Cuoco, M., Ortix, C. & Gentile, P. (2017). "Tuning pairing amplitude and spin-triplet texture by curving superconducting nanostructures", *Phys. Rev. B*, 96 (10), p. 100506. DOI: https://doi.org/10.1103/PhysRevB.96.100506.

[76] Ying, Z., Gentile, P., Ortix, C. & Cuoco, M. (2016). "Designing electron spin textures and spin interferometers by shape deformations", *Phys. Rev. B*, 94 (8), p. 081406. DOI: https://doi.org/10.1103/PhysRevB.94.081406.

[77] Baltz, V., Manchon, A., Tsoi, M., Moriyama, T., Ono, T. & Tserkovnyak, Y. (2018). "Antiferromagnetic spintronics", *Rev. Mod. Phys.*, 90 (1), p. 015005. DOI: https://doi.org/10.1103/RevModPhys.90.015005.

[78] Francica, G., Couco, M. & Gentile, P. (2020). "Topological superconducting phases and Josephson effect in curved superconductors with time reversal invariance", *Phys. Rev. B*, 101 (9), p. 094504. DOI: https://doi.org/10.1103/PhysRevB.96.100506.

[79] van Remortel, N. (2016). "The nature of natural units", *Nature Phys*, 12 (11), p. 1082. DOI: https://doi.org/10.1038/nphys3950.

# A
# Vector calculus in curvilinear coordinates

In this appendix physical vectors are denoted with a bold font and physical vector components are denoted with parenthesis around the index i.e. $\boldsymbol{A}$ is a physical vector with physical components $A_{(i)}$. The covariant and contravariant vector components are denoted without parenthesis and with a sub- and superscript respectively. Einstein summation is implied for covariant/contravariant contractions if not stated otherwise. This appendix contains all the needed vector identities in this thesis when considering curvilinear coordinates.

The metric tensor in curvilinear coordinates is given by

$$\eta_{ij} = \begin{pmatrix} H(s,n)^2 & 0 & 0 \\ 0 & 1 & 0 \\ 0 & 0 & 1 \end{pmatrix}, \tag{A.1}$$

where $H(s,n) = 1 - \kappa(s)n$ is the curvature dependent curvilinear scale factor. Using the metric tensor the non-zero Cristoffel symbols in curvilinear coordinates are

$$\begin{aligned} \Gamma^s_{ss} &= \frac{1}{H(s,n)}\partial_s H(s,n), \\ \Gamma^n_{ss} &= -H(s,n)\partial_n H(s,n), \\ \Gamma^s_{ns} &= \Gamma^s_{sn} = \frac{1}{H(s,n)}\partial_n H(s,n). \end{aligned} \tag{A.2}$$

Consider an arbitrary vector in Cartesian coordinates $\boldsymbol{A}(x,y,z)$. The same vector in curvilinear coordinates has the physical components

$$A_{(i)}(s,n,b) = \boldsymbol{A}(x,y,z) \cdot \hat{\boldsymbol{e}}_{(i)}, \tag{A.3}$$

where $\hat{\boldsymbol{e}}_{(i)}$ are the orthonormal basis vectors in curvilinear coordinates.

The scalar product and ordinary components of a cross product of two vectors in curvilinear coordinates can be expressed as

$$\boldsymbol{u} \cdot \boldsymbol{v} = u_i v^i = \eta^{ij} u_i v_j = u_{(i)} v_{(j)}, \tag{A.4}$$

$$(\boldsymbol{u} \times \boldsymbol{v})_{(i)} = \epsilon^{ijk} u_{(i)} v_{(j)}, \tag{A.5}$$

where $\epsilon^{ijk}$ is the Levi-Cevita symbol.

The gradient of a scalar field $\phi$ in curvilinear coordinates is given by

$$\nabla\phi = \frac{1}{h_{(i)}}(\partial_i\phi)\hat{\boldsymbol{e}}_{(i)} = \frac{1}{H(s,n)}(\partial_s\phi)\hat{\mathcal{T}}(s) + (\partial_n\phi)\hat{\mathcal{N}}(s) + (\partial_b\phi)\hat{\mathcal{B}}(s), \tag{A.6}$$

where the repeated index should not be interpreted as a summation and $h_{(i)}$ are the scale factors. The divergence of a vector $\boldsymbol{F}$ in curvilinear coordinates

can be derived using the coordinate covariant derivative

$$\begin{aligned}\nabla \cdot \boldsymbol{F} &= \mathcal{D}_i F^i = \eta^{ij}\mathcal{D}_i F_j = \eta^{ij}(\partial_i F_j - \Gamma^k_{ij} F_k) \\ &= \frac{1}{H(s,n)}\partial_s F_{(T)} + \frac{1}{H(s,n)}\partial_n(H(s,n)F_{(N)}) + \partial_b F_{(B)}.\end{aligned} \tag{A.7}$$

The coordinate covariant Laplacian of a scalar $\phi$ can be found by taking the divergence of the coordinate covariant derivative of $\phi$

$$\begin{aligned}\nabla^2\phi = \nabla\cdot(\nabla\phi) &= \mathcal{D}_i\mathcal{D}^i\phi = \eta^{ij}(\partial_i\partial_j\phi - \Gamma^k_{ij}\partial_k\phi) \\ &= \left[\frac{1}{H(s,n)}\partial_s(\frac{1}{H(s,n)}\partial_s) + \frac{1}{H(s,n)}\partial_n(H(s,n)\partial_n) + \partial_B^2\right]\phi.\end{aligned} \tag{A.8}$$

The contravariant components of the coordinate covariant curl of a vector $\boldsymbol{F}$ is given by

$$(\nabla\times\boldsymbol{F})^i = c^i = E^{ijk}\mathcal{D}_j F_k = \frac{1}{\sqrt{\eta}}\epsilon^{ijk}\mathcal{D}_j F_k, \tag{A.9}$$

where $E^{ijk} = \frac{1}{\sqrt{\eta}}\epsilon^{ijk}$ is the contravariant Levi-Cevita tensor and $\eta = |\det(\eta_{ij})|$. In curvilinear coordinates the physical components of the vector $\boldsymbol{c}$ are

$$c_{(T)} = [\partial_n F_{(B)} - \partial_b F_{(N)}], \tag{A.10}$$

$$c_{(N)} = \frac{1}{H(s,n)}[H(s,n)\partial_b F_{(T)} - \partial_s F_{(B)}], \tag{A.11}$$

$$c_{(B)} = \frac{1}{H(s,n)}[\partial_s F_{(N)} - \partial_n(H(s,n)F_{(T)})]. \tag{A.12}$$

The Jacobian in the transformation from Cartesian coordinates (x) to curvilinear coordinates (s) can be computed directly from the metric

$$|J| = |\partial_x s| = \sqrt{\frac{\eta(s)}{\eta(x)}} = \sqrt{\eta(s)} = H(s,n), \tag{A.13}$$

where $\eta(x) = 1$ is the determinant of the Cartesian metric.

# B
# Riccati parametrized Usadel equation

The Usadel equation for a nanowire arc reads

$$iD_F\tilde{\partial}_s(\hat{g}^R\tilde{\partial}_s\hat{g}^R) = [\epsilon\hat{\tau}_z - \hat{\Delta} - \boldsymbol{h}\cdot\hat{\boldsymbol{\sigma}}, \hat{g}^R], \tag{B.1}$$

where the retarded component of the quasiclassical Green's function in Nambu space is defined as

$$\hat{g}^R = \begin{pmatrix} \underline{g}^R & \underline{f}^R \\ -\underline{\tilde{f}}^R & -\underline{\tilde{g}}^R \end{pmatrix}. \tag{B.2}$$

In the Riccati parametrization, the retarded component of the quasiclassical Green's function may be written in terms of the gamma matrix and the N-matrix

$$\hat{g}^R = \begin{pmatrix} N & 0 \\ 0 & -\tilde{N} \end{pmatrix} \begin{pmatrix} 1+\gamma\tilde{\gamma} & 2\gamma \\ 2\tilde{\gamma} & 1+\tilde{\gamma}\gamma \end{pmatrix}. \tag{B.3}$$

The right hand side of the Usadel equation may be written explicitly as

$$\begin{aligned} \tilde{\partial}_s(\hat{g}^R\tilde{\partial}_s\hat{g}^R) = \partial_s(\hat{g}^R\partial_s\hat{g}^R) - i\partial_s(\hat{g}^R\hat{A}_T\hat{g}^R) + i\partial_s\hat{A}_T \\ - i[\hat{A}_T, \hat{g}^R\partial_s\hat{g}^R] - [\hat{A}_T, \hat{g}^R\hat{A}_T\hat{g}^R]. \end{aligned} \tag{B.4}$$

The reoccurring terms are $\hat{g}^R\tilde{\partial}_s\hat{g}^R$ and $\hat{g}^R\hat{A}_T\hat{g}^R$. These terms may be written in matrix form using equation (B.2)

$$\hat{g}^R\partial_s\hat{g}^R = \begin{pmatrix} \underline{g}^R\partial_s\underline{g}^R - \underline{f}^R\partial_s\underline{\tilde{f}}^R & \underline{g}^R\partial_s\underline{f}^R - \underline{f}^R\partial_s\underline{\tilde{g}}^R \\ \underline{\tilde{g}}^R\partial_s\underline{\tilde{f}}^R - \underline{\tilde{f}}^R\partial_s\underline{g}^R & \underline{\tilde{g}}^R\partial_s\underline{\tilde{g}}^R - \underline{\tilde{f}}^R\partial_s\underline{f}^R \end{pmatrix}, \tag{B.5}$$

$$\hat{g}^R\hat{A}_T\hat{g}^R = \begin{pmatrix} \underline{g}^R\underline{A}_T\underline{g}^R + \underline{f}^R\underline{A}_T^*\underline{\tilde{f}}^R & \underline{g}^R\underline{A}_T\underline{f}^R + \underline{f}^R\underline{A}_T^*\underline{\tilde{g}}^R \\ -\underline{\tilde{g}}^R\underline{A}_T\underline{\tilde{f}}^R - \underline{\tilde{f}}^R\underline{A}_T^*\underline{g}^R & -\underline{\tilde{g}}^R\underline{A}_T\underline{\tilde{g}}^R - \underline{\tilde{f}}^R\underline{A}_T^*\underline{f}^R \end{pmatrix}. \tag{B.6}$$

Due to the symmetry of equation (B.2), only the terms on the top row is needed. The top row terms in equation (B.4) can be expressed in the Riccati parametrization as

$$\begin{aligned} [\partial_s(\hat{g}^R\partial_s\hat{g}^R)]^{(1,1)} = 2N[(\partial_s^2\gamma) + 2(\partial_s\gamma)\tilde{N}\tilde{\gamma}(\partial_s\gamma)]\tilde{\gamma}N \\ - 2N\gamma[(\partial_s^2\tilde{\gamma}) + 2(\partial_s\tilde{\gamma})N\gamma(\partial_s\tilde{\gamma})]N, \end{aligned} \tag{B.7}$$

$$\begin{aligned} [\partial_s(\hat{g}^R\partial_s\hat{g}^R)]^{(1,2)} = 2N[(\partial_s^2\gamma) + 2(\partial_s\gamma)\tilde{N}\tilde{\gamma}(\partial_s\gamma)]\tilde{N} \\ - 2N\gamma[(\partial_s^2\tilde{\gamma}) + 2(\partial_s\tilde{\gamma})N\gamma(\partial_s\tilde{\gamma})]\gamma\tilde{N}, \end{aligned} \tag{B.8}$$

$$\begin{aligned}[\partial_s(\hat{g}^R\hat{A}\hat{g}^R)]^{(1,1)} &= 4N\gamma\underline{A}_T^*\tilde{N}[(\partial_s\tilde{\gamma})+\tilde{\gamma}(\partial_s\gamma)\tilde{\gamma}]N\\ &+4N[(\partial_s\gamma)+\gamma(\partial_s\tilde{\gamma})\gamma]\tilde{N}\underline{A}_T^*\tilde{\gamma}N\\ &+2N(1+\gamma\tilde{\gamma})\underline{A}_TN[\gamma(\partial_s\tilde{\gamma})+(\partial_s\gamma)\tilde{\gamma}]N\\ &+2N[\gamma(\partial_s\tilde{\gamma})+(\partial_s\gamma)\tilde{\gamma}]N\underline{A}_T(1+\gamma\tilde{\gamma})N\\ &+(2N-1)(\partial_s\underline{A}_T)(2N-1)\\ &+4N\gamma(\partial_s\underline{A}_T^*)\tilde{N}\tilde{\gamma},\end{aligned} \tag{B.9}$$

$$\begin{aligned}[\partial_s(\hat{g}^R\hat{A}\hat{g}^R)]^{(1,2)} &= 4N\gamma\underline{A}_T^*\tilde{N}[\tilde{\gamma}(\partial_s\gamma)+(\partial_s\tilde{\gamma})\gamma]\tilde{N}\\ &+4N[\gamma(\partial_s\tilde{\gamma})+(\partial_s\gamma)\tilde{\gamma}]N\underline{A}_T\tilde{\gamma}\tilde{N}\\ &+2N(1+\gamma\tilde{\gamma})\underline{A}_TN[(\partial_s\gamma)+\gamma(\partial_s\tilde{\gamma})\gamma]\tilde{N}\\ &+2N[(\partial_s\gamma)+\gamma(\partial_s\tilde{\gamma})\gamma]\tilde{N}\underline{A}_T^*(1+\tilde{\gamma}\gamma)\tilde{N}\\ &+(2N-1)(\partial_s\underline{A}_T)2N\gamma\\ &+2N\gamma(\partial_s\underline{A}_T^*)(2\tilde{N}-1),\end{aligned} \tag{B.10}$$

$$\begin{aligned}[[\hat{A}_T,\hat{g}^R\partial_s\hat{g}^R]]^{(1,1)} &= 2\underline{A}_TN[(\partial_s\gamma)\tilde{\gamma}-\gamma(\partial_s\tilde{\gamma})]N\\ &-2N[(\partial_s\gamma)\tilde{\gamma}-\gamma(\partial_s\tilde{\gamma})]N\underline{A}_T,\end{aligned} \tag{B.11}$$

$$\begin{aligned}[[\hat{A}_T,\hat{g}^R\partial_s\hat{g}^R]]^{(1,2)} &= 2\underline{A}_TN[(\partial_s\gamma)-\gamma(\partial_s\tilde{\gamma})\gamma]\tilde{N}\\ &+2N[(\partial_s\gamma)-\gamma(\partial_s\tilde{\gamma})\gamma]\tilde{N}\underline{A}_T^*,\end{aligned} \tag{B.12}$$

$$\begin{aligned}[[\hat{A}_T,\hat{g}^R\hat{A}_T\hat{g}^R]]^{(1,1)} &= 4\underline{A}_TN(\underline{A}_T+\gamma\underline{A}_T^*\tilde{\gamma})N-4N(\underline{A}_T+\gamma\underline{A}_T^*\tilde{\gamma})N\underline{A}_T\\ &-2[\underline{A}_T^2,N],\end{aligned} \tag{B.13}$$

$$\begin{aligned}[[\hat{A}_T,\hat{g}^R\hat{A}_T\hat{g}^R]]^{(1,2)} &= 4\underline{A}_TN(\underline{A}_T\gamma+\gamma\underline{A}_T^*)\tilde{N}+4N(\underline{A}_T\gamma+\gamma\underline{A}_T^*)\tilde{N}\underline{A}_T^*\\ &-4\underline{A}_TN\gamma\underline{A}_T^*-2(\underline{A}_T^2N\gamma+N\gamma(\underline{A}_T^*)^2).\end{aligned} \tag{B.14}$$

The top row of the right-hand side of the Usadel equation may be expressed in the Riccati parametrization as

$$\begin{aligned}[[\epsilon\hat{\tau}_z-\hat{\Delta}-\boldsymbol{h}\cdot\hat{\boldsymbol{\sigma}},\hat{g}^R]^{(1,1)} &= 2\underline{\Delta}\tilde{N}\tilde{\gamma}+2N\gamma\underline{\Delta}^*\\ &-\boldsymbol{h}\cdot\boldsymbol{\sigma}(2N-1)+(2N-1)\boldsymbol{h}\cdot\boldsymbol{\sigma},\end{aligned} \tag{B.15}$$

$$\begin{aligned}[[\epsilon\hat{\tau}_z-\hat{\Delta}-\boldsymbol{h}\cdot\hat{\boldsymbol{\sigma}},\hat{g}^R]^{(1,2)} &= 4\epsilon N\gamma+\underline{\Delta}(2\tilde{N}-1)+(2N-1)\gamma\underline{\Delta}^*\\ &-2\boldsymbol{h}\cdot\boldsymbol{\sigma}N\gamma+2N\gamma\boldsymbol{h}\cdot\boldsymbol{\sigma}^*.\end{aligned} \tag{B.16}$$

To simplify the left-hand side of the Riccati parametrized Usadel equation, we operate $[\tilde{\partial}_s(\hat{g}^R\tilde{\partial}_s\hat{g}^R)]^{(1,1)}$ with $\gamma$ from the right, subtract this from $[\tilde{\partial}_s(\hat{g}^R\tilde{\partial}_s\hat{g}^R)]^{(1,2)}$ and operate with $\frac{1}{2}N^{-1}$ from the left

$$\begin{aligned}
&\frac{1}{2}N^{-1}([\tilde{\partial}_s(\hat{g}^R\tilde{\partial}_s\hat{g}^R)]^{(1,2)} - [\tilde{\partial}_s(\hat{g}^R\tilde{\partial}_s\hat{g}^R)]^{(1,1)}\gamma)\\
&= (\partial_s^2\gamma) + 2(\partial_s\gamma)\tilde{N}\tilde{\gamma}(\partial_s\gamma) - 2i(\partial_s\gamma)\tilde{N}(\underline{A}_T^* + \tilde{\gamma}\underline{A}_T\gamma)\\
&- 2i(\underline{A}_T + \gamma\underline{A}_T^*\tilde{\gamma})N(\partial_s\gamma) - 2(\underline{A}_T\gamma + \gamma\underline{A}_T^*)\tilde{N}(\underline{A}_T^* + \tilde{\gamma}\underline{A}_T\gamma)\\
&- (\underline{A}_T^2\gamma - \gamma(\underline{A}_T^*)^2) + i(\partial_s\underline{A}_T)\gamma + i\gamma(\partial_s\underline{A}_T^*).
\end{aligned} \tag{B.17}$$

Similarly for the right hand side

$$\begin{aligned}
&\frac{1}{2}N^{-1}([\epsilon\hat{\tau}_z - \hat{\Delta} - \boldsymbol{h}\cdot\hat{\boldsymbol{\sigma}} - \check{\Sigma}_{sf}, \check{g}]^{(1,2)}\\
&- [\epsilon\hat{\tau}_z - \hat{\Delta} - \boldsymbol{h}\cdot\hat{\boldsymbol{\sigma}} - \check{\Sigma}_{sf}, \check{g}]^{(1,1)}\gamma)\\
&= 2\epsilon\gamma - (\gamma\underline{\Delta}^*\gamma - \underline{\Delta}) + \boldsymbol{h}\cdot(\boldsymbol{\sigma}\gamma - \gamma\boldsymbol{\sigma}^*).
\end{aligned} \tag{B.18}$$

Finally, the Riccati parametrized Usadel equation is achieved

$$\begin{aligned}
&D[(\partial_s^2\gamma) + 2(\partial_s\gamma)\tilde{N}\tilde{\gamma}(\partial_s\gamma)]\\
&= i(\gamma\underline{\Delta}^*\gamma - \underline{\Delta}) - i\boldsymbol{h}\cdot(\boldsymbol{\sigma}\gamma - \gamma\boldsymbol{\sigma}^*) - 2i\epsilon\gamma + 2Di(\partial_s\gamma)\tilde{N}(\underline{A}_T^* + \tilde{\gamma}\underline{A}_T\gamma)\\
&+ 2Di(\underline{A}_T + \gamma\underline{A}_T^*\tilde{\gamma})N(\partial_s\gamma) + 2D(\underline{A}_T\gamma + \gamma\underline{A}_T^*)\tilde{N}(\underline{A}_T^* + \tilde{\gamma}\underline{A}_T\gamma)\\
&+ D(\underline{A}_T^2\gamma - \gamma(\underline{A}_T^*)^2) - iD[(\partial_s\underline{A}_T)\gamma + \gamma(\partial_s\underline{A}_T^*)].
\end{aligned} \tag{B.19}$$

The Kuprianov Lukichev boundary conditions for a nanowire arc is given by

$$2L_j\zeta_j\hat{g}_j^R\tilde{\partial}_s\hat{g}_j^R = [\hat{g}_1^R, \hat{g}_2^R]. \tag{B.20}$$

The derivative term on the left-hand side of equation (B.20) may be written explicitly as

$$\hat{g}_j^R\tilde{\partial}_s\hat{g}_j^R = \hat{g}_j^R\partial_s\hat{g}_j^R - i\hat{g}_j^R[\hat{A}, \hat{g}_j^R]. \tag{B.21}$$

The upper row of the two terms on the right-hand side of equation (B.21) may be expressed in the Riccati parametrization as

$$[\hat{g}_j^R\partial_s\hat{g}_j^R]^{(1,1)} = 2N_j[(\partial_s\gamma_j)\tilde{\gamma_j} - \gamma_j(\partial_s\tilde{\gamma_j})]N_j, \tag{B.22}$$

$$[\hat{g}_j^R\partial_s\hat{g}_j^R]^{(1,2)} = 2N_j[(\partial_s\gamma_j) - \gamma_j(\partial_s\tilde{\gamma_j})\gamma_j]\tilde{N}_j, \tag{B.23}$$

$$\begin{aligned}
[g_j^R[\hat{A}, g_j^R]]^{(1,1)} &= 4N_j(\underline{A}_T + \gamma_j\underline{A}_T^*\tilde{\gamma}_j) - 2N_j\underline{A}_T(1 - \gamma_j\tilde{\gamma}_j)N_j\\
&\quad - 2N_j(1 - \gamma_j\tilde{\gamma}_j)\underline{A}_T N_j,
\end{aligned} \tag{B.24}$$

$$[g_j^R[\hat{A}, g_j^R]]^{(1,2)} = 2N_j(1 + \gamma_j\tilde{\gamma}_j)\underline{A}_T\gamma_j\tilde{N}_j + 2N_j\gamma_j\underline{A}_T^*(1 + \tilde{\gamma}_j\gamma_j)\tilde{N}_j. \tag{B.25}$$

By combining the terms, the final form of the Riccati parametrized Kuprianov Lukichev boundary conditions are achieved

$$\partial_s \gamma_1 = i(\gamma_1 \underline{A}_T^* + \underline{A}_T \gamma_1) + \frac{1}{L_1 \zeta_1}(1 - \gamma_1 \tilde{\gamma}_2) N_2 (\gamma_2 - \gamma_1), \tag{B.26}$$

$$\partial_s \gamma_2 = i(\gamma_2 \underline{A}_T^* + \underline{A}_T \gamma_2) + \frac{1}{L_2 \zeta_2}(1 - \gamma_2 \tilde{\gamma}_1) N_1 (\gamma_2 - \gamma_1). \tag{B.27}$$

# C
# MATLAB code

The MATLAB code utilizes the nonlinear differential equation solver bvp6c, a 6th order method implementing the Cash-Singhal 6 formula. The bvp6c-method returns a solution which is both continuous and has a continuous first derivative, useful when computing physical observables dependent on the derivative of the quasiclassical Green's function like the current density.

The code is split in two scripts; One solver-script using the bvp6c-function to solve the Riccati parametrized Usadel equation with the Kuprianov-Lukichev boundary conditions, and one script where user specific variables are defined and the physical observables are calculated. The superconductor is assumed to have the bulk solution which is used in the boundary conditions. In order to work with two separate scripts global variables are used.

# D
# Paper draft

The following paper was submitted for publication.

# Curvature-induced long ranged supercurrents in diffusive SFS Josephson Junctions, with dynamic $0-\pi$ transition

Tancredi Salamone,[1,*] Mathias B.M. Svendsen,[1] Morten Amundsen,[2] and Sol Jacobsen[1]

[1] *Center for Quantum Spintronics, Department of Physics, NTNU Norwegian University of Science and Technology, NO-7491 Trondheim, Norway*

[2] *Nordita, KTH Royal Institute of Technology and Stockholm University, Roslagstullsbacken 23, SE-106 91 Stockholm, Sweden*

We report that spin supercurrents can be induced in diffusive SFS Josephson junctions without any magnetic misalignment or intrinsic spin orbit coupling. Instead, the pathway to spin triplet generation is provided via geometric curvature, and results in a long ranged Josephson effect. In addition, the curvature is shown to induce a dynamically tunable $0-\pi$ transition in the junction. We provide the analytic framework and discuss potential experimental and innovation implications.

*Introduction.*— In the last two decades there have been substantial advances in the experimental realization of curved nanostructures. Since the realization of nanotubes by rolling up thin solid films [1], many new techniques of bending, wrinkling and buckling nanostructures in up to three dimensions have been developed [2, 3], as well as direct growth on curved templates [4], electron-beam lithography [5–7] and many more (see e.g. [8] and references therein). These techniques open a broad new range of spintronic device design, and have already been shown to enable independent control of spin and charge resistances [4].

Geometric curvature introduces two main effects: a quantum geometric potential, producing many interesting phenomena at the nanoscale [9–12], and a strain field leading to a curvature-induced Rashba spin-orbit coupling (SOC), with strength proportional to the curvature [13]. Several studies have investigated new properties triggered by curvature, e.g. in semiconductors [14–18], magnets [4, 7, 8] and superconductors [19–21]. Curved nanostructures with induced superconductivity can display geometric control of spin-triplet correlations in the clean limit [22], and proximizing a superconductor with a curved semiconductor can result in topological edge states [15]. The curved topological superconductor/straight semiconductor Josephson junction counterpart has been predicted to display a $0-\pi$ transition and $\phi$-junction behaviour [20].

Hybrid structures of superconductors and ferromagnets are of great interest for the field of superconducting spintronics [23, 24] since at the superconductor/ferromagnet (SF) interface the proximity effect allows the property of one material to "leak" into the other [25–27]. A coexistence of superconductivity and magnetism may therefore enable data processing, encoded in spin and charge degrees of freedom, to be performed without the heat loss associated with traditional electronics. In diffusive heterostructures, which cover a range of commonly available materials that may have impurities or sub-optimal interface transparencies, conventional $s$-wave superconducting correlations typically penetrate a ferromagnet for extremely short distances, proportional to $\sqrt{D_F/h}$, with $D_F$ the diffusion constant and $h$ the exchange field strength. Significant theoretical and experimental effort has focused on the conversion of singlet correlations into so-called long range triplet correlations (LRTC), which penetrate for longer distances, on the order of $\sqrt{D_F/T}$, where $T$ is the temperature. This conversion can take place in the presence of magnetic inhomogeneities [28–30] or due to intrinsic spin-orbit coupling either in the superconductor or in the ferromagnet [31, 32]. The role of geometric curvature as a source of designable and dynamically alterable SOC in diffusive structures has not been investigated in this context, and we address this here. By considering a model SFS junction with constant curvature shown in Fig. 1, we show that the curvature alone can induce long ranged supercurrents due to the generation of triplet correlations. Moreover, we show that these systems display a tunable $0-\pi$ transition.

The possibility of $0-\pi$ state switching has been of much interest, in part due to its potential role in solid state quantum computing [25, 33–37]. Investigations

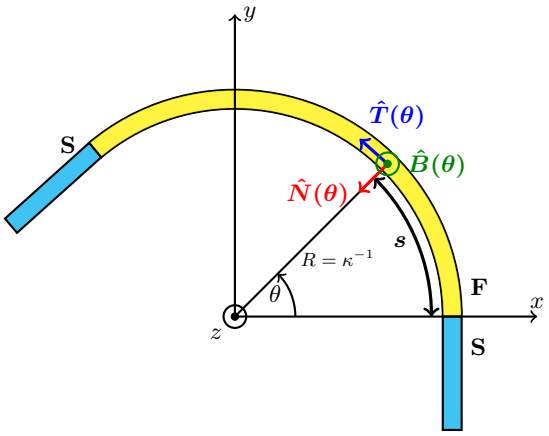


FIG. 1. Model system. SFS junction having a ferromagnet with constant curvature as weak link. The three orthonormal unit vectors $\hat{T}(\theta)$, $\hat{N}(\theta)$ and $\hat{B}(\theta)$ identifying the curvilinear coordinates are also shown.

have confirmed the transition can be governed by altering the length of the ferromagnetic weak link. However, this is not practicable to do in-situ and must be done by preparing multiple samples of different lengths. In this Letter, we show that dynamically changing the curvature of the magnet via in-situ strain manipulation, for example via photostriction, piezoelectrics or thermoelectric effects [38, 39], allows for a single-sample $0-\pi$ transition in the diffusive regime. Moreover, we show that curvature can yield long-ranged Josephson currents without any magnetic inhomogeneities or intrinsic SOC.

*Theoretical framework.*— A fundamental tool for the study of curved structures is the thin-wall quantization procedure, where the quantum motion of a particle in a 2D curved surface is treated as equivalent to the motion in a 3D space with the addition of lateral quantum confinement [40, 41]. This procedure allows one to derive the Hamiltonian for the motion of electrons constrained to a curved planar one-dimensional structure [42, 43].

When dealing with a ferromagnet, further effects of the curvature must be taken into account, namely in how it affects its exchange field. Recent studies have developed a fully 3D approach for thin magnetic shells of arbitrary shape and extended it to 2D shells and 1D wires [44, 45]. This showed that curvature induces two effective magnetic interactions: an effective magnetic anisotropy and an effective Dzyaloshinskii-Moriya interaction (DMI). When dealing with a 1D curved wire below a certain critical curvature, the magnetic anisotropy and the DMI, which results in an effective Rashba SOC, both combine to give an effective field tangential to the wire. The geometrically defined SOC is therefore both designable and tunable, and gives greater freedom in the manipulation of superconducting proximity effects.

We parametrize the curve by its arc length $s$, and define a set of three orthonormal unit vectors $\hat{T}(s)$, $\hat{N}(s)$, $\hat{B}(s)$ representing the tangential, normal and binormal curvilinear coordinates respectively, as indicated in Fig. 1. These obey the following Frenet-Serret-type equation of motion:

$$\begin{pmatrix} \partial_s \hat{T}(s) \\ \partial_s \hat{N}(s) \\ \partial_s \hat{B}(s) \end{pmatrix} = \begin{pmatrix} 0 & \kappa(s) & 0 \\ -\kappa(s) & 0 & 0 \\ 0 & 0 & 0 \end{pmatrix} \begin{pmatrix} \hat{T}(s) \\ \hat{N}(s) \\ \hat{B}(s) \end{pmatrix}, \tag{1}$$

where $\kappa(s)$ is the curvature of the wire, whose role and effect will be discussed in detail below. Deriving the Hamiltonian for a wire, which may include intrinsic SOC in general, we find [43]:

$$\begin{aligned} H = &-\frac{\hbar^2}{2m}\partial_s^2 - \frac{\hbar^2}{8m}\kappa(s)^2 - i\hbar\alpha_N\sigma_B\partial_s \\ &+ i\hbar\alpha_B\left(\sigma_N\partial_s - \frac{\kappa(s)}{2}\sigma_T\right). \end{aligned} \tag{2}$$

The SOC constants $\alpha_{N,B}$ represent the spin-orbit field with axis along the normal and binormal direction respectively, and $\sigma_{T,N,B}(s) = \boldsymbol{\sigma}\cdot\{\hat{T},\hat{N},\hat{B}\}(s)$ are the set of three Pauli matrices in curvilinear coordinates. By using Eqs. (1) we can incorporate the last three terms in Eq. (2) in a SU(2) spin-orbit field term:

$$\boldsymbol{A} = (\alpha_N\sigma_B - \alpha_B\sigma_N, 0, 0), \tag{3}$$

which has a vector structure in the geometric space and a $2\times 2$ matrix structure in spin space. It is worth distinguishing between the two terms entering the SU(2) field, namely $\alpha_B$ and $\alpha_N$. The former represents the intrinsic, not induced by the curvature, SOC term which may or may not exist according to the material taken into consideration. The latter is curvature-induced, and is proportional to the curvature strength. In natural units we have $\alpha_N = g\lambda\kappa(s)/(4m)$, where $g$ is the g-factor and the parameter $\lambda > 0$ is a characteristic energy scale for the material. Inspection of the relevant diffusion equations for the system shows that $\alpha_N$ and $\kappa(s)$ appear together in such a way that the former always acts as a strengthening factor for the latter. Therefore, considering a material with no intrinsic term we can ignore spin-orbit coupling as a whole, and consider the $\kappa(s)$ term only.

Having set up the Hamiltonian, we employ Green functions in the diffusive limit at equilibrium. Here the dynamics are describable by the second-order partial differential Usadel equation [46], which, with suitable boundary conditions, describes the diffusion of superconducting correlations inside the ferromagnet. Treating the case of diffusive equilibrium, it is sufficient to consider just the retarded component $\hat{g}_R$ of the quasiclassical Green function to describe the system [47]. Using Eq. (2) the Usadel equation in a curved ferromagnet with constant curvature reads (from now on we set $\hbar = 1$):

$$D_F\partial_s\left(\hat{g}_R\partial_s\hat{g}_R\right) + i\left[\varepsilon\hat{\tau}_3 + \hat{M}, \hat{g}_R\right] = 0, \tag{4}$$

with $\hat{\tau}_3 = \mathrm{diag}(1,1,-1,-1)$, $\varepsilon$ the quasiparticle energy and magnetization $\hat{M} = \boldsymbol{h}\cdot\mathrm{diag}(\boldsymbol{\sigma},\boldsymbol{\sigma}^*)$. The components of both vectors $\boldsymbol{h} = (h_T, h_N, h_B)$ and $\boldsymbol{\sigma} = (\sigma_T, \sigma_N, \sigma_B)$ are expressed in curvilinear coordinates. To solve the Usadel equation we employ the Kuprianov-Lukichev boundary conditions [48]:

$$L_j\zeta_j\hat{g}_{Rj}\nabla_I\hat{g}_{Rj} = [\hat{g}_{R1}, \hat{g}_{R2}]. \tag{5}$$

Here $\nabla_I$ is the derivative at the interface, $j$ refers to the various components of the hybrid system, with $j = 1, 2$ denoting the materials on the left and right side of the relevant interface, $L_j$ represents the length of the material and $\zeta_j = R_B/R_j$ is the interface parameter given by the ratio between the barrier resistance $R_B$ and its bulk resistance $R_j$.

If desirable, the intrinsic SOC can be retained, in which case one also introduces the gauge covariant derivative [32]:

$$\partial_s(\,\cdot\,) \to \widetilde{\partial}_s(\,\cdot\,) \equiv \partial_s(\,\cdot\,) - i\left[\hat{A}_T, \cdot\right], \tag{6}$$

with $\hat{A}_T = \mathrm{diag}(A_T, -A_T^*)$ and $A_T$ is the tangential component of the SO field of Eq. (3).

To treat the system we will use the Riccati parametrization [49, 50] for the quasiclassical Green function:

$$\hat{g}_R = \begin{pmatrix} N(1+\gamma\tilde{\gamma}) & 2N\gamma \\ -2\tilde{N}\tilde{\gamma} & -\tilde{N}(1+\tilde{\gamma}\gamma) \end{pmatrix}, \tag{7}$$

where the normalization matrices are $N = (1-\gamma\tilde{\gamma})^{-1}$ and $\tilde{N} = (1-\tilde{\gamma}\gamma)^{-1}$ and the tilde operation denotes $\tilde{\gamma}(\varepsilon) = \gamma^*(-\varepsilon)$. The Usadel equation (4) thus becomes:

$$\begin{aligned} D_F\left\{\partial_s^2\gamma + 2(\partial_s\gamma)\tilde{N}\tilde{\gamma}(\partial_s\gamma)\right\} = \\ -2i\varepsilon\gamma - i\boldsymbol{h}\cdot(\boldsymbol{\sigma}(s)\gamma - \gamma\boldsymbol{\sigma}^*(s)). \end{aligned} \tag{8}$$

Here the dependence on the curvature is implicitly contained in the Pauli matrices $\sigma_{T,N,B}(s)$.

We will consider our one-dimensional curved wire to be lying in the $xy$ plane as represented in Fig.1, so that the set of three unit vectors is:

$$\hat{T}(s) = -\sin\theta(s)\hat{x} + \cos\theta(s)\hat{y}, \tag{9a}$$

$$\hat{N}(s) = -\cos\theta(s)\hat{x} - \sin\theta(s)\hat{y}, \tag{9b}$$

$$\hat{B}(s) \equiv \hat{z}, \tag{9c}$$

with $\theta(s) = \kappa s$. It is useful to note that, when considering Eq. (8), the curved ferromagnet can be regarded as equivalent to a straight wire with a rotating exchange field, *i.e.* a tangential exchange field in a curved wire is equivalent to a position dependent exchange field in a straight wire, varying as $\vec{h}(s) = h_0(\sin\theta(s), -\cos\theta(s), 0)$, with $\theta(s) = \pi s/L_F$ and $L_F$ being the length of the ferromagnet.

*Results.*— Solving the Usadel equation, and therefore finding the quasiclassical Green function of the system, allows us to calculate many interesting quantities. In this work we will focus mainly on the charge current given by:

$$\frac{I_Q}{I_{Q0}} = \int_{-\infty}^{+\infty} d\varepsilon \mathrm{Tr}\left\{\hat{\tau}_3\left(\hat{g}_R\partial_s\hat{g}_R - \hat{g}_A\partial_s\hat{g}_A\right)\right\}\tanh(\beta\varepsilon/2). \tag{10}$$

Here $\hat{g}_A = -\hat{\tau}_3\hat{g}_R^\dagger\hat{\tau}_3$ is the advanced quasiclassical Green function and $\beta = (k_BT)^{-1}$ is the inverse temperature, with $k_B$ being the Boltzmann constant. Moreover, $I_{Q0} = N_0eD_FA\Delta_0/4L_F$, where $N_0$ is the density of states at the Fermi energy, $A$ the interfacial contact area and $\Delta_0$ the bulk gap of the two superconductors. Lengths and energies have been normalized to $L_F$ (which in turn is scaled with the superconducting coherence length $\xi_S$) and superconducting bulk gap $\Delta_0$ respectively, so that the integral on the right side of Eq.(10) is dimensionless.

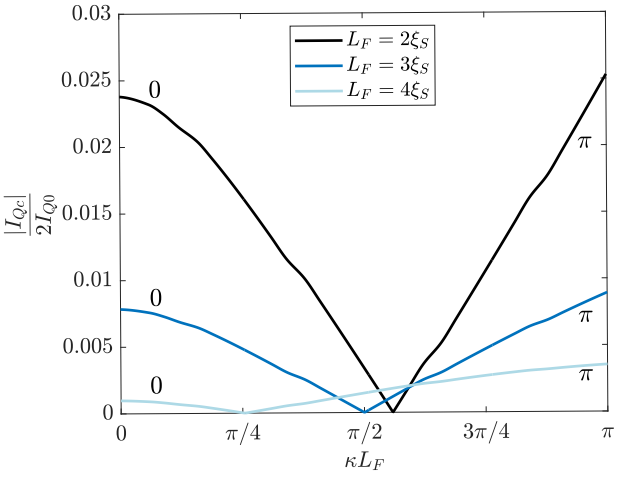


FIG. 2. Magnitude of the critical current as a function of the curvature for different lengths $L_F$ of the ferromagnet, with $T = 0.005T_c$, $\vec{h} = \Delta_0\hat{T}$, $\zeta = 3$. A $0-\pi$ transition occurs when changing the curvature of the wire.

We investigate the system portrayed in Fig. 1 by solving numerically Eq. (8) for various lengths $L_F$ of the ferromagnet and multiple curvatures $\kappa$ for each length. We set the interface parameter with both superconductors to be $\zeta = 3$ and the temperature to $T = 0.005T_c$. We consider the exchange field inside the curved ferromagnet to be tangential to its curvature profile at each point, $\boldsymbol{h}(s) \parallel \hat{T}(s)$, which we expect to be the case in 1D curved structures below a certain critical curvature [45].

Two interesting effects of the curvature appear immediately from our results. First, we show in Fig. 2 that it is possible to induce a $0-\pi$ transition in the junction by changing the curvature of the ferromagnetic wire while keeping its length fixed. Secondly, we will show in Fig. 3 that even for a long junction, where the singlet contribution to the supercurrent is negligible, a Josephson effect still appears for a non-zero $\kappa$ due to the presence of long ranged triplets.

In Fig. 2 we plot the absolute value of the critical current as given by Eq. (10) as a function of the curvature $\kappa$ of the ferromagnet across the junction for different lengths $L_F$. From the figure we see that starting in the 0 state with a straight wire, increasing the curvature results in a decreasing magnitude of the critical current, until it completely disappears for a certain $\kappa$, indicating a $0-\pi$ transition. A further increase in the curvature produces a revival of the critical current, which now flows in the

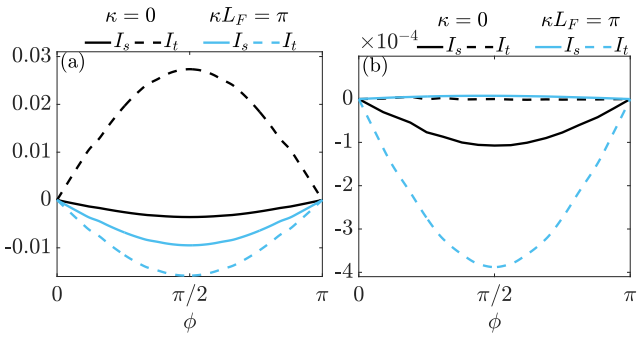


FIG. 3. Charge current as a function of the phase difference $\phi$, showing separately the singlet (solid lines) and triplet (dashed lines) contributions with $T = 0.005T_c$, $\vec{h} = \Delta_0\hat{T}$, $\zeta = 3$, for a straight ($\kappa = 0$) and semi-circular ($\kappa L_F = \pi$) ferromagnetic wire. (a) $L_F = 2\xi_S$ Increasing the curvature causes the triplet contribution to change sign. (b) $L_F = 6\xi_S$ Increasing the curvature causes the singlet contribution to be negligible with respect to the triplet one, signaling that the charge current is transported almost exclusively by the triplet correlations.

opposite direction with respect to the straight case. We also note that increasing the length of the ferromagnet reduces not only the overall magnitude of the critical current but also the curvature at which the $0-\pi$ transition takes place.

In order to better understand how this $0-\pi$ transition appears, and to show that the role of the triplets is crucial in tuning it, we split the charge current into singlet and triplet contributions, $I_s$ and $I_t$ respectively. It can be shown that the charge current given by Eq. (10) only depends on the anomalous Green function $f$ which is the off-diagonal block matrix in the retarded Green function. We define $f = (f_0 + \boldsymbol{d}\cdot\boldsymbol{\sigma})i\sigma_y$, with $f_0$ representing the singlet contribution and $\boldsymbol{d} = (d_T, d_N, d_z)$ the d-vector representing the triplet contribution, and obtain that the charge current can be written as $I_Q/I_{Q0} = I_s + I_t$, where $I_t = I_T + I_N + I_z + I_\kappa$ and:

$$I_s = -8\int_0^\infty d\varepsilon \mathrm{Re}\left\{\tilde{f}_0\partial_s f_0 - f_0\partial_s\tilde{f}_0\right\}\tanh(\beta\varepsilon/2), \quad (11a)$$

$$I_j = 8\int_0^\infty d\varepsilon \mathrm{Re}\left\{\tilde{d}_j\partial_s d_j - d_j\partial_s\tilde{d}_j\right\}\tanh(\beta\varepsilon/2), \quad (11b)$$

$$I_\kappa = 16\kappa\int_0^\infty d\varepsilon \mathrm{Re}\left\{\tilde{d}_N d_T - \tilde{d}_T d_N\right\}\tanh(\beta\varepsilon/2), \quad (11c)$$

with $j = (T, N, z)$. The terms $I_s$ and $I_j$ represent the contribution coming from the singlet and triplets with spin aligned in the $j$ direction respectively. The last term $I_\kappa$ instead defines an inverse Edelstein term due to the curvature.

In Fig. 3(a) we plot these two different contributions to the charge current for two different values of $\kappa$ and $L_F = 2\xi_S$. It can be seen that for $\kappa = 0$ triplets and singlet charge currents have opposite sign, with the triplets contribution being generally bigger than the singlet one. Interestingly however, when increasing the curvature the triplet current changes sign, i.e. starts flowing in the opposite direction, while the singlet contribution does not. Hence, the $0-\pi$ transition is tuned by the curvature through its effect on the triplets. Furthermore, we note from Fig. 3(a) that in the $\pi$-phase for $\kappa = \pi/L_F$ the singlet and triplet currents have the same sign and thus flow in the same direction. Consequently, the two contributions add up, resulting in a larger critical current in the $\pi$-phase at $\kappa = \pi/L_F$ compared to the 0-phase at $\kappa = 0$.

We point out that curvature also introduces a spin current to the system, which is absent in a straight nanowire. This *exchange* spin current, as it is known in the literature, is caused by the misalignment of the magnetization in the system and is non-zero even at phase differences of $\phi = 0$ and $\phi = \pi$, where there are no charge currents [51, 52]. The magnitude of the spin current is affected by the curvature, thereby providing means by which it can be externally manipulated.

To highlight that the triplets generate a long range Josephson effect, we consider a long junction, $L_F = 6\xi_S$, and plot in Fig.3(b) separately singlet and triplet contributions for a straight ($\kappa = 0$) and semi-circular ($\kappa L_F = \pi$) wire. We see that, while for $\kappa = 0$ the triplet term is essentially zero and the singlet term is finite, for $\kappa L_F = \pi$ the singlet contribution is negligible compared to the triplet one. Going from a straight to a semi-circular ferromagnet produces a significant singlet to triplet conversion, and given the significant length of the wire we can state that the SFS junction with a semi-circular nanowire exhibits long-ranged triplets.

*Concluding remarks.*— We have shown that curvature is a designable and tunable parameter that can generate and control long-ranged supercurrents in diffusive SFS Josephson junctions without any magnetic inhomogeneities or intrinsic SOC. The system displays a curvature-controlled $0-\pi$ transition, which can be manipulated dynamically in-situ with a single sample. This can facilitate experimental investigation of the transition, and improve our understanding of the coexistence of superconductivity and magnetism in different phases. In the longer term this opens a diverse new toolkit for design and control of diffusive superconducting spintronic systems, and may be a useful implementation in solid state quantum computing. Since this field is still in its infancy, with several exciting directions still to be explored, we anticipate that curvature in such systems will be integral to the new generation of spintronic designs.

We thank P. Gentile for useful discussions and H. G. Hugdal for his helplful insights. The computations have been performed on the SAGA supercomputer provided by UNINETT Sigma2 - the National Infrastructure for High Performance Computing and Data Stor-

age in Norway. We acknowledge funding via the "Outstanding Academic Fellows" programme at NTNU, the Research Council of Norway Grant number 302315, as well as through its Centres of Excellence funding scheme, project number 262633, "QuSpin".

* Corresponding author: tancredi.salamone@ntnu.no

[1] O. G. Schmidt and K. Eberl, Nature **410**, 168 (2001).
[2] P. Cendula, S. Kiravittaya, Y. F. Mei, C. Deneke, and O. G. Schmidt, Phys. Rev. B **79**, 085429 (2009).
[3] S. Xu, Z. Yan, K.-I. Jang, W. Huang, H. Fu, J. Kim, Z. Wei, M. Flavin, J. McCracken, R. Wang, A. Badea, Y. Liu, D. Xiao, G. Zhou, J. Lee, H. U. Chung, H. Cheng, W. Ren, A. Banks, X. Li, U. Paik, R. G. Nuzzo, Y. Huang, Y. Zhang, and J. A. Rogers, Science **347**, 154 (2015).
[4] K. S. Das, D. Makarov, P. Gentile, M. Cuoco, B. J. Van Wees, C. Ortix, and I. J. Vera-Marun, Nano letters **19**, 6839 (2019).
[5] E. R. Lewis, D. Petit, L. Thevenard, A. V. Jausovec, L. O'Brien, D. E. Read, and R. P. Cowburn, Applied Physics Letters **95**, 152505 (2009).
[6] D. M. Burn, M. Chadha, S. K. Walton, and W. R. Branford, Phys. Rev. B **90**, 144414 (2014).
[7] O. M. Volkov, A. Kákay, F. Kronast, I. Mönch, M.-A. Mawass, J. Fassbender, and D. Makarov, Phys. Rev. Lett. **123**, 077201 (2019).
[8] R. Streubel, P. Fischer, F. Kronast, V. P. Kravchuk, D. D. Sheka, Y. Gaididei, O. G. Schmidt, and D. Makarov, Journal of Physics D: Applied Physics **49**, 363001 (2016).
[9] G. Cantele, D. Ninno, and G. Iadonisi, Phys. Rev. B **61**, 13730 (2000).
[10] H. Aoki, M. Koshino, D. Takeda, H. Morise, and K. Kuroki, Phys. Rev. B **65**, 035102 (2001).
[11] M. Encinosa and L. Mott, Phys. Rev. A **68**, 014102 (2003).
[12] C. Ortix and J. van den Brink, Phys. Rev. B **81**, 165419 (2010).
[13] P. Gentile, M. Cuoco, and C. Ortix, SPIN **03**, 1340002 (2013).
[14] F. Nagasawa, D. Frustaglia, H. Saarikoski, K. Richter, and J. Nitta, Nature communications **4**, 1 (2013).
[15] P. Gentile, M. Cuoco, and C. Ortix, Phys. Rev. Lett. **115**, 256801 (2015).
[16] Z.-J. Ying, P. Gentile, C. Ortix, and M. Cuoco, Phys. Rev. B **94**, 081406 (2016).
[17] C.-H. Chang and C. Ortix, Nano letters **17**, 3076 (2017).
[18] G. Francica, P. Gentile, and M. Cuoco, EPL (Europhysics Letters) **127**, 30001 (2019).
[19] A. M. Turner, V. Vitelli, and D. R. Nelson, Rev. Mod. Phys. **82**, 1301 (2010).
[20] G. Francica, M. Cuoco, and P. Gentile, Phys. Rev. B **101**, 094504 (2020).
[21] P.-H. Chou, C.-H. Chen, S.-W. Liu, C.-H. Chung, and C.-Y. Mou, Phys. Rev. B **103**, 014508 (2021).
[22] Z.-J. Ying, M. Cuoco, C. Ortix, and P. Gentile, Phys. Rev. B **96**, 100506(R) (2017).
[23] J. Linder and J. W. Robinson, Nature Physics **11**, 307 (2015).
[24] M. Eschrig, Phys. Today **64**, 43 (2011).
[25] A. I. Buzdin, Rev. Mod. Phys. **77**, 935 (2005).
[26] F. S. Bergeret, A. F. Volkov, and K. B. Efetov, Rev. Mod. Phys. **77**, 1321 (2005).
[27] I. F. Lyuksyutov and V. L. Pokrovsky, Advances in Physics **54**, 67 (2005).
[28] F. S. Bergeret, A. F. Volkov, and K. B. Efetov, Phys. Rev. Lett. **86**, 4096 (2001).
[29] T. S. Khaire, M. A. Khasawneh, W. P. Pratt, and N. O. Birge, Phys. Rev. Lett. **104**, 137002 (2010).
[30] J. W. A. Robinson, J. D. S. Witt, and M. G. Blamire, Science **329**, 59 (2010), https://science.sciencemag.org/content/329/5987/59.full.pdf.
[31] F. S. Bergeret and I. V. Tokatly, Phys. Rev. Lett. **110**, 117003 (2013).
[32] F. S. Bergeret and I. V. Tokatly, Phys. Rev. B **89**, 134517 (2014).
[33] A. I. Buzdin, L. Bulaevskii, and S. Panyukov, JETP lett **35**, 147 (1982).
[34] A. Buzdin and A. E. Koshelev, Phys. Rev. B **67**, 220504 (2003).
[35] V. V. Ryazanov, V. A. Oboznov, A. Y. Rusanov, A. V. Veretennikov, A. A. Golubov, and J. Aarts, Phys. Rev. Lett. **86**, 2427 (2001).
[36] T. Kontos, M. Aprili, J. Lesueur, F. Genêt, B. Stephanidis, and R. Boursier, Phys. Rev. Lett. **89**, 137007 (2002).
[37] J. E. Mooij, T. P. Orlando, L. Levitov, L. Tian, C. H. van der Wal, and S. Lloyd, Science **285**, 1036 (1999).
[38] B. Kundys, Applied Physics Reviews **2**, 011301 (2015).
[39] S. Matzen, L. Guillemot, T. Maroutian, S. K. K. Patel, H. Wen, A. D. DiChiara, G. Agnus, O. G. Shpyrko, E. E. Fullerton, D. Ravelosona, P. Lecoeur, and R. Kukreja, Advanced Electronic Materials **5**, 1800709 (2019).
[40] H. Jensen and H. Koppe, Annals of Physics **63**, 586 (1971).
[41] R. C. T. da Costa, Phys. Rev. A **23**, 1982 (1981).
[42] C. Ortix, S. Kiravittaya, O. G. Schmidt, and J. van den Brink, Phys. Rev. B **84**, 045438 (2011).
[43] C. Ortix, Phys. Rev. B **91**, 245412 (2015).
[44] Y. Gaididei, V. P. Kravchuk, and D. D. Sheka, Phys. Rev. Lett. **112**, 257203 (2014).
[45] D. D. Sheka, V. P. Kravchuk, and Y. Gaididei, Journal of Physics A: Mathematical and Theoretical **48**, 125202 (2015).
[46] K. D. Usadel, Phys. Rev. Lett. **25**, 507 (1970).
[47] W. Belzig, F. K. Wilhelm, C. Bruder, G. Schön, and A. D. Zaikin, Superlattices and Microstructures **25**, 1251 (1999).
[48] M. Y. Kuprianov and V. Lukichev, Zh. Eksp. Teor. Fiz **94**, 149 (1988).
[49] N. Schopohl and K. Maki, Phys. Rev. B **52**, 490 (1995).
[50] S. H. Jacobsen, J. A. Ouassou, and J. Linder, Phys. Rev. B **92**, 024510 (2015).
[51] S. H. Jacobsen, I. Kulagina, and J. Linder, Scientific reports **6**, 1 (2016).
[52] W. Chen, P. Horsch, and D. Manske, Phys. Rev. B **89**, 064427 (2014).